THESIS FOR THE DEGREE OF DOCTOR OF PHILOSOPHY

Application of 3-D Computation of Magnetic Fields to the Design of Claw Pole Motors

SONJA K. TIDBLAD LUNDMARK

Department of Energy and Environment
Division of Electric Power Engineering
CHALMERS UNIVERSITY OF TECHNOLOGY
Göteborg, Sweden 2005

Application of 3-D Computation of Magnetic Fields to the Design of Claw Pole Motors
SONJA K. TIDBLAD LUNDMARK
ISBN 91-7291-631-1

Doktorsavhandlingar vid Chalmers tekniska högskola
Ny serie nr 2313
ISSN 0346-718x

Technical Report No. 3
Division of Electric Power Engineering
Department of Energy and Environment
Chalmers University of Technology
SE-412 96 Göteborg
Sweden
Telephone +46 (0)31-772 1000

Mediagruppen Intercopy AB
Göteborg, Sweden 2005

Application of 3-D Computation of Magnetic Fields to the Design of Claw Pole Motors

SONJA K. TIDBLAD LUNDMARK
Division of Electric Power Engineering
Department of Energy and Environment

ABSTRACT

The main advantage of claw-pole machines lies in their ability to yield higher torque density values than is obtainable from a conventional machine. However, the high torque density has its price; leakage flux is often high resulting in low power factor and efficiency. This thesis is mainly concerned with the design of a claw-pole motor that meets application requirements of reasonably high torque density and a power factor comparable to conventional topologies.

After critically reviewing previously proposed designs of Transverse-flux and Claw-pole machines, the thesis focuses on a special type of claw pole motor having claws in both the stator and the rotor. The claws are made of Soft Magnetic Composites (SMC); consisting of iron powder particles that are individually insulated and can be readily pressed into complex geometries. Detailed explanation of the operation of such a design is then provided.

Internal design of the claw-pole motor is investigated with the aid of three-dimensional finite-element field computation. In particular, the effect of the following parameters on the motor's performance has been investigated: number of poles, main dimensions, magnet material and dimensions, pole-face profile and claw angle. This theoretical work was verified, to some extent, against measurements obtained from an experimental machine especially constructed for this purpose. Details of this experimental motor are also presented.

The investigation of the internal design of the claw-pole motors presented in this thesis provides a physical insight into their operation and, therefore, can be utilised for their general design. Indeed, this work enabled realisation of a claw-pole servomotor that is capable of achieving a torque density of about 1.5 Nm/Kg at a power factor of 0.9. The decisions made in arriving at the servomotor design are presented and clearly related to the conclusions of the internal design investigation.

Keywords: Permanent-magnet machines, Transverse flux, Claw-pole motor, Soft magnetic composites (SMC).

Acknowledgements

The financial support granted by Elforsk, ABB, and Danaher Motion is gratefully acknowledged. I also wish to acknowledge the general support from Höganäs AB. The last few months of my studies were financed from Professor Hamdis start-up grant and Thanks are due to the Chalmers Foundation for this.

I would like to take this opportunity to express my deepest gratitude to my supervisor, Professor Essam Hamdi, who with his wisdom, kindness, and joy gave me the best guidance and support, ever possible. I am also grateful to him for giving me a chance and the encouragement to come back after a long interruption of having a family. Because of the parental leave, I have been a PhD student at Chalmers for many years (since 1993). During the first three years, Professor Jorma Luomi, who is now at Helsinki University of Technology, supervised me to the Licenciate degree and examined most of the 40 credit points necessary for the PhD degree, and I am very grateful to him for his excellent supervision. Since 2003, I have been working on the subject of this thesis under the supervision of Professor Essam Hamdi.

As it is not possible to mention all colleagues that have been helpful and kind during these years, I would still like to express special thanks to Dr Raj Kasinathan for patiently introducing me to MagNet, Valborg Ekman for her kindness and honesty, Eva Palmberg who is one of my role models, and finally all in the group of Electrical Machines and Drives (Essam, Hasan, Mohamed, Ehab, Raj, Helmi and Hassan) who gave me a feeling of coming home when I came to work.

I also wish to give special thanks to Dr Öystein Krogen, Jerry Brown, Axel Öhman, and Laszlo Bartha at Danaher Motion for their expert help and encouragement with the claw-pole prototype construction and testing. I am also indebted to Dr Lars-Olov Pennander and Göran Nord at Höganäs AB for help, ideas and enthusiasm concerning the soft magnetic composites.

Last but not least, my family's support during my studies has been a condition for its realisation. I am very thankful to my beloved husband David for his support and patience. Thanks also to my children, Alice, Edvin, Jessica, and Miriam for giving me inspiration and motivation. Warm thanks to my parents and parents in law for helping out in numerous occasions and a special thanks to my grandmother Karin, who together with my late grandfather Erland, are also my role models.

Table of Content

List of symbols

Abbreviations:

FE	finite element
FEM	finite element method
ID	inner diameter
OD	outer diameter
PM	Powder Metallurgical
PWM	Pulse Width Modulated
SMC	Soft Magnetic Composite
TFM	Transverse Flux Machine
TFRM	Transverse Flux Reluctance Motor
TM	Torque Magnification
VRPM	Variable Reluctance Permanent Magnet
Z-TFM	Zweygberk- Transverse Flux Machine
+z assembly	way of rotor assembly as in Fig. 4.1
3D	three dimensions

Symbols:

ac	electric loading
A_c	conductor area
A_{coil}	area of the coil cross section
A_{Cu}	area of the bare copper wire
A_m	area of the magnet
A_g	area of the air gap
b	half-length of the conducting material
B	magnetic flux density
B_r	remanence
B_n	normal component of B
B_p	peak flux density
B_g	air gap flux density
B_m	magnet flux density
cosφ	power factor
C_h	constant associated with P_h
C_e	constant associated with P_e
d	bare wire diameter
D	stator bore
E, emf	induced voltage at no load
f	frequency
f_c, f_{cm}	fill factors
H_g	air gap field intensity
H_m	magnet field intensity
H_c	coercivity
I	current
I_d, I_q	current in d- and q-directions
j	current density
K_e	back emf constant
K_l	leakage flux factor
K_r	reluctance factor

K_T	torque constant
l	mean length of one turn
l_g	air gap length
l_m	magnet length
l_{sc}	stator claw length
L	inductance
m	number of phases
N	number of turns
p	number of poles
P_{core}	core losses in the stator and rotor cores
P_{Cu}	copper losses in the stator winding
P_e	eddy current losses
P_{em}	electromagnetic power
P_h	hysteresis losses
P_{in}	input power
P_{mech}	mechanical losses
P_{out}	output power
P_{rot}	rotational losses
r_o	outer radius of the magnet
r_i	inner radius
r_s	inner radius of the stator
R	resistance
V	voltage
W	energy
X	reactance
X_d, X_q	reactance in *d*- and *q*-directions
α	rotor angular position
β	overlapping angle of the claws
γ	phase advance angle
δ	load angle
ρ	resistivity
τ	pole pitch
ψ	flux linkage
ω_e	electrical angular frequency
ω_m	mechanical angular frequency
Φ_r	flux induced by the rotor magnets
Φ_s	flux induced by the stator winding
Φ	magnetic flux

1 Introduction

1.1 Background

The search for improvement in the performance of electrical machines has been going on for a long time. Lately, these efforts have been facilitated by advances in power electronics, and by the introduction of new materials. Both hard and soft magnetic materials have improved, the latter with the introduction of the Soft Magnetic Composites (SMC) that allows construction of machines in which the magnetic flux path is three-dimensional. Design and research work has been facilitated by the availability of commercial software capable of modelling complex geometries and providing numerical solutions to the field problems in three-dimensions.

The goal of the machine designer would of course depend on the application, but common goals include achieving high torque density, high efficiency, and low cost. Other goals would, for example, be long lifetime, high power factor (to keep the cost of the power electronics converter down) and ease of control.

Considering environmental issues and the limited global resources, the goal of achieving the highest possible efficiency is becoming increasingly important. A high efficiency implies of course low losses. Unfortunately, optimising the efficiency often means choosing more expensive materials. To follow that route, the machine producer must see a significant difference in performance. An example of relatively new machines with better performance is the brushless dc-machine, which gives better performance than the induction machines. As the induction machine is less expensive, it is still the first choice in many cases, in spite of the better performance of brushless dc-machines. If the total cost of the losses is considered over the whole lifetime of the machine, the one having better efficiency could be more economical. However, keeping the cost calculations to the short perspective, the choice falls often on the cheaper to produce machine. From a motor manufacture perspective, the motivation is to find a design topology that could achieve higher output or efficiency (or an efficiency value comparable to that of an existing design) at lower production cost.

One possible solution is the use of Soft Magnetic Composites (SMC) in the so-called claw-pole motors; a kind of transverse flux machines (TFMs). TFMs are known for their ability to yield high torque density values: a reported figure is about 20 Nm/kg compared to 2 Nm/kg of a servo machine of the same size, as seen in (Maddison, Mecrow et al. 1998), (Harris, Pajooman et al. 1997) and (Henneberger and Bork 1998). The SMC material offers the possibility to lead the flux in three-dimensions, it restricts the eddy currents and can be produced in complex shapes relatively easy. On the other hand, TFMs are also known to suffer from high leakage fields and, consequently low power factor. Additionally, SMC materials are characterised with high iron losses compared to the laminated electrical steels used in conventional radial-flux machines.

One other characteristic of the SMC materials is their brittleness. While this is viewed as a disadvantage during assembly and normal operation, it improves the recycling of copper used in the machine winding. Considering that electric motor manufacturers aim to increase product quality while minimizing scrap, this is an interesting fact that may assume a greater importance in the future.

Realisation of the potential benefits of the claw-pole topology is not a straightforward process. This is not only because of the large number of design variables that can affect the performance but also because a conflict exists between the torque density and the power factor; both are important in industrial drive applications. In the available literature, several electrical machines built with SMC are reported, where most of these are intended for moderate performance applications, where the main advantages seem to be low cost and easy assembly. It is believed that the potential for this type of machines in industrial drive applications is yet to be assessed. This can be achieved when their operation and internal design are fully understood.

1.2 Objectives and scope of thesis

The objectives of the work reported in this thesis are:

- to improve understanding of operation and internal design of claw-pole machines, and
- to develop one such a design for servo applications and to compare its performance and cost with a conventional design

After critically reviewing available relevant literature (Chapter 2), the first objective is addressed in Chapter 3. It begins by investigating different design parameters of the claw-pole machine, and identifying aspects that have most effect on torque density and power factor. These are then investigated one at a time, while reasonable conditions of the other parameters are assumed, and the sensitivity of the torque density and power factor values is determined. This work yielded design roles that can assist in meeting design targets. The investigation relies on 3-D finite element computations and the accuracy of the models used are assessed against test results obtained from an experimental machine, especially built for this purpose. The constructional details of the experimental machine and the testing programme are also given in Chapter 3.

In Chapter 4, the practical value of the theoretical investigation is demonstrated, where the conclusions of Chapter 3 are used to design a claw-pole servomotor. After arriving at a suitable design, modifications were introduced to take into account limitations imposed by the method used in building a pre-production prototype. Constructional details and predicted performance are given for both the mass-production and prototype designs.

Chapter 5 summarises the conclusions of the work and gives suggestions for further work.

1.3 Contributions

The work improves the understanding of the effect various design parameters have on the performance of claw-pole motors. It provides a physical insight into their operation and clearly identifies design trade-offs, i.e. it has a *design office* value.

As is the case of many engineering research projects, this work is undertaken in collaboration with industry. While it is accepted that the detailed prototype design

described in this thesis, on its own, does not constitute a major advance of knowledge, it is believed to have a significant engineering value.

1.4 Publications

Lundmark, S. T., et al. (2004). Effect of Pole Face Profile on Performance of a Class of Claw-pole Motors. Norfa Summer Seminar, Tallinn, Estonia.

Lundmark, S. T. and Hamdi, E. S. (2004). "Construction, Operation and Internal Design of Transverse-Flux Machines." WSEAS Transactions on Circuits and Systems **3**(8): 1724-1728.

Lundmark, S. T. and Hamdi, E.S. (2004). "Design of Claw-Pole Machines Using SMC Cores." WSEAS Transactions on Circuits and Systems **3**(8): 1729-1734.

Lundmark, S. T. and E. S. Hamdi (2005). "Construction, Operation and Internal Design of a Claw-Pole Servo Motor." Submitted for publication in *Electromotion* Journal.

2 Literature review

2.1 Introduction

The development of new machine topologies has increased in recent years, as new and improved hard- and soft-magnetic materials are introduced. For example, Soft Magnetic Composite materials (SMC) give the opportunity to lead 3D alternating or rotating fields. SMCs manufacturing process allows construction of complex machine topologies, such as claw-pole, transverse flux, and combined axial and radial flux motors. An advantage of the SMC material is that the conductivity is low (with an isotropic permeability) resulting in low eddy currents. The result concerning output torque from the new machine topologies seem promising, although, new problems arise, as for instance a high armature reactance (giving a low power factor), the construction of the complicated geometry, and the modelling of the three-dimensional flux path. As the claw-pole machine is a special kind of the transverse flux machine (TFM), both the transverse flux machine and the claw-pole machine will be analyzed in detail. First the different machine models and their performance will be treated. Then, the use of SMC in electric machines will be described.

The characteristics of transverse flux machines and claw-pole machines are that the number of poles can be increased, without decreasing the conductor volume, resulting in a high torque density. This is to be compared with a conventional machine where the electric and magnetic parts compete for the same space, and a higher number of poles only give less flux per pole and thus no change in torque. According to (Qin, Ronghai et al. 1999), the transverse flux machine and the claw-pole machine can be included in the family of torque magnification (TM) machines. In (Harris and Mecrow 1993), they calculated a possible torque density of 28 kNm/m^3 (compared to 5,75 kNm/m^3 for a comparable induction motor). According to (Hasubek and Nowicki 2000), transverse flux machines are capable of producing torque densities that are three to five times higher than conventional machines. In (Henneberger and Bork 1998), they explain the possible high torque density for transverse flux machines with this equation of the specific electric loading:

$$ac = \frac{I}{2\tau}, \tag{2.1}$$

where I is the armature current, and τ is the pole pitch.

As the torque density is proportional to the electric loading, the torque can be increased by decreasing the pole pitch (or increasing the pole numbers for a given machine size). However, according to (Henneberger and Bork 1998) there is a limit of number of poles, as a too high number of poles results in a high leakage field, and the optimal pole pitch depends also on the stator current because the leakage flux is encouraged by saturation. This is also found in (Kastinger 2003).

One clear difference between TFM and claw-pole machines is that TFM often have a 2-D flux path in a plane transverse to the direction of motion and thus may have laminated material in the rotor and stator, whereas the flux path in claw-pole machines is truly three-dimensional. However, the TFM is mostly analyzed and modelled in three-dimensions (just as the claw-pole machine) to enable consideration of such effects as leakage and fringing fluxes.

2.2 Transverse flux machines

2.2.1 Construction and different types

As its name implies, a transverse flux machine is a permanent magnet machine in which the flux path is transversal to the direction of motion. The rotor may consist of surface mounted permanent magnets, polarized in the radial direction, or of buried magnets polarized in the peripheral direction (giving flux concentration). There is also a special version with a ring magnet magnetised axially, as presented in (Kastinger 2003). According to (Henneberger and Bork 1998), buried magnets give higher specific torque than surface mounted magnets but the rotor will be difficult to manufacture. In (Harris, Pajooman et al. 1997), the flux concentrated rotor is also found to yield better performance, both concerning torque production and the power factor. Both constructions, however, give radial flux in the air gap. The stator consists of the core and a ring winding. The current carrying coil, fed with ac current, produces alternating flux, which is lead through the stator pole pieces and passes the air gap in the radial direction, as shown in Fig. 2.1.

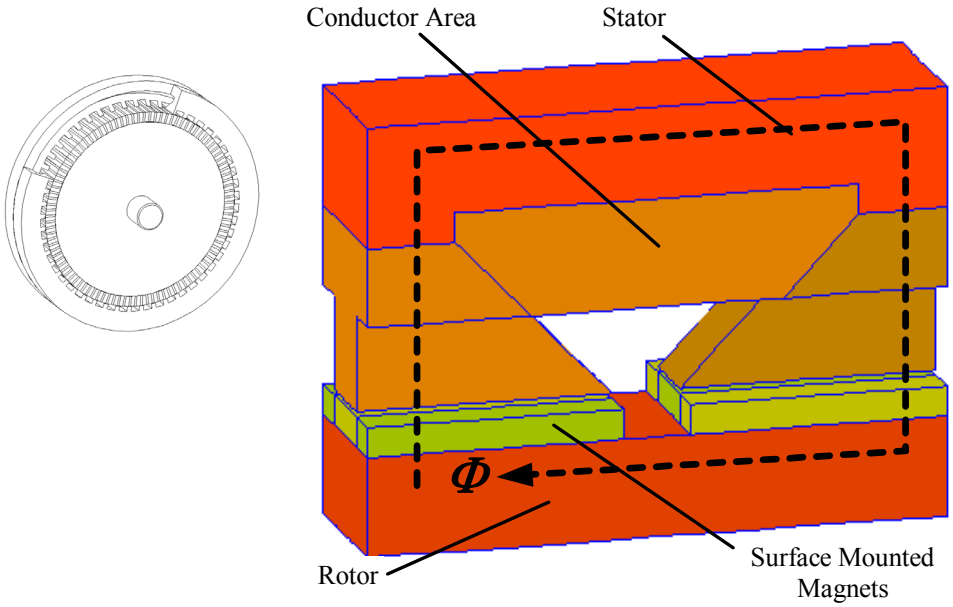

Figure 2.1: Transverse flux motor, single sided version with surface mounted magnets in the rotor. Picture from (Maddison, Mecrow et al. 1998).

There is one package (stack) for each phase. Several one-phase machines can be added in the axial direction to build a poly-phase machine. A three-phase machine would then have three ring windings, giving alternating fields electrically shifted 120 degrees. However, in (Henneberger and Bork 1998) they found it best, from a production point of view, to put the stator currents in phase and to shift the rotor magnets instead. To overcome the problem of leakage between phases, magnetic insulation techniques need to be employed. For example, in (Mecrow, Jack et al. 2002) and (Henneberger and Bork 1998), a small air gap between phases is used while in (Njeh, Masmoudi et al. 2003) aluminium barriers are employed. In (Cros and Viarouge 2004) the use of barriers between phases was avoided by placing all three stator windings in the same stack. For rotors with surface mounted magnets, the

leakage between phases is much smaller than with flux concentration, and in (Guo, Zhu et al. 2003) the induced emf of the three phases was nearly symmetrical without using barriers.

The stator can be single-sided or double-sided, and with different shapes of the core, as is illustrated in Figs. 2.2 and 2.3. It is reported that a double-sided transverse flux machine is the variation that gives the highest specific output (torque per unit volume or mass) and a relatively high power factor but it is complicated to construct (Maddison, Mecrow et al. 1998).

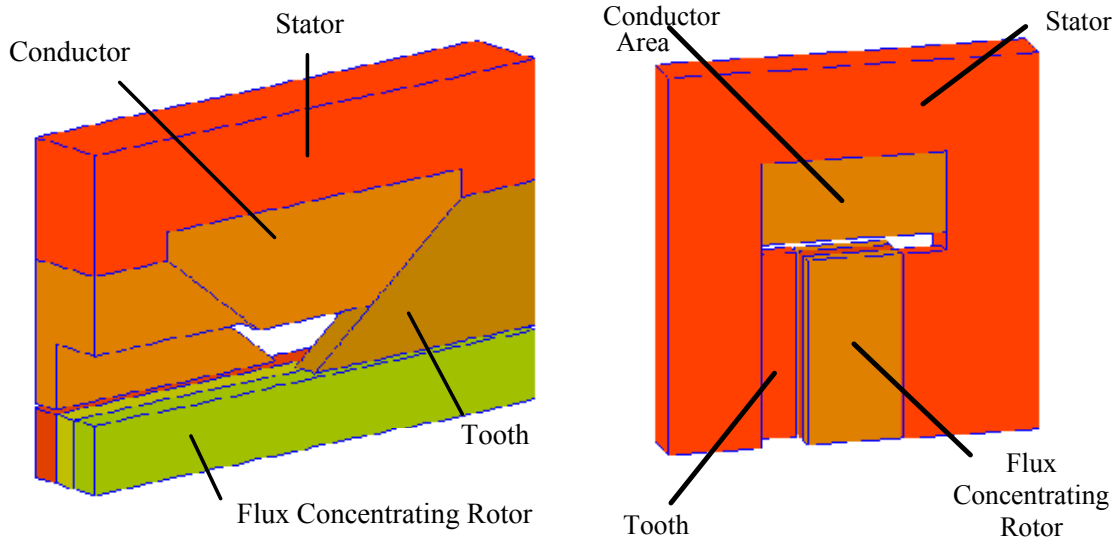

Figure 2.2: Transverse flux motors; single sided version with flux-concentrated rotor (left) and double sided version (right). Picture from (Maddison, Mecrow et al. 1998).

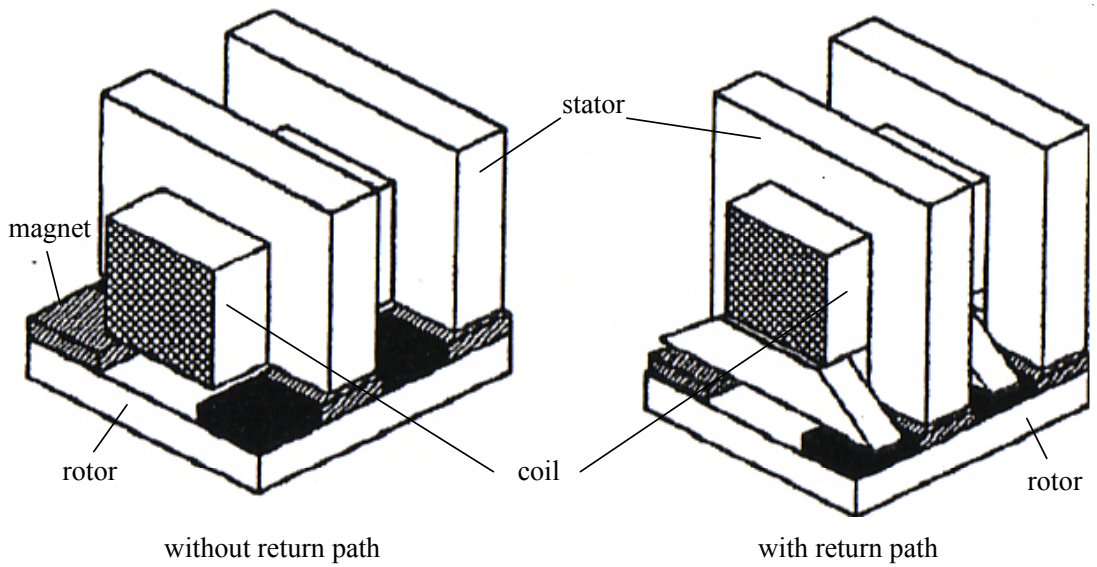

Figure 2.3: Transverse flux motors; single sided version with surface mounted magnets in the rotor and different stator constructions. Picture from (Henneberger and Bork 1998).

In (Rang, Gu et al. 2002) a 20 kW, double sided TFM is compared with a TFM with a C-shaped stator core, surrounding the rotor (see Fig. 2.4). This C-shaped design was found to be mechanically strong and easy to manufacture. It can be used in ship propulsion applications at speeds below 200 rpm. Also in (Payne, Husband et al. 2002), a C-shaped stator core is investigated for a marine propulsion application (a 20 MW machine with a rated speed of 308 rpm).

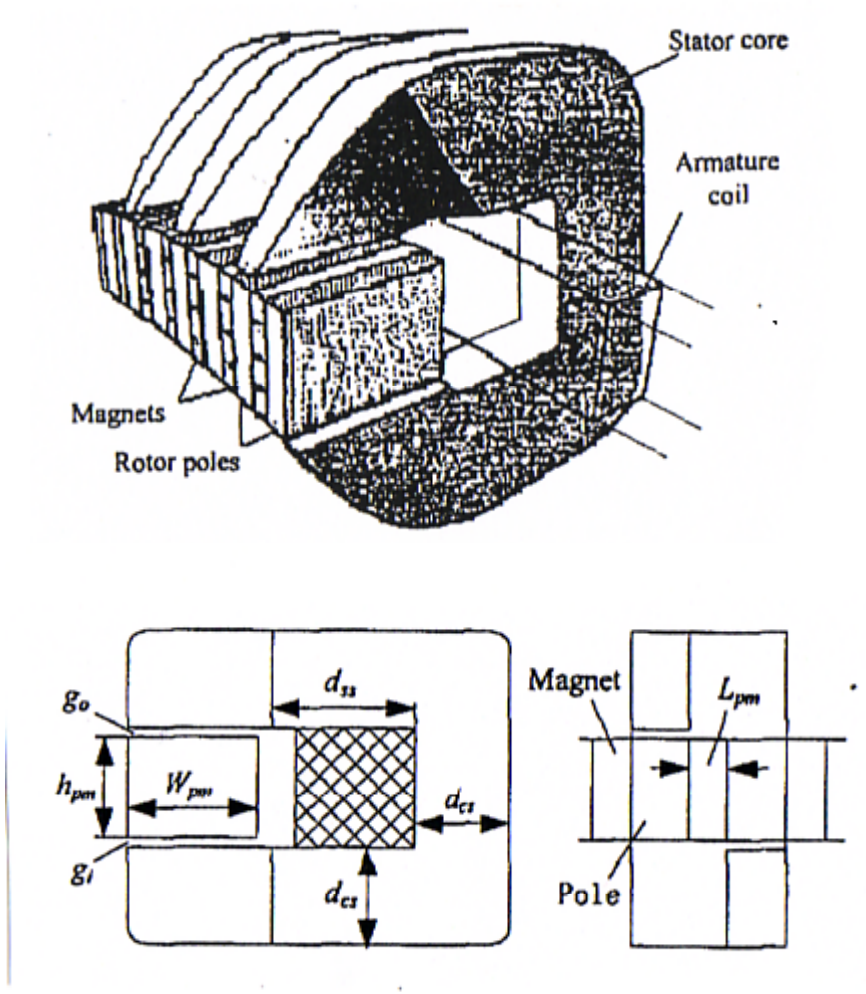

Figure 2.4: A transverse flux motor with C-shaped stator core. Picture from (Rang, Gu et al. 2002).

There are some other types of transverse flux machines; the claw-pole machine (described in the next chapter) and the variation of Zweygberk (The Z-TFM), which is reported in (Arshad, Backstrom et al. 2002). As conventional transverse flux machines with surface mounted magnets only use half the magnets at any one time and half of the winding, an improvement might be achieved by adding intermediate poles in the stator. It was found in (Arshad, Backstrom et al. 2002) that the improvement was counteracted by a large amount of additional leakage. However, this design was used after some modification in a linear double-sided TFM of 5 kW by (Arshad, Thelin et al. 2003). Comparing surface mounted magnets and buried magnets; they found that the surface mounted magnets lead to a very high armature leakage flux between adjacent poles with core parts of different polarity. The leakage flux path was thus only around the armature winding (passing two adjacent poles) and did not cross the active air gap. With surface mounted magnets the active air gap is

larger than with buried magnets, and the reluctance path of the leakage will be relatively lower (than with buried magnets). Using buried magnets, the armature leakage could be reduced but then the rotor leakage would increase (as the leakage-areas between two adjacent poles were moved from the stator to the rotor). However, the rotor leakage could also be decreased, if the rotor magnets are magnetised in the axial direction (the leakage flux direction). With such a design, the power factor was improved (as the leakage was decreased).

There is also reported the work of (Henneberger and Bork 1998) who added intermediate poles with a special triangular shape to minimize stray flux (see Fig. 2.3). Doing this, they could separate the rotor in two parts, giving less used material and allowing for a laminated rotor. The same stator concept as in the work of (Henneberger and Bork 1998) was used in (Kastinger 2003). However, he used another type of rotor, similar to the ones used in hybrid stepping motors. The rotor thus has an axially magnetized permanent magnet ring and laminated rotor elements with tooth-slot geometry.

In (Harris, Pajooman et al. 1996) three alternative topologies of the TFM are compared; two single-sided with and without intermediate poles, and one double-sided. It is found that intermediate poles give no additional torque but instead reduce the available space for the stator winding. However, the eddy currents in the rotor may be reduced, as the bridges reduce the flux pulsations in the rotor. Also in (Maddison, Mecrow et al. 1998) a comparison of different transverse flux machines is performed. They compare a single-sided TFM, a double-sided TFM, the variation with intermediate poles and the claw-pole machine. They also compared different rotor constructions. They concluded that a single-sided TFM has high rotor leakage fields but nevertheless, it has a specific output about 50% greater than that of a conventional machine. They also found that although the intermediate poles reduce the rotor leakage flux, the armature leakage becomes higher. The double-sided TFM produced an extremely high specific output and a high power factor but it was considered too complicated to build and assemble because of the need to place the rotor within the stator assembly (the stator core investigated is similar to the C-core). Finally (Maddison, Mecrow et al. 1998) suggested an improved design that is a claw-pole machine. It will be described further in the next section.

Another special kind of TFM is suggested by (Dubois, Polinder et al. 2002). They modify the TFM in several steps in order to obtain a machine geometry that allows easy production and low mass of active material. One modification is the toothed rotor structure (laminated) that enables an easier magnet assembly. This construction is further optimized for lowest cost/torque and tested in (Dubois, Polinder et al. 2002). In comparison with a conventional PM synchronous machine, the cost/torque is found lower for the TFMs with a diameter of 0,5m and 1m but higher for a diameter of 2m (Dubois and Polinder 2004).

In (Henneberger and Bork 1998) the outer rotor is found favourable, as it is easier to wind the copper in an inner stator and also this construction yields less motor volume. However, the rotor needs more support. In (Jack, Mecrow et al. 1999) they found the outer rotor concept to be thermally disadvantageous because the heat generated in the stator has poor thermal paths to dissipation.

Another special version of the TFM is the transverse flux reluctance motor (TFRM) presented by (Kruse, Pfaff et al. 1998). They use no permanent magnets in the rotor, only salient poles as in a switched reluctance motor. However, as it is still a transverse flux machine, increasing the pole number can increase the torque. This machine was aimed for direct servo drive applications. Compared to the TFM, the TFRM does not use any expensive permanent magnets but the salient poles cause high torque ripple and the torque has to be smoothed by phase shifting of the rotor poles and by appropriate converter control. The same concept is investigated by (Jeong 2001), but they also try with adding permanent magnets in the stator to shield the leakage flux. They found the motor design with shields better than a TFM with permanent magnets in the rotor. This is because the control is simpler. Also in (Hasubek and Nowicki 2000), they model a motor which is built with a passive rotor. In fact, they propose a special kind of passive rotor design with two rotor parts surrounding the stator, which is built with the core, the winding and permanent magnets. They mean that by having the permanent magnets in the stator and not in the rotor, the cooling is simpler. For the high torque density motor with surface mounted permanent magnets on the rotor, heat may be a problem as this can demagnetise the magnets. However, they found that passive rotor design often require more magnet material than active rotor transverse flux machines.

As a higher pole number gives a higher torque, the TFM is usually used in lower speed applications. It can thus be a solution for direct drive applications as traction motors in trains (Kang, Chun et al. 2003), or for generation of electricity by wind-energy or for the electric propulsion of naval ships.

2.2.2 Operation of TFMs

The current carrying coil produces one flux component in the radial-axial plane, and the magnets in the rotor give radial flux in the air gap. The total flux passes through the stator pole pieces, through the air gap into the rotor pole pieces, and then returns to the rotor, as is illustrated in Figs 2.1 and 2.5. The path is therefore in the radial-axial plane (transverse to the direction of motion). For the C-core TFM, there is also some part of the total flux that pass through all the stator poles (Rang, Gu et al. 2002). Of course, there is also leakage flux and fringing flux.

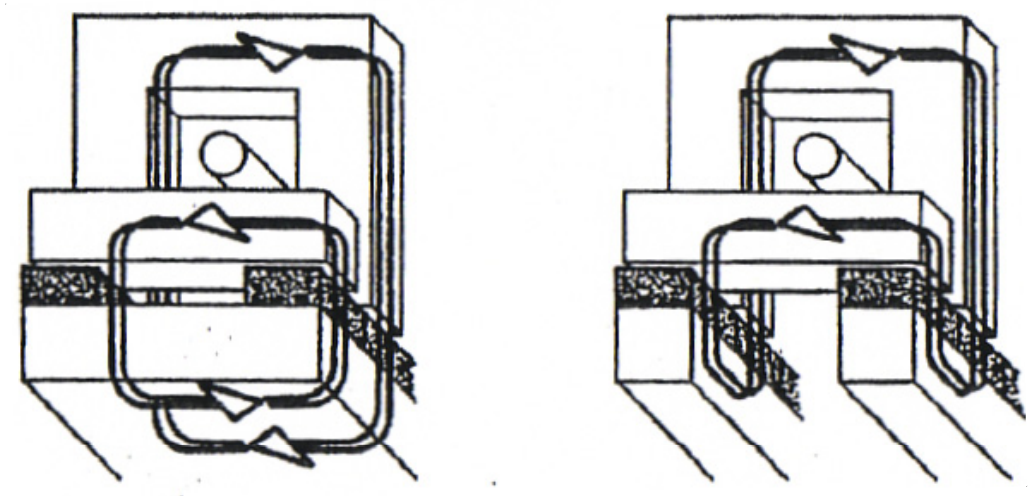

solid rotor separated rotor parts

Figure 2.5: Flux paths in transverse flux motors; single sided version with surface mounted magnets in the rotor but different rotor constructions. Picture from (Henneberger and Bork 1998).

Torque results by the interaction of the rotor flux in the radial direction and the stator mmf in the axial direction, producing motion in the circumferential direction (Jack, Mecrow et al. 1997). Also, operation of TFM can be explained by a close study of the total flux lines and the fact that the lines of flux try to shorten themselves, as is done in (Payne, Husband et al. 2002). In (Harris and Mecrow 1993), the surface mounted magnets are represented as an array of equivalent currents placed in the flux density field produced by the slotted structure. The radial flux density and the axial equivalent currents thereby develop a force in the circumferential direction. This is also illustrated in (Anpalaham 2001).

2.2.3 Assessment of TFMs

The main and obvious advantage of the TFM is its ability to yield high torque density values. Another advantage is that the phases are electromechanically decoupled as the phases are separated (even though there could be rather high leakage between phases in some cases). Also, the position of the rotor or stator parts can be varied in the circumferential direction to decrease cogging torque, as is explained below. Another advantage is that there is no need for end windings (unless the motor is linear).

The disadvantages of all these type of machines are a low power factor (because of large armature leakage fields), a complex construction, and three-dimensional fields, which make lamination difficult (Maddison, Mecrow et al. 1998).

Reported power factor values are as low as 0.3 (Arshad, Backstrom et al. 2002). Thorough investigation on the effect of the power factor is done in (Harris, Pajooman et al. 1997) for different physical features. They compare conventional machines and variable reluctance permanent magnet (VRPM) machines (that are the same as transverse flux machines) and discuss the reasons for the difference in power factor. They found that very limited improvement is possible for the VRPM machine, and that low working power factor seems to be the price that must be paid for the high specific output. The lowest power factor (about 0.35) is found in machines with surface mounted permanent magnets, whereas the machines with flux concentration has a power factor of about 0.55. This is because the flux concentrated rotor has a superior magnetic circuit. The investigated machines have a specific output of about 5-10 times that of a standard industrial induction motor. (They found that the flux component excited by stator current is much greater than that excited by the rotor magnets. Thus, with both sources of excitation present, the problem of saturation in the magnetic circuit is dominated by stator excited flux, rather than rotor-magnet flux. This feature, they write, is a characteristic of VRPM machines, and is the reverse of what is usually found in classical synchronous machines.) In order to find means of improving the power factor, they used the inverter to control the angle between the phase current and the back emf. By lowering this angle, the power factor should be higher for the same current (set by a thermal limit). The price to pay would be a lower running torque. They found, however that there were no major improvement by doing this. At least not for machines with already low power factors. If the power factor is about 0.7 though, this is a possibility to improve the power factor. If a large loss of output torque is acceptable, they suggest another way of improving the power factor; by leaving the phase of current unchanged and simply lower the rated current and torque (and also reduce the ohmic loss). By doing this, the flux ratio is changed (the stator flux will be lowered compared to the rotor flux) and the power factor will improve.

As in other types of machines with salient structures, there will be reluctance torque (because the self-inductance of the stator winding changes with position, and thus the magnetic field produced by the phase currents is a function of position) and cogging torque (because the field from the permanent magnets seeks a minimum reluctance path), apart from the useful alignment torque (produced by the mutual coupling between the rotor- and the stator winding magnetic field). Cogging torque may be a major drawback and can neither be reduced by fractional pitch winding nor skewing (skewing is inefficient as the stator tooth span is approximately equal to a pole span according to (Arshad, Backstrom et al. 2002)). However, the stators of different phases can be shifted to reduce reluctance torque, as is done in (Deliege, Vande Sande et al. 2002) where a linear two-phase transverse flux actuator intended for operation in a computer device is modelled. The configuration investigated utilised buried magnets and C-shaped stator cores. Also in (Kastinger and Schumacher 2002) phase shifting was used to suppress the cogging torque and other harmonics of second order in a two-phase TFM. They also investigated the possibility of shifting some stator elements relative to other stator elements within a pole pitch. They show that an optimization with respect to the amplitude of the fundamental and harmonic waves can be realized by such a shift. This is also done in (Kruse, Pfaff et al. 1999) where it is concluded that the pole shifting yields a smoother torque but at the expense of the average total torque (which was decreased by about 15%).

According to (Kastinger 2003), the transverse flux machine is generally considered to be complicated to manufacture and thus too expensive. This would prevent most companies from using this type of motor.

2.3 The claw-pole machine

2.3.1 Types and construction

Claw-pole alternators have for many years (since 1960s) been used as automobile generators, supplying power to electronic components in the car. Construction of such a machine is illustrated in Fig. 2.6. They offer high pole number excitation with a simple field coil and pole systems. According to (Guo, Zhu et al. 2003), claw-pole alternators are capable of producing power densities up to three times greater than the conventional machines. The field system (in the rotor) is formed from a coil arranged to act along the axis of the machine. The flux produced by this coil is then carried into the air gap of the machine by metal claws arranged to interlock with similar claws from the other pole of the coil (Jack, Mecrow et al. 1997). Thus the rotor consists of metal claws and a field coil (so there must be slip-rings), whereas the stator is laminated and consists of poly-phase windings like in a conventional machine. The claws in the rotor carry a dc magnetic field, thus there are no eddy currents due to the rotor field and the material of the claws (in car alternators) are made of solid steel. There will however be some eddy currents in the rotor parts close to the stator due to the stator field. In (Kuppers and Henneberger 1998) the eddy currents in the rotor were found to be twice as high as the eddy currents in the stator. The same authors investigated different rotor designs, by varying the shape of the claws and the pole-pitch, and the introduction of additional magnets in the rotor. They found that adding magnets to enforce the magnetic field was not a good option. However, using the extra magnets to cancel out leakage fields was more effective. They also found that

the leakage between claws was 30-50% of the main flux. According to (Guo, Zhu et al. 2003), the excessive eddy currents limit the claw-pole designs to small sizes and/or low speeds and results in low efficiency.

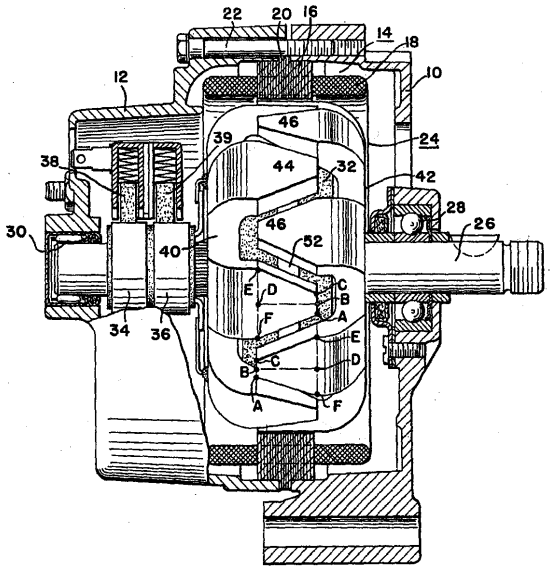

Figure 2.6: A claw-pole alternator. Picture from (Collins 1966).

Lately, new designs of *stators* in small high performance AC machines have been tried using the claw-pole structure. The stator consists of the core with claws and the coil, as seen in Fig. 2.7, where a one-phase module is shown. The design of the stator winding is mostly of a single-phase ring type. However, some designs deal with poly-phase stator windings and a claw-pole structure, as in (Cros and Viarouge 2004). A possible core material is Soft Magnetic Composites (SMC) having very low conductivity and isotropic magnetic properties in 3-D (Höganäs). Thus, the SMC can both lead the flux in three dimensions and restrict the iron losses. Laminated steel, as used in conventional stators, is out of the question, as it cannot cater for the three-dimensional flux path.

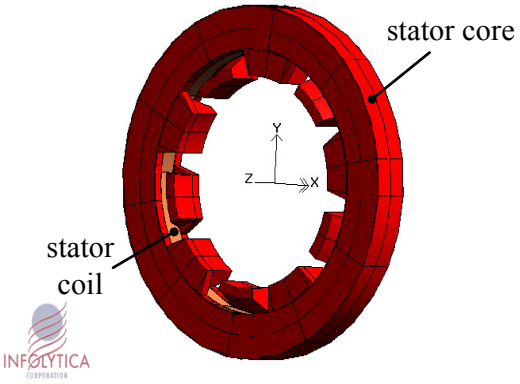

Figure 2.7: A claw-pole stator

There are, however, several solutions using steel sheets to stamp out the claw-shaped stator core, like in stepping motors (Ishikawa, Takakusagi et al. 2000) where the iron loss is not a problem. Though there are some examples where this type of claws is used in motors with higher speeds, like in the work of (Felicetti and Ramesohl 2003). They built a small claw-pole motor for a water pump application with a simple claw-

pole stator and a bonded-ferrite rotor. There is also the work of (Suzuki, Fujitani et al. 1998) who in different ways modified the solid thin steel claws as to decrease the iron losses in the claws and thereby allow the motor to run at higher frequencies, see Fig. 2.8. This of course reduces the possible output torque.

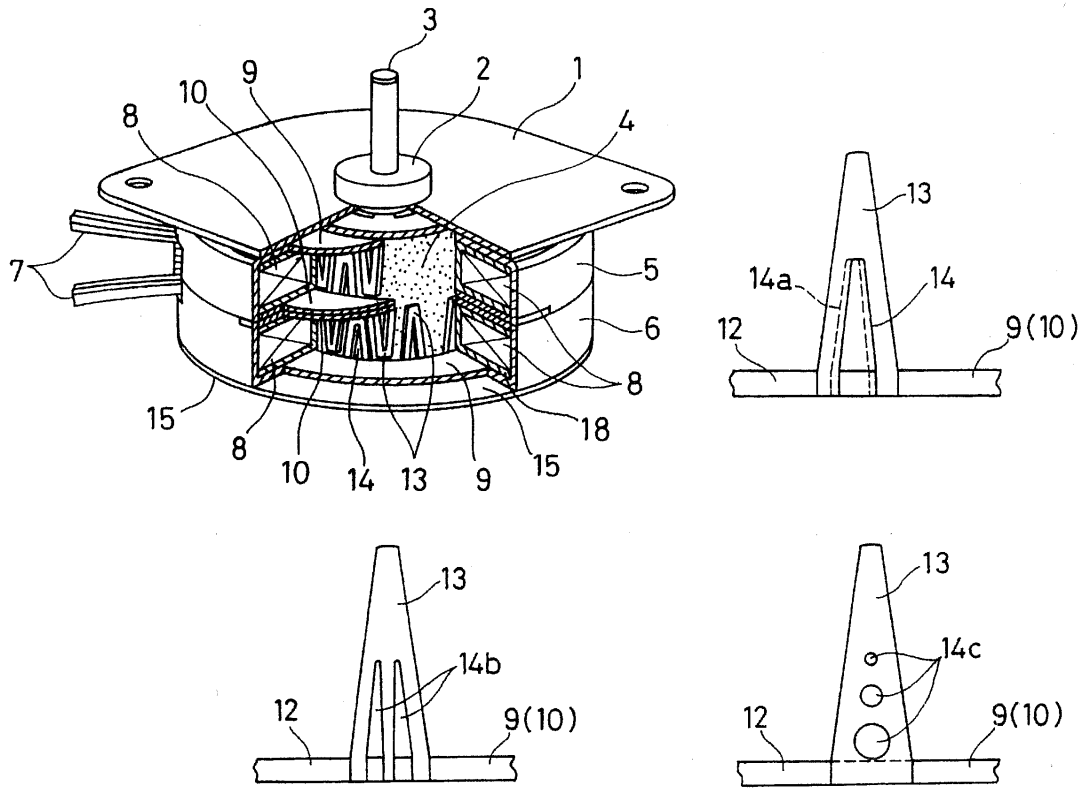

Figure 2.8: A claw-pole motor with modified stator claws (top left) and differently shapes claws. Picture from (Suzuki, Fujitani et al. 1998).

Just as with the transverse flux machine, the full winding mmf of the stator appears across every pole, and a major problem is the high armature leakage flux. The torque capability of the machine is also increased when the number of poles is increased. The optimum pole number is generally high. According to (Jack, Mecrow et al. 1997), the upper limit of the number of poles is set by the leakage flux (a high number of poles leads to a smaller distance between the poles and hence higher leakage flux), by the switching speed of the inverter, and by the iron and stray losses.

The rotor can be magnetised with permanent magnets, as in (Maddison, Mecrow et al. 1998), or consist of an armature winding as in the universal motor of (Cros, Viarouge et al. 2001). The magnets can be bonded to the surface or buried in the rotor core, giving flux concentration. In (Ishikawa, Matsuda et al. 1998) it is shown that polar orientation of the magnets in the rotor give more torque than magnets with radial orientation, for the stepping motor. So, the comparison of flux concentration and surface mounted magnets give the same conclusions as for transverse flux machines. This is also the case regarding the leakage between phases (which is much smaller with surface mounted magnets than with flux concentration). A pole-pitch of a simple claw-pole machine, presented in (Guo, Zhu et al. 2002), is shown in Fig. 2.9. The model has an outer rotor with surface mounted permanent magnets and an inner stator with a claw-pole structure.

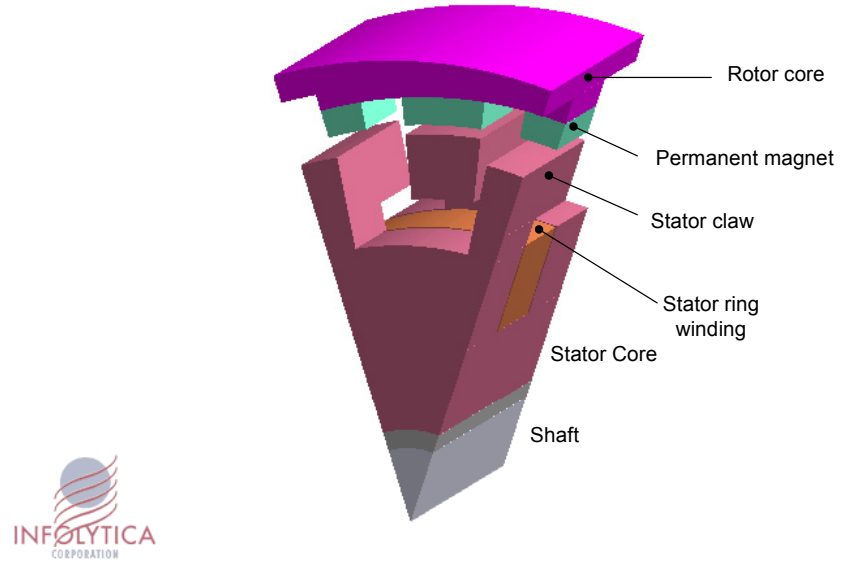

Figure 2.9: A pole-pitch pair of a claw-pole machine with an outer rotor

The different designs mainly have a common goal to maximize the torque density and to minimize the leakage flux, but also to minimize the cogging torque, and to yield an easy to produce topology. Different shapes of the claws can be adapted to adjust the harmonic content of the no-load electromotive force and to control the amplitude of the cogging torque. The most common shapes are triangular, rectangular or trapezoidal. The claws can also be skewed to reduce the cogging torque by using the same skewing method used in conventional machines, as explained in (Cros and Viarouge 2004).

The cogging torque and its harmonics were calculated in (Guo, Zhu et al. 2002). They found that the fundamental component and most of the harmonics could be cancelled out by the effect of shifting the three stator stacks. For single stack motors, the claw-pole shape should be optimized to minimize the cogging torque, usually by using an irregular shape with tapered width and height along the pole. More investigation on cogging-torque reduction is performed in (Njeh, Masmoudi et al. 2003). They compared different combinations of the 120 degrees electrical angle shift between the three axially arranged phases of a claw-pole machine, and found that the topology where the 120 degrees electrical angle shift is applied to the stator magnetic circuits is the most beneficial. In contrast to the paper of (Arshad, Backstrom et al. 2002) concerning transverse flux machines, it is described in (Njeh, Masmoudi et al. 2003) that it can be a good idea to skew the rotor of a claw-pole machine. A slot pitch skew yields a reduction of about 25% of the cogging torque without reducing the electromagnetic torque.

In (Maddison, Mecrow et al. 1998), they have investigated different claw-pole structures (as well as transverse flux machines structures) and developed a design with axially shortened claws (100 poles). This design feature limits the armature inter polar leakage flux. However, the magnets in the rotor must be buried (giving flux concentration). They also investigated the effect of increasing the radial rotor depth, and found a breakpoint up to which it is most efficient to increase the radial rotor depth.

For an easy assembly of the stator, the core is often divided into, at least, two parts. The three-part assembly for a two-phase motor is described in the patent of (Ichimura 1994) for small stepping motors. In (Maddison, Mecrow et al. 1998) they have built one stator phase core of four different parts using SMC material (not counting the winding and the support); two core back sections and two rings with the claws. A special way of assembly is described in (Masahiro, Noboyuki et al. 2005) where a three phase claw-pole motor stator can be made with two slot openings and three stator core parts. Thus the length of the stator can be smaller than in a common three-phase claw-pole-stator, which has three slot openings and a minimum of four stator core parts.

A special kind of claw-pole machine is studied and compared to a conventional permanent magnet machine in (Martinez-Munoz and Alakula 2003). The claw-pole rotor has neither permanent magnets nor a field winding. The stator, however, has a three-phase winding and additional field coils, placed in magnetically conducting end plates, attached to the stator. Thus, the rotor is electrically magnetized, eliminating the need for slip rings. Although the permanent magnet machine gave more torque and less leakage, the authors imply that the claw-pole machine could be advantageous in field weakening operations. In (Reinap and Alakula 2003), a similar approach is adopted. They investigate a three-phase claw-to-claw-pole machine, also with no source of magnetic energy in the rotor, and also for the possibility to use field weakening. However, they also use the claw-pole structure for the stator design. The stator then consists of three parts (each consisting of a core and an armature- and an excitation winding) adjacent to each other in the axial direction (but shifted 120 electrical degrees). Also for this design, the torque density was found rather poor, due to excessive leakage flux.

2.3.2 Operation of claw-pole machines

In literature, there are a few descriptions of how the claw-pole motor works. One description is found in (Jack, Mecrow et al. 1997), stating that the rotor permanent magnets give radial flux in the air gap (from the rotor to the claws), which reacts with the armature mmf, effectively carried into an axial sense by the claw-pole structure thereby producing circumferential motion. In (Maddison, Mecrow et al. 1998), the path of the flux produced by the rotor magnets with flux concentration is described as circumferentially through a magnet, into a soft iron rotor piece, axially down the rotor pole, radially across the air gap and into a stator tooth, then round the core back and into the tooth on the other side of the stator, then back across the air gap and into the adjoining rotor pole on the other side of the magnet. A detailed description of the flux paths and behaviour is also found in (Reinap 2005) and in (Martinez-Munos 2005).

In the next chapter, a full description of the operation of the claw-pole motor topology considered in the present work is provided.

2.3.3 Assessment of claw-pole machines

Just as in transverse flux machines, claw-pole *armature* machines have high specific torque outputs, and can use simple and easily manufactured coils. However, they suffer from high per unit reactance (resulting in a low power factor) and high leakage flux (because there are poles of opposite polarity in close proximity) and high core loss at higher frequencies. If the SMC is used, a high frequency in the armature is not such a big drawback, since the eddy currents are reduced by the low conductivity of

the SMC. Compared to transverse flux machines, the claw-pole machine would be mechanically stronger at the expense of the reduced specific torque output (Jack, Mecrow et al. 1997). Another comparison of claw-pole machines and transverse flux machines is done in (Guo, Zhu et al. 2002). Both motors considered in the comparative study utilised outer rotors with permanent magnets. The study showed that the transverse flux machine uses twice as many permanent magnets and copper material and produces more than twice the electromagnetic power at a given rotor speed.

The high leakage flux has an adverse effect on the performance of claw-pole machines. However, considering their low production cost, they are attracting interest in some applications with a power range below 3kW (Cros, Viarouge et al. 2001). According to (Maddison, Mecrow et al. 1998), their design with the shorter claws (of about 0.5 kW), compares favourably with the double-sided TFM as it gives higher output and a simpler construction. The same experience is reported in (Njeh, Masmoudi et al. 2003), where they state that the optimal length of the claws is 30% of the axial stack length per phase.

A comparison between a claw-pole machine and a conventional laminated surface magnet servo motor, concerning cost per kW, is performed in (Hultman and Jack 2003). They found that the servomotor comes out 38% better than the claw-pole machine. They thus conclude that the claw-pole machine is at present state of development better suited to lower speed applications. A similar conclusion is made in (Mecrow, Jack et al. 2002) where they compare designs for power hand tool applications, which typically require a high output torque at modest speed. Two new designs are compared: one uses conventional laminated construction for a radial field machine, the other uses powdered iron for a claw-pole armature machine. The claw-pole machine was found to produce 40% more torque than the laminated machine but it has a less short-term overload capability.

2.4 Soft Magnetic Composites (SMC)

Soft Magnetic Composites (SMC) are metal powders developed by Höganäs AB, Sweden. They are also called Ferromagnetic Composite Powders and offered by Quebec Metal Powders Limited, Canada.

The SMC has an isotropic relative permeability of about 500 (thus much lower than electrical steel) and low conductivity (low enough to restrict eddy currents), as the grains of the material are individually insulated. An approximate value of the resistivity is 150 $\mu\Omega$m, which can be compared with 0,16 $\mu\Omega$m for electrical steel. Due to their magnetic isotropy, SMC makes it possible to construct electrical machines with 3-dimensional magnetic field paths, achieving increased design flexibility and thereby increased specific output.

The material's advantages include efficient, environmentally friendly manufacturing, with minimal material waste, through the powder metallurgical (PM) method. According to the producers, it is up to 50% more cost-effective than conventional production. Also there is an advantage of an easy recycling of copper (Hultman and Jack 2003). However, there are some disadvantages of the SMC material: The

unsaturated magnetic permeability is low; the hysteresis loss is high; the mechanical strength is low (the SMC is brittle). The brittleness of the material may be a problem when SMC is used in claw-pole machines, as the radial forces acting on the claws may break the claws. According to (Kuppers and Henneberger 1998), the radial forces for their claw-pole alternator was five to ten times the tangential forces.

The bulk thermal conductivity is similar to lamination steel, and is isotropic, unlike lamination steel, which have a higher thermal conductivity in the plane of the laminations than normal to the plane (Jack, Mecrow et al. 1997).

2.4.1 Manufacturing

First the iron powder of high purity and compressibility (sponge and water atomized) is electrically insulated with a thin inorganic surface coating (an alloy) and then the powder is mixed with a lubricant and sometimes with a binder. The binder is added to keep the material together which is not so good if one wants a high density. The lubricant is added to facilitate the pressing and the ejecting of the piece from the pressing tool, and it is later heated off. The size of the particles are typically 5-200 μm, to be compared with the thickness of steel sheets which is normally 200-1000 μm (Hultman and Ye 2002). By powder metallurgy techniques, the mixed material is poured into a die and then compacted with the tool at a high pressure, the higher the better for the density but also more expensive. Some shapes are not possible to create because of the difficulty in making the proper tools. After the compaction, the produced piece is ejected. This can also cause a problem. If the ejection is not done properly, the piece can get cracks. Thereafter, the material is heat-treated at about 150-500 °C (the higher value if no binder is used). This will reduce the lubricant and partly relieve the stresses that arise during the compaction. The material is not sintered nor annealed, as higher temperatures would destroy the insulation. The powder metallurgy process for sintered metal powder components is the same as for SMC but the temperature is higher (about 1200 degrees). The powder metallurgy gives then sintered products with higher strength (and not insulated particles). (However, the same tools for compaction can be used.) A general rule of thumb concerning the choice of lubricant/binder and choice of temperature is given in (Hultman and Jack 2003); Less additive and higher heat treatment will improve the magnetic properties but also result in lower strength. An example of a lubricant is Kenolube, which is used in the SMC material Somaloy^{TM}. There are two types of Somaloy^{TM}: Somaloy^{TM}550 has higher permeability than Somaloy^{TM}500 due to a larger particle size. Much higher relative permeability than 550 is not possible because when the particle size is increased, the strength of the produced component is decreased. Prototypes can be constructed by cold machining but the injection moulding technique should be used for commercial production which would simplify the manufacturing process and hence the cost.

2.4.2 Losses and magnetic and electric properties:

The losses in soft magnetic materials consist of eddy current and hysteresis loss. The losses are due to a time varying magnetic field affecting the material and the result is heat. A common approximation is that eddy current loss increase with f^2, while the hysteresis loss increase with f (the frequency). In SMC, the eddy currents can be kept low but the hysteresis loss is rather high. So, if laminated steel and SMC are compared, laminated steel would be better for low frequencies and SMC better for

high frequencies, where the impact of low eddy currents show off. According to (Narasimhan 2003), the frequency threshold is at about 1 kHz. However, in applications with three-dimensional flux-paths, use of a laminated material is not an option and the comparison between SMC and laminated steel is of little practical value. The main goal would then be to find the SMC material best suited for the given application. For completion, the results of such comparisons will still be reported in this review. The losses are normally measured and given for alternating fields but rotational flux may increase the iron losses in motors and transformer cores (thus in laminated steel) with 50% (Moses and Leicht 2004). Rotational losses exist due to the variation of the direction of the magnetic flux in the lamination planes (Hamdi 1994). The rotational core losses in SMC was calculated and measured by (Guo, Zhu et al. 2002). The iron losses depend also on the amplitude and order of harmonics. The harmonic content of the magnetic flux and the resulting losses may in fact be an increasingly important factor due to an increasing use of pulse width modulated (PWM) voltage sources, and to the growing numbers of inductive loads, both increasing the harmonic content of the magnetic flux in the machines (Moses and Leicht 2004).

The *eddy current losses* in SMC depend not only on the size and shape of the iron particles but also on the geometry of the SMC piece (Nord and Pennander 2004). This is because the insulation between the particles is not perfect. Thus, if a test value is given for certain geometry, another loss value might be found after machining or for another geometry. This is further explained in (Lefebvre and Gélinas 2001) and in (Skarrie 2001). In (Guo, Zhu et al. 2003) they say that the ratio of the material dimensions to skin depth is a critical parameter. If the skin depth is smaller than the material dimensions, the magnetic field will be distorted, and the skin effect must be included in the analysis. In (Jack, Mecrow et al. 1999), it is investigated whether the SMC material shows additional iron losses due to manufacturing (punching procedures, mechanical stress etc). It was found that the difference in iron losses before and after manufacturing was not so significant as was found in a laminated core. They also found that the iron loss in a SMC machine was about twice that of a similar laminated machine, but when expressed as a percentage of output power the figures of the iron loss become much closer.

The *hysteresis loss* is a result of the domain structure of the material being changed when an external magnetic field is applied to the material. If the material suffers from strain and poor domain structure, the hysteresis loss will be higher. As the SMC material cannot be annealed (which would relieve the material from stress), unlike electrical steels, the hysteresis losses are rather high. It is further explained in (Jack, Mecrow et al. 1999): “The forming process requires very high pressure to obtain high densities (and thereby high permeability and saturation) and this, coupled with the lack of grain control, (inherent in the powder forming process) leads to high hysteresis loss.” As with the measurement of eddy currents, the measurements of hysteresis loss can be unpredictable. For the same material, there are different hysteresis loops for different frequencies, and different measurement methods and geometries can give different results.

Because of the factors discussed above, the *iron losses* given in the data sheets and the measured values of an application may not be the same. Also, the loss values of different research groups may also not be the same, as seen in (Chen and Pillay 2002).

The calculations of the iron losses when using finite element software is addressed by (Nord and Pennander 2004), where a formula like the one used for laminations is given for the SMC material in order to calculate the hysteresis losses. The eddy current losses should then be calculated with a time dependent solver, using the conductivity of the material. However, to obtain a good agreement between calculations and measurements for simple ring samples, the conductivity values had to be modified.

Some examples of loss values and other data for the SMC materials, and lamination steel are given in Table 2.1. The figures concerning the SMC come from the manufacturer's data sheet, and from (Hamdi 1994) concerning the lamination (except the value of the iron loss in the lamination at 1000 Hz, which is found in (Chen and Pillay 2002)).

	Somaloy^{TM}500	Somaloy^{TM}550	ATOMET-EM1	Standard motor lamination
Initial relative DC permeability	500	550	290	8000
Saturation flux density	1.7 T at 30 kA/m and 1.4 T at 10 kA/m	1.7 T at 30 kA/m and 1.5 T at 10 kA/m	1.5 T at **20** kA/m and 1.3 T at 10 kA/m	2.0 T at 30 kA/m and 1.8 T at 10 kA/m
Iron losses at 1.0 T/60 Hz	8 W/kg	9.5 W/kg	11 W/kg	2 W/kg at 1.0 T/**50 Hz**
Iron losses at 1.0 T/400 Hz	65 W/kg	80 W/kg	77 W/kg	11.5 W/kg
Iron losses at 1.0 T/1000 Hz	150 W/kg	220 W/kg	218 W/kg	140 W/kg

Table 2.1: Magnetic properties and losses of SMC and laminations

In (Jack, Mecrow et al. 1997), it is found that the iron loss of SMC is competitive with laminations for frequencies above 100 Hz, giving about 20 W/kg at 1.5 T. However, for lower frequencies, SMC is only competitive with low quality lamination steel. They give as an example, losses of 5 W/kg at 1.5 T and 50 Hz for lamination steel, to be compared with twice that amount of loss for the SMC material. However, looking at Table 2.1, it seems more likely that (Narasimhan 2003) is more correct, saying that the frequency must be higher than 1000 Hz before the SMC material can be competitive with a good lamination.

The unsaturated *magnetic permeability* of SMC materials is much lower than that of unsaturated electrical steel (see Table 2.1). This is because of the space factor effects, as the material is micro porous. According to (Jack, Mecrow et al. 1997), the relative permeability is limited to a value less than 1/(1-effective space factor) and it is unlikely that powder materials can achieve any where near the maximum permeability of lamination steel. However, the saturated magnetic permeability is comparable to that of saturated electrical steel (Hultman and Jack 2003). The saturation flux density is near to the figure for laminated steel but slightly lower due to a less than unity space factor.

The SMC material is most appropriate for use in permanent magnet machines, for which the magnetic reluctance of the magnet dominates the magnetic circuit, making the performance of such motors less sensitive to the core permeability. The low permeability can be a problem for some machines, such as induction and reluctance motors because they are magnetized from the armature and the magnetization current is relatively large. It is far less a problem for permanent magnet machines, whose magnetic circuit is basically determined by the large effective air gaps presented by the magnets. (Guo, Zhu et al. 2002)

Some applications where SMC material is used are transverse flux machines and claw-pole machines (Hultman and Jack 2003), axial flux machines (Zhang, Profumo et al. 1997), and combined radial and axial permanent magnet motors (Jack, Mecrow et al. 1999). The universal motor (Jack, Mecrow et al. 2000) and dc machines are given as an option, as those kind of motors are driven in saturation, resulting in a low permeability for both SMC and laminations (Hultman and Jack 2003). In (Dubois, Polinder et al. 2002), a linear transverse flux machine is modelled with laminations in the stator, after comparison with SMC in the stator. The choice of laminations is possible due to the planar flux path in the TFM. Also in (Harris, Pajooman et al. 1996), it is concluded that the use of SMC in transverse flux machines is not advantageous. However, recently two new applications are reported in (Höganäs 2005); two mass-produced linear compressors, one for sewage aeration and the other for a cooling box. The reported advantages include low-cost, good efficiency, easy assembly, and eliminating the need for secondary machining.

3 Design of claw-pole motors

3.1 Introduction

The objective of the work presented in this chapter is to investigate different design parameters of the claw-pole machine, in order to identify design aspects that have most effect on torque density and power factor. This investigation would then enable tailoring of the design to meet a specific application requirement. In view of the number of design parameters that can be changed, rather than trying to incorporate all variables in a mathematical formulation and then seek its theoretical optimum, which would probably be unsolvable, a more practical approach is adopted. Design parameters are investigated one at a time, while reasonable conditions of the other parameters are assumed, and the sensitivity of the torque density and power factor values is determined. Such an approach does not only serve to provide a physical insight into the operation and design of claw-pole motors, it also have a *design office* value. Indeed, the practical value of this approach is demonstrated in the work presented in the next chapter, where it is presented a design for a given servomotor application that is based on the investigation described below.

The theoretical investigation presented in this chapter involves the use of 3-D finite element computation. The work makes use of a commercially available finite element suite of programmes (Infolytica 2004). While such a commercial finite element package, nowadays, facilitates modelling of complex devices such as claw-pole machines, the computations would still be sensitive to the chosen mesh, solution parameters and post-processing procedures. Therefore, accuracy of computation must be validated, ideally, against test results. This is achieved in the present work utilising a specially built experimental claw-pole machine (which is referred to below as Mark 0). Constructional details of this machine as well as description of the testing procedure are provided in this chapter.

While the importance of cogging torque is recognised, it is not treated in detail in the present work. This is because the operating speed of the intended application of the servomotor developed in the next chapter is about 3000 rpm. Thus the cogging torque will only be a fraction of the output torque at any reasonable operating point (Hamdi, Licariao-Nogueira et al. 1993). Still, the investigation identifies the design topologies that yield a relatively large cogging torque. Also, measures for reducing this torque component are discussed.

It is appreciated that the servomotor is a motor used for torque, speed or position control, and that the torque characteristics should be smooth and equal in both directions of rotor rotation. Because of this, the cogging torque should be considered. However, the difficulty of calculating and measuring the cogging torque in an exact way implies that this matter should be dealt with in any future work when the general design process is finished.

3.1.1 General description of the investigated claw-pole motor

The investigated claw-pole motor consists of a stator with a claw-construction surrounding a ring coil and a rotor with permanent magnets and a rotor core. The permanent magnets may be placed on the rotor surface, as in Fig. 3.1, or they may be

buried in the rotor core, giving flux concentration. As flux concentration (buried magnets) yields better torque density and power factor than surface mounted magnet topologies, and as one of the main design objectives considered here is to obtain a high power factor, the flux concentrated rotor is preferred (even though surface mounted magnets give more symmetric flux linkage and less leakage between stacks). Because of this, the rotor with surface mounted magnets is only considered at the beginning of the investigation, when it was compared with a flux concentrated rotor topology.

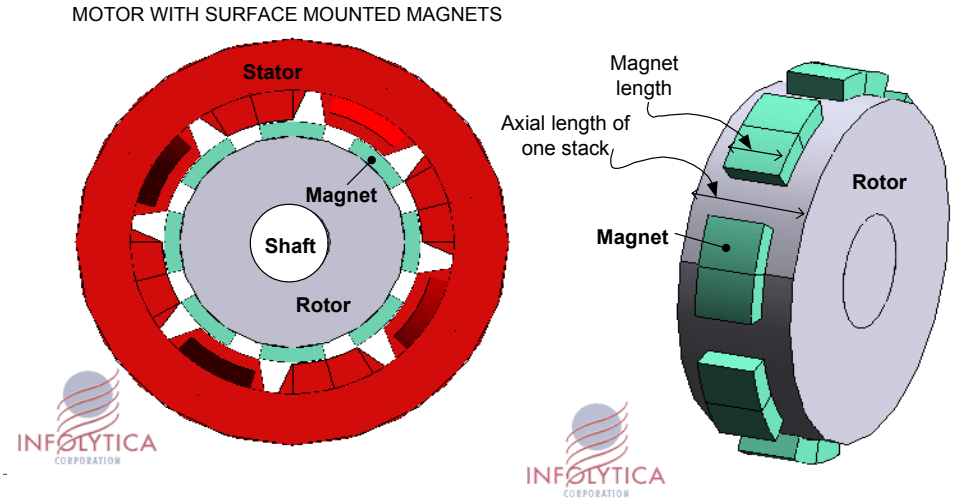

Figure 3.1: A motor with surface mounted magnets

There are several examples of rotor structures with flux concentration, as is described in Chapter 2. In the following investigations, the flux concentrated rotor is used with a permanent magnet shaped as a ring and magnetised in the axial direction, as shown in Fig. 3.2. Such a rotor construction is believed to be easy to produce. The core material may be solid steel or made of SMC. With solid steel as the core material, the eddy current losses will be very high for motors operating at high frequency stator currents. This type of steel rotor can only be used in low speed applications or for low-speed and static tests. A high-speed machine will require a SMC core.

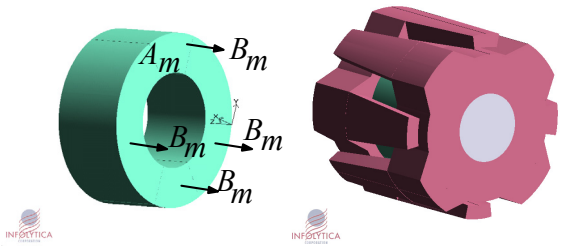

Figure 3.2: A ring-magnet, magnetized in the axial direction and a rotor core claw-structure

For a three-phase motor, there could be one, two or three ring-magnets and two to six core parts. The core parts should be simple and few to allow low cost manufacturing. However, for the three-phase motor with one ring magnet, the flux would be concentrated to the middle part of the rotor and, therefore, would link more with the middle stator stack than with the outer stator stacks. Also, the flux path will be the path of least reluctance, thus the main rotor flux will go through the stator phase that is aligned with the rotor. This is not optimal as it is around the unaligned positions

that the torque production is highest (as is explained in Section 3.2). To get a more even distribution of rotor flux in the stator stacks, it is better to use two or three ring magnets instead of one. These options also allow shorter rotor claws, which makes the manufacturing of the rotor claws made of SMC easier (bearing in mind that the SMC is brittle). Also, with three rotor-stacks and three stator-stacks, the design process with the finite element model could be simplified to two pole-pitches of one of the phases, as shown in Fig. 3.3.

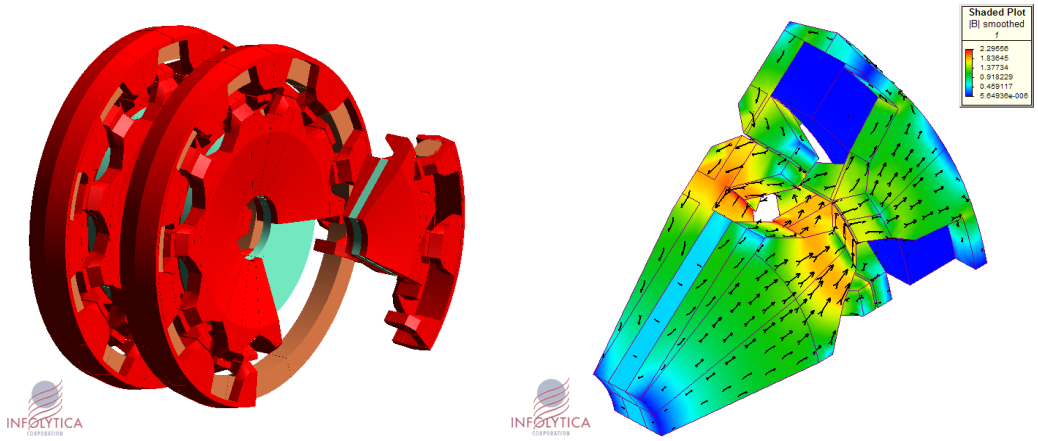

Figure 3.3: Claw-pole motor with three claw-pole stacks (left). Only parts of phase 2 and 3 are shown for clarity. The solution of the flux density in the two-pole-pitch model of one phase (right).

The stator must be large enough to contain the winding, and to keep the leakage and the saturation at a reasonable level. However, a short motor is preferable together with the axially magnetised magnet. There is more space for the winding if the stator claws are thin but the claws should not be too thin as the SMC material is brittle and because this will give saturation in the claws. The claws should not be too close to each other, as this will give leakage flux. The cross section of the coil can be circular with the advantage of avoiding corners in the stator core. As seen in Fig. 3.4, the core part closest to the top left corner of the squared coil cross section, carries a high flux density. This, and the associated saturation, can be avoided with the circular coil cross section. However, with a rectangular cross section, the cross section area can be larger (for the same motor length). The rectangular cross section area is selected for the preliminary investigations, simply because it is easier to model in the finite element program. The length of the motor is decided mainly by the rotor side core parts, for a given magnet radius. This is because the rotor core side parts will become saturated if they are made too thin.

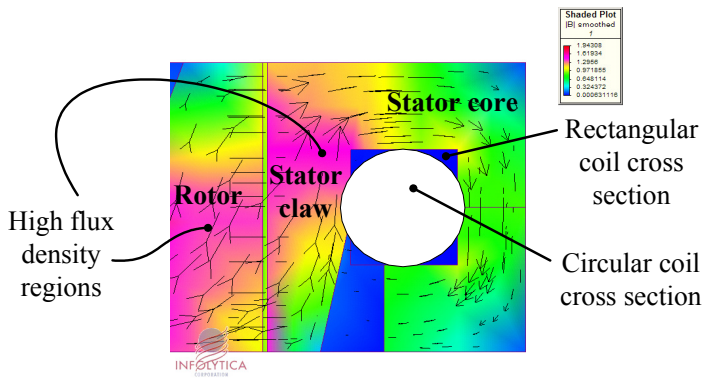

Figure 3.4: Different shapes of the coil-cross-section

The demagnetising effect of the armature field is not a problem if the magnet is a ring magnet inside the rotor as the rotor will rotate at synchronous speed and there will only be high eddy currents on the rotor surface depending on the rotor material. The shaft must definitely be non magnetic, otherwise all the flux from the magnet would go through the shaft. The shape of the claws must be designed with due consideration of the resulting flux linkage so that the back emf is symmetric.

As the core parts are to be made of SMC material, because of the three-dimensional nature of the flux path, the outer diameter of the stator was restricted to 115 mm, which is the diameter of an available pressed blank. The length of the motor can be more freely varied. However, the brittleness of the material restricts the core parts to a length-to-width ratio of less than 8:1 (MPIF 1999) or even less than 6:1 according to (Reinap 2005). Other decided fixed values during the design process in this chapter are the fill factor, which is set to 0.5, and a current density below 6 A/mm for a rated current of 2 A. Further, the air gap should not be below 0.3 mm, and the shaft diameter is set to 10 mm. The number of turns of the stator winding is also fixed to 100. Other parameters are varied during the design process, as is described below.

A picture of the used model is shown in Fig. 3.3, showing two pole-pitches of one phase of the motor. Positive (even) periodic boundary conditions are used on the slices in the radial-axial plane, and a gliding surface is defined in the air gap as shown in Fig. 3.5, allowing the modelling of the rotation of the rotor. The Neumann boundary condition is used on the other planes. The boundary condition constrains to zero the normal component of the magnetic flux density thus the flux is made to flow tangential to (along the side of) the boundary. In the design process, the used air box is made small in order to minimize the model size and thus the solution time. This restriction will neglect the fringing flux, and a larger air box is consequently used in the calculations of the predicted performance of the suggested model Mark 1 (in Chapter 4).

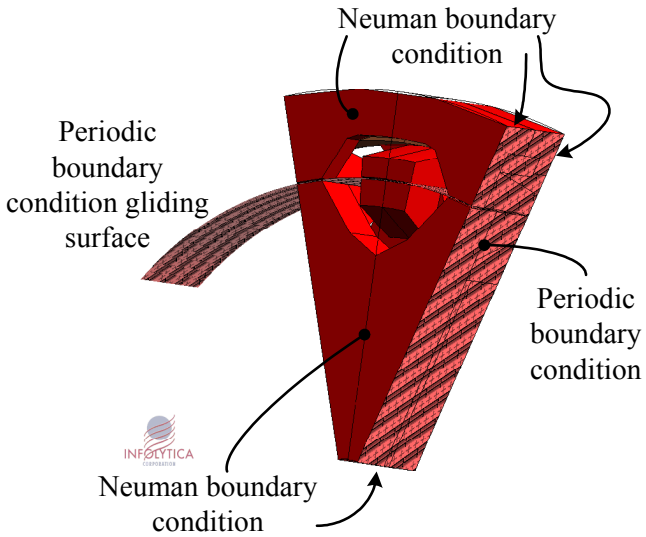

Fig. 3.5: Boundary conditions of the two pole-pitch model

A description of the parameters that are varied and investigated here is given in Figs. 3.6 and 3.7. The first figure (Fig. 3.6) describes a construction with rounded claws to the left and long claws to the right. The rounded claws allow the claws to be shorter

than the motor length and simplify using circular cross sections of the coil. It also adds barriers between phases for the claws. The extra barriers would lead to less leakage between phases, less core material, and better cooling.

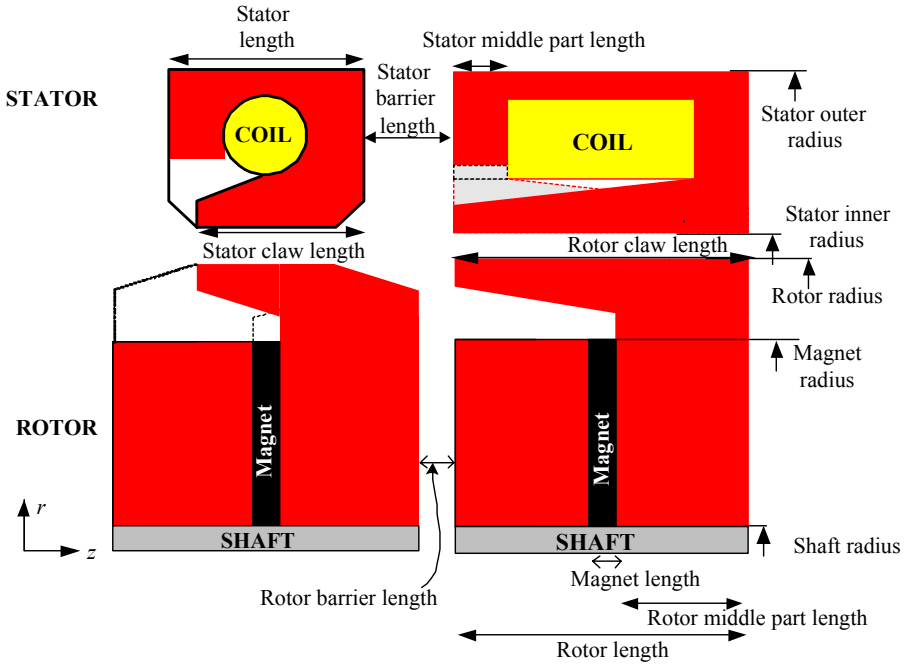

Figure 3.6: Drawing of two stacks of a motor with rounded claws to the left and long claws to the right. Two alternative stator cross-sections of the coils are also illustrated.

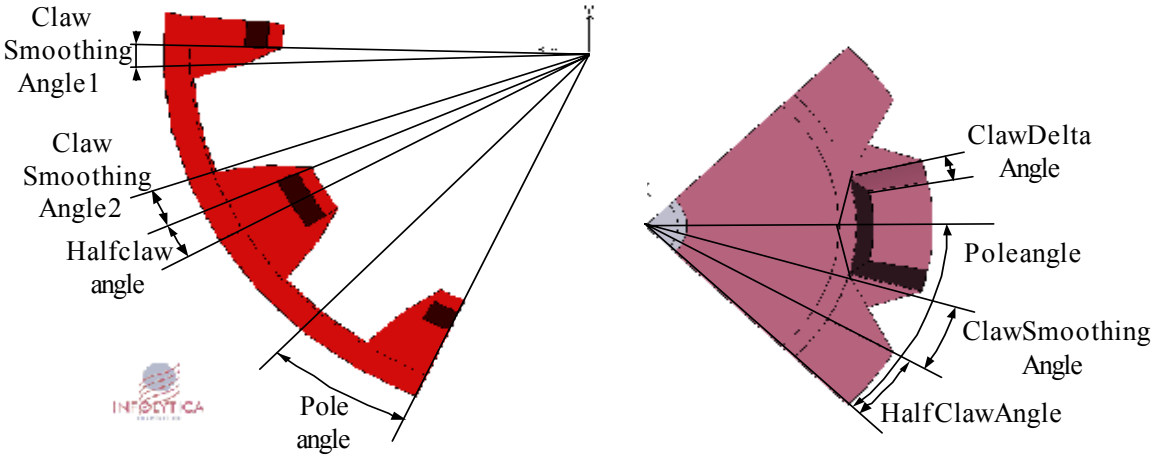

Figure 3.7: Drawing of part of a stator and part of a rotor

When the magnet is a ring magnet, axially magnetised, the remanence must be high. This is because the area of the magnet, A_m, cannot be so large compared to the air gap area, as the rotor is an inner rotor. To get a large A_m, the shaft should be made as thin as possible (but not less than 10 mm diameter as that would give a too week shaft). However, the major change in magnet area is achieved by changing the magnets outer diameter. If the magnet area is increased, the core parts need to be modified to be able to lead the increased flux without being saturated. Thus, for a given air gap flux, and a

given magnet length, the minimum claw size and the minimum length of the core parts enclosing the magnet are set. The magnet length and the core parts length will give the total rotor length, as seen in Figs. 3.6 and 3.7.

The finite element mesh adaption tolerance is set to 1.5% for the two pole-pitch model and 5% when the whole three-phase motor is modelled. This means that the finite element program's adaption process automatically identifies and refines the areas of the mesh most in need of refinement to improve the quality of the solution. During mesh adaption process, the finite element program compares the change in the stored energy between solver runs with the specified adaption convergence tolerance. If the change in the value of the stored energy is greater than the tolerance, the mesh is refined and another solution is run. The mesh refinement is based on the error in the magnetic field continuity across element edges. For 3-D solutions, the mesh can be refined through subdivision (h-type adaption) or by increasing their polynomial order (p-type adaption). For the two pole-pitch model, h-adaption is used with the polynomial order of two. The mesh in the air gap needed to be improved by setting the maximum length of the finite elements. The value of this element size varies with the used pole number, the more poles the smaller elements.

3.2 Operation of claw-pole machines

Common for transverse flux machines is that the rotor permanent magnets give radial flux in the air gap (from the rotor to the stator claws) and that the rotor flux does not cross the stator current. Thus torque production cannot be readily explained by the *Bil* principle. The movement can instead be explained as the rotor and stator fluxes trying to align; sometimes the rotor and stator flux components are in the same direction and sometimes in the opposite direction, but the mean produced torque is always unidirectional.

The pulsating flux produced by the stator winding passes through the stator core, alternating in the positive and in the negative axial direction. Consequently, the rotor flux should be lead through the stator core, alternating in the positive and in the negative axial direction also. The rotor flux may be delivered from different rotor constructions. The following description of the operation of the claw-pole motor is based on a rotor construction incorporating a ring-magnet magnetised in the axial direction and a rotor core with claws. With this construction, the rotor poles (claws) align with the stator claws of alternating sides as the rotor rotates. The main rotor flux paths are drawn in Figs. 3.8 and 3.9 for different rotor positions. The rotor magnet, axially magnetized, gives flux in the positive axial direction (towards the right). This particular design utilises only one rotor (with two core parts and one ring magnet) with the three-stator stacks (one stack for each phase). Only the middle of the three-stator stacks is shown. The magnet flux passes through a rotor claw and enters the air gap in the radial direction, goes into the closest stator claw, travels through the stator core, around the coil, to the neighbouring stator claw on the opposite side, and then returns to the magnet via the air gap and the closest rotor claw. It can be seen that when claws on the same side (at the same axial position) are aligned, the main rotor flux passes the stator-core in the negative axial direction (Fig. 3.8), and thus has the opposite axial direction compared to the magnet magnetization.

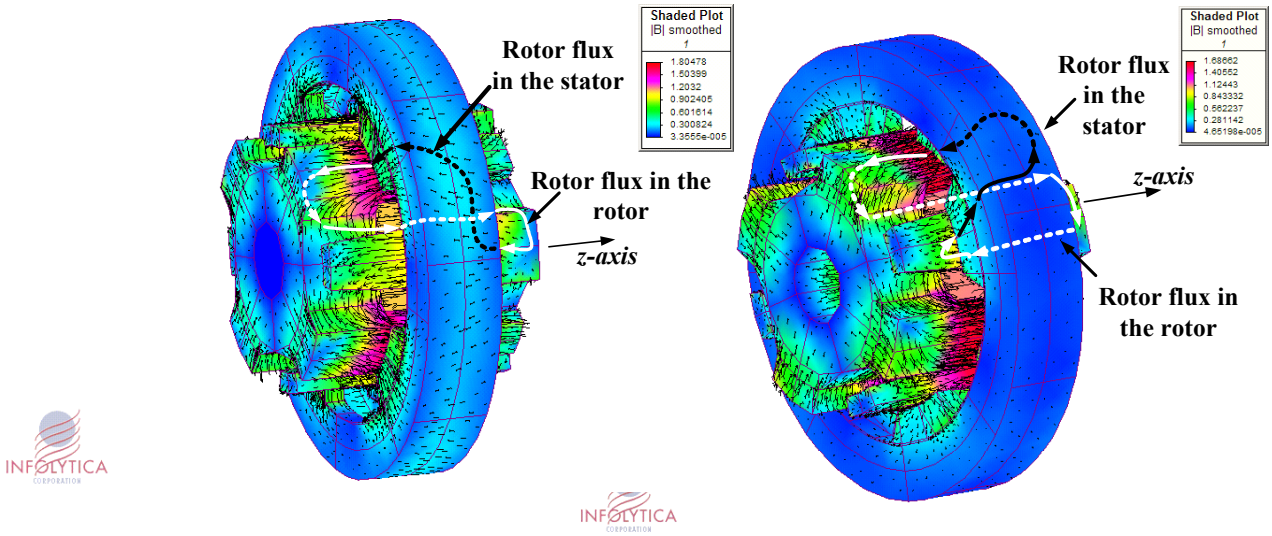

Figure 3.8 (left): The middle stator stack is aligned with the rotor. Stator and rotor claws on the same side are aligned.
Figure 3.9 (right): The middle stator stack is aligned with the rotor. Stator and rotor claws on the opposite sides are aligned.

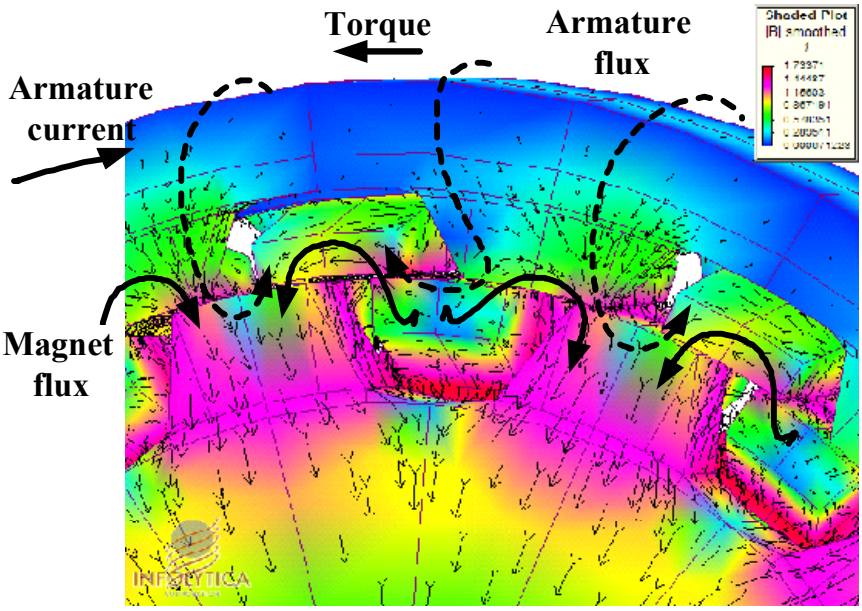

Figure 3.10: The rotor poles are unaligned with the stator claws.

On the other hand, when claws on the opposite sides (at different axial positions) are aligned, the main rotor flux passes the stator core back in the positive axial direction (Fig. 3.9), and thus has the same axial direction as the magnet magnetization. The stator current should then be controlled to react with this rotor flux. The highest torque is achieved if the current is in phase with the induced electromotive force at no load (displaced 90 electrical degrees from the magnet flux linking the stator winding). With this type of current control, the peak stator flux will occur when the rotor poles are out of alignment with respect to the stator claws. Then the stator flux will pass the air gap and react with the rotor flux in the rotor pole, returning to the stator via the air gap. The rotor magnet flux passes from one rotor claw, via the air gap and into the

closest stator claw and then the flux returns to the rotor without linking with the stator coil. This can be seen in Fig. 3.10. The flux induced by the rotor magnets, Φ_r, and the flux induced by the stator winding, Φ_s, cancel each other out in parts of the stator and rotor claws, and add up in other parts. The adding up gives torque in the direction of alignment, and the cancelling out gives torque in the direction away from alignment. Thus, in Fig. 3.10, the direction of rotation is anticlockwise (the opposite direction to the current at this instant). The torque is thus highest in (and around) the unaligned positions, and the flux linkage due to the magnet flux is zero at the unaligned position. This is seen in Fig. 3.11, where the normalised flux linkage, resulting emf, current, and torque as a function of the rotor position are illustrated for one phase. The torque will be negative at some rotor positions. This is due to the relatively large cogging torque in combination with the low current. The normalised cogging torque can be seen in Fig. 3.12. Observe that the current may also be a square shaped current. This would in fact give a slightly higher torque. However, in the testing of the experimental machine, as is described below, sinusoidal current control was used.

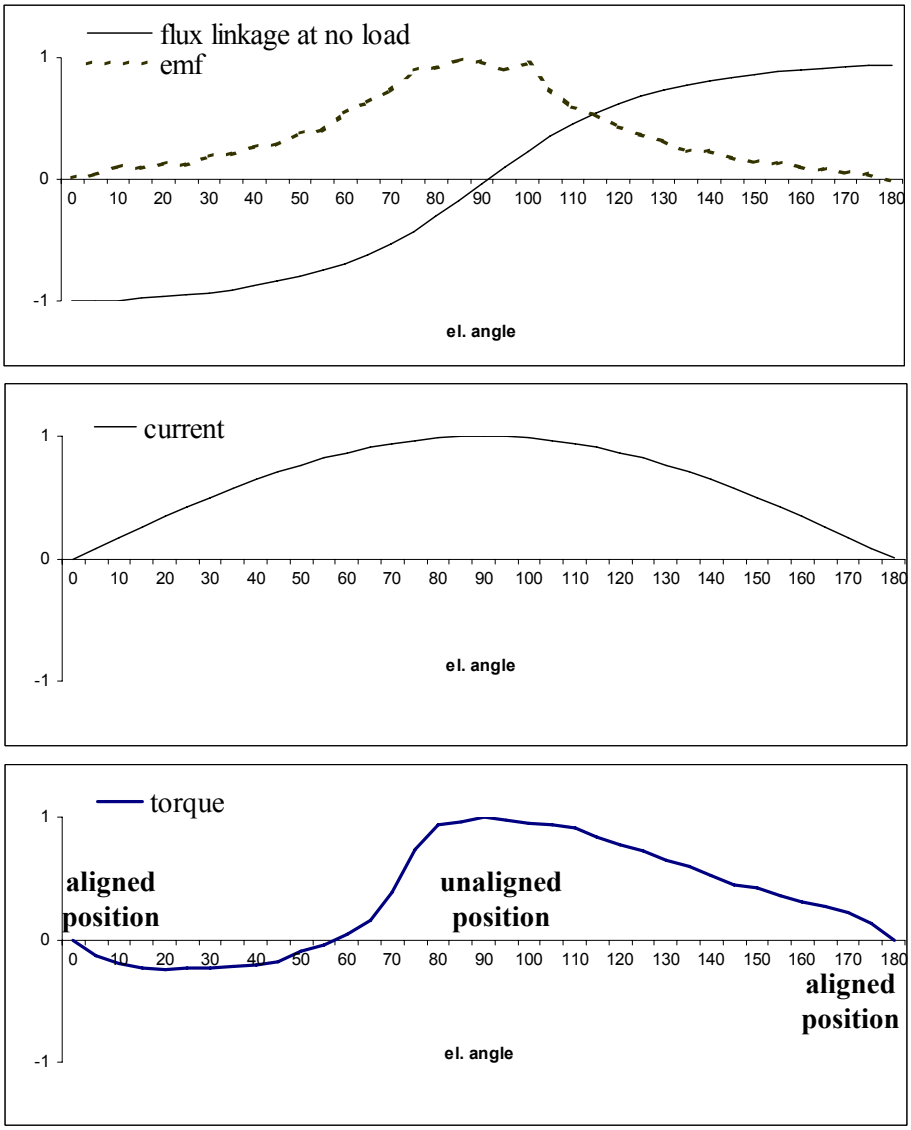

Figure 3.11: Normalised flux linkage, resulting emf, current and torque as a function of rotor position.

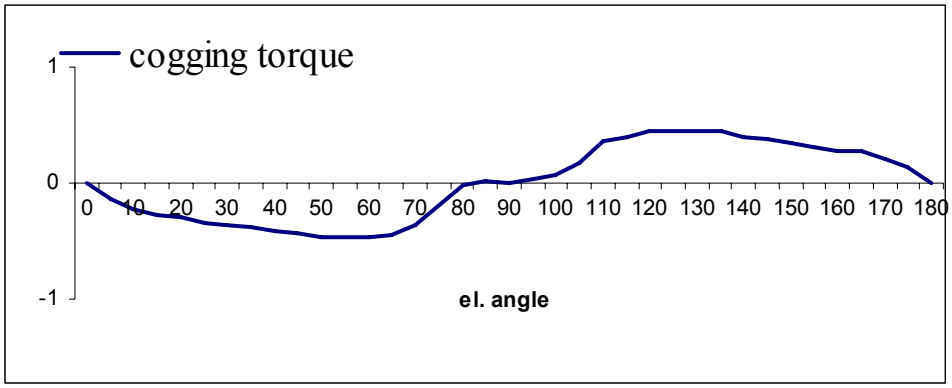

Figure 3.12: Normalised cogging torque as a function of rotor position.

The way of operation of a claw-pole motor with surface mounted magnets is similar to the motor with axial rotor magnetisation. The magnets on the surface must of course be magnetised in opposite directions (north and south poles alternating around the rotor surface). The stator then has a similar flux path but the path of the flux in the rotor is different compared to the motor with the interior ring magnet. The motor with the surface mounted magnets will have a well-defined flux path under the magnets for the flux induced by the magnets, within the rotor core. The flux induced by the armature winding must pass the relatively larger air gap due to the magnet thickness.

3.3 The experimental machine

In order to evaluate the accuracy of the results obtained from the 3-D finite element field computation, a simple experimental machine was built and tested, and is referred to here as Mark 0. This motor has three-phases and eight poles and its active parts consist of a stator core with claws made of soft magnetic composite material (SMC), three stator ring windings (one for each phase), and a solid steel (EN 10025-E335) single-piece rotor also with claws, magnetized with a ring magnet (NdFeB), as illustrated in Figs. 3.13 to 3.15. The shaft is made of non-magnetic steel (EN-1.4301). All dimensions are given in Appendix 1. Because an SMC-rotor was too brittle to produce, a rotor of solid steel was built. This of course gives a low performance due to expected large eddy currents, but the results would still enable comparison with computations to be made. The motor parts were first assembled with appropriate sensors, and then the motor was tested. The performed tests were: measurements of the induced voltage at no load (emf), measurements of the resistance and the inductance, load measurements (current at different speeds and different load torques) and temperature tests.

Magnetic field calculations were performed with the aid of a commercial 3-dimensional finite-element package (Infolytica 2004). The tolerance of the finite element calculations must be chosen carefully. A tight tolerance results in long solution times and sometimes non-solvable problems. On the other hand, a lower accuracy will solve the problem and might give reasonable results of the flux linkage but inaccurate result of the developed torque. Also the step angle must be carefully selected, when the torque is calculated, as the torque changes abruptly at certain rotor positions. For these reasons it was important to be able to compare computations with experimental results (in order to determine appropriate solution parameters) prior to using the FE in serious design work. In this case the whole motor had to be modelled

due to the rotor structure. However, for Mark 1, having one rotor part for each of the three stator-phases, it is enough to model two pole pitches of one phase only, except when considering the inter-phase leakage.

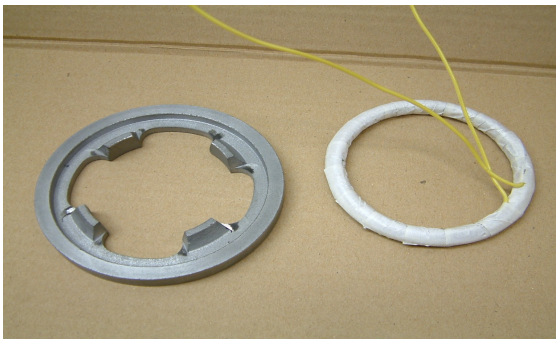

Figure 3.13: a) The rotor b) The stator parts

3.3.1 Construction and assembly

The different parts and the assembly can be seen in the following figures: Fig. 3.13 a) shows the rotor made of solid steel and a ring magnet of NdFeB. On both sides of the core, on the shaft, there is a ball bearing. Fig. 3.13 b) shows one part of the stator core of one stack, and one phase winding. The winding is wound on a specially made tool. The winding is then detached from the tool and formed with insulation scotch. While adding the scotch, the winding cross sectional area became circular which was not the idea in the original design. The number of turns needed to be at least 100, in order to get a reasonable induced voltage. These facts lead to that the wire diameter had to be smaller (0.71 mm), yielding a higher current density than planned for (a rated current of 2.5 A give a current density of 6.3 A/mm^2). This gave problems of high temperatures at rated speed, as the current then became higher than the rated value.

The winding is then put in place, in between the stator core parts (Fig. 3.14). The stator core parts had to be pressed together to get contact between the parts. Even so, the contact was not perfect, as the glue took some space, so it must be accounted for a small air gap between the stator parts. A temperature sensor (PTI) was attached to one of the phase windings. This sensor was set to signal warning if the temperature exceeds 155 °C (the windings' insulation can support 200 °C). In another winding, a thermocouple (type J) was attached, so that the temperature of the winding could be under continuous observation during the measurements.

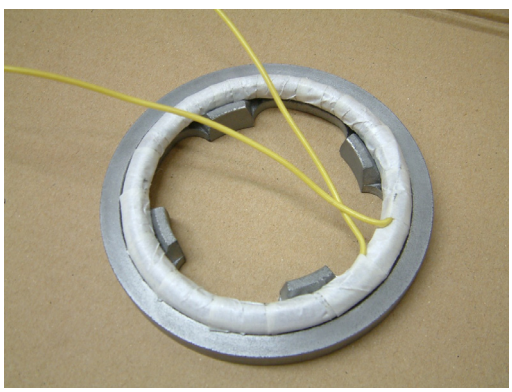

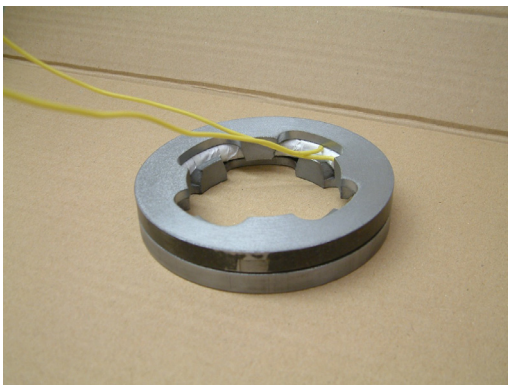

Figure 3.14: The stator winding placed in the stator core

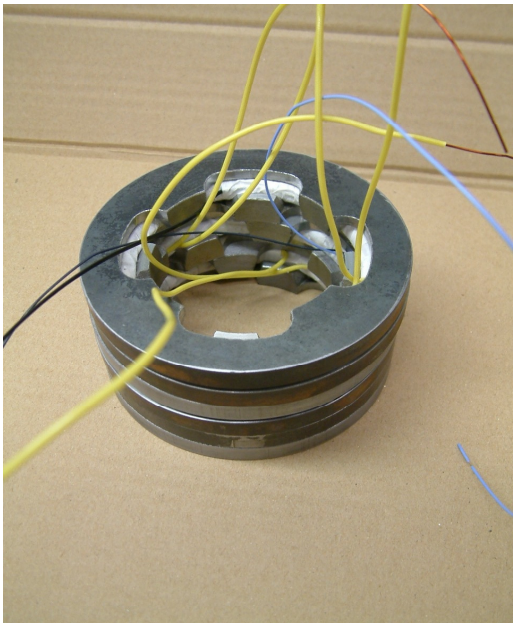

Figure 3.15: The three-phase stator

In Fig. 3.15, the three stator stacks are put together. The relative displacement of the stator stacks should be 30 degrees (120 electrical degrees). As the diameter of the stacks is 115 mm, this means that the second stack was turned 30.1 mm relative to the first stack, and the third stack was turned 30.1 mm in the other direction. The end windings of the phase windings and the temperature sensors are attached to the inner stator surface between the claws. This is done with the insulation scotch and epoxy glue. The glue used for gluing the stacks together was primarily meant to be Loctite 603, which would soften at 150 °C, thus the parts could be detached after the measurements. However, this type of glue could not harden, it showed, because the SMC material is porous, and therefore the surfaces were not free of air, a necessity for the hardening of this type. Therefore, another type of glue had to be used; a two-component epoxy resin. It was allowed to dry for one hour at room temperature, and then about thirty minutes at 70 °C. The glued part was allowed to cool down before the assembly process was completed. The stator was then assembled with the rotor and the shaft position sensor and the clamping plates. The clamping plates were attached with long screws. Thus, there were no screws in the stator core; only the pressure of the clamping plates holds the stator in position.

After the production of the parts and after the assembly, some dimensions showed a discrepancy to the expected values. The outer diameter of the stator core showed to be 115.3 mm instead of 115 mm. The stator claws had individual shapes due to the brittleness of the core material. The circumferential outer claw lengths along the air gap (see Fig. 3.16) were measured to be between 18.7 mm and 19 mm. Also the lengths of the three stator-stacks were found to be 60.3 mm instead of the expected 60 mm. This of course means that the glue introduced a total air gap of 0.3 mm between the six stator-parts. The magnetic properties of the stator core may also have been weakened during the machine tooling process.

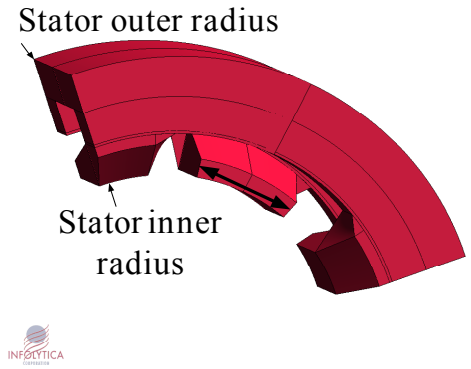

Figure 3.16: The circumferential outer claw length along the air gap is shown with a thick black double-arrow.

3.3.2 Measurements

The measuring system is illustrated in Fig. 3.17. The measuring equipment was as follows:

1. The power inverter/controller: Digital Motion controller ATLAS DMC 310 25P, 3x240 V, continuous current 10 A, peak current 25 A, 9 kHz switch frequency.
2. The load torque is produced by a synchronous generator (3 phases, 4 poles) connected to a torque reaction arm with a possibility to place certain weights on predefined positions on the arm.
3. Resolver: LTN Mod RE-21-1-V02, 2 poles
4. Thermocouple type J (Iron and Constantan) is coupled to a FLUKE 52 K/J thermometer.

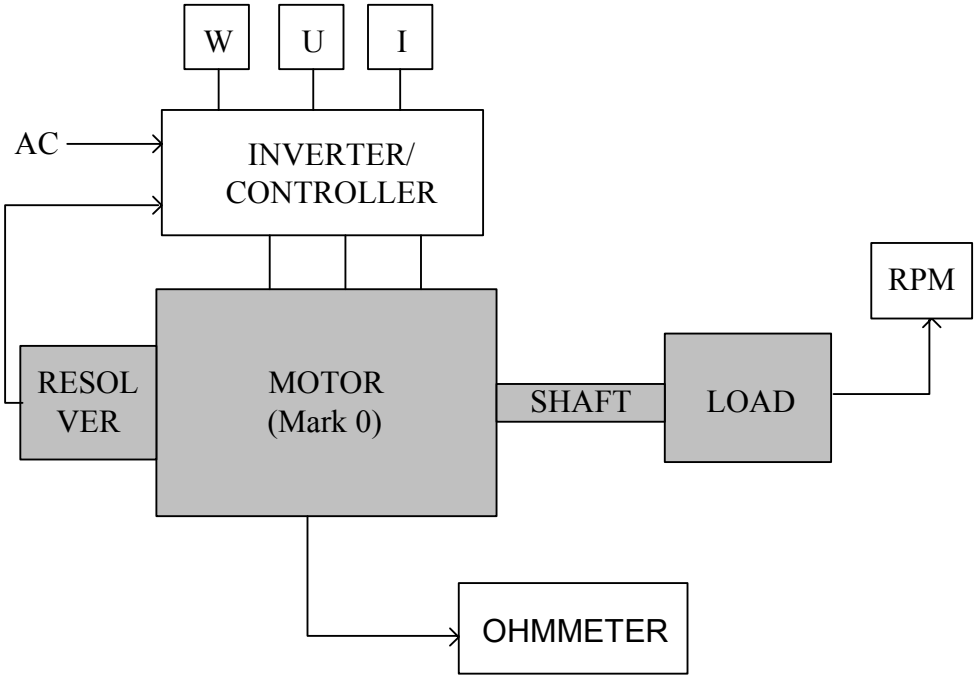

Figure 3.17: Measurement setup

Back emf

The machine was tested, as a generator for back emf measurements, with the recognition that back emf is an indicator for good torque characteristics. As the rotor rotates, the flux linking the stator winding varies and an electromotive force, emf, is induced. The rotor was rotated with another motor (a drilling machine), at a measured speed, 503 rpm, and the terminal voltage was measured with a voltmeter (to get the rms value of the emf). The rms values for the phase voltages were as follows:

phase 1: 4.67 V
phase 2: 4.03 V
phase 3: 5.0 V

Also, the voltage was measured with an oscilloscope (to get the emf as a function of time). The speed was set to 1022 rpm, giving a frequency of 67.9 Hz. The rms value of phase 1 was calculated from the oscilloscope readings to be 9.06 V, and for phase 2 the rms voltage was 8.249 V. The open-circuit voltage waveform is shown in Fig. 3.18.

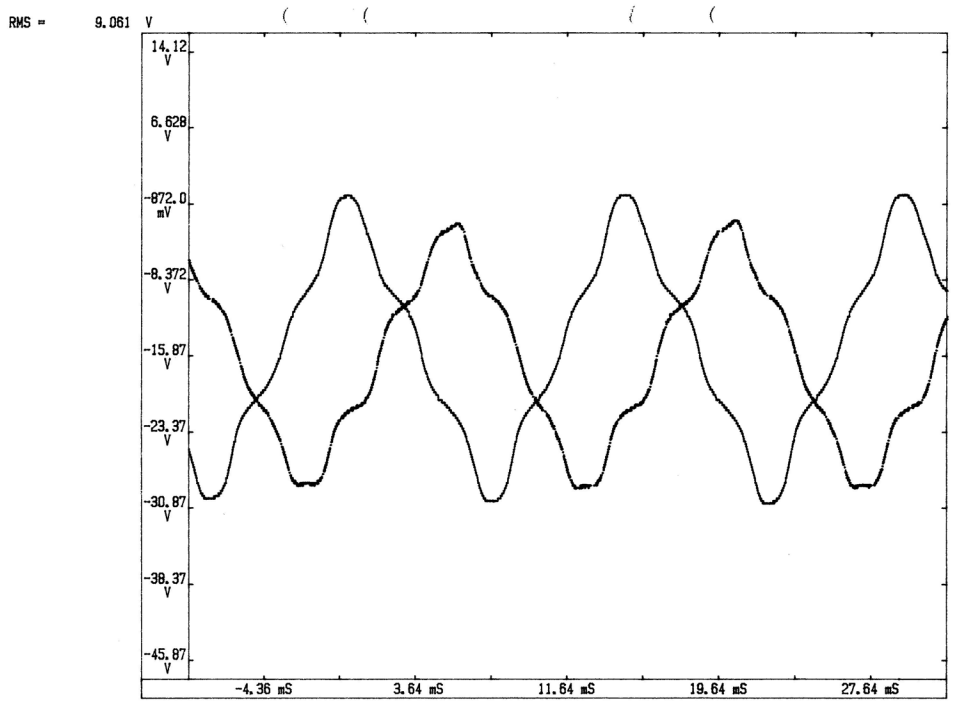

Figure 3.18: Voltage per time at no load and 1022 rpm.

Stator resistance

The stator resistance varies with temperature. Thus, the resistance should be measured at known temperature (room temperature). Then it can be corrected for the working temperatures. The phase resistance and the phase-to-phase resistance were measured with a multimeter. A discrepancy of more than 2-3% between phases or between line-line values may be an indication of an incorrect winding or connection. The phase resistance and the phase-to-phase resistance were measured at room temperature. The phase-to-phase resistances were 2.50 Ω, 2.49 Ω, and 2.49 Ω, with a mean value of 2.493 Ω. The discrepancy between the phases is small (under 1%).

Inductance
The line-to-line inductance was measured with the aid of an inductance meter, where the frequency could be varied. The inductance values at different rotor positions were recorded. In rotors with surface mounted magnets, the inductance values should not differ for different rotor positions but for rotors with flux concentration (and thus salient poles) the inductance values will differ for different rotor positions. The test frequency was also varied, as the value of the frequency and the currents will affect the permeability of the core and the magnitude of the induced eddy currents in the core. Thus, a test frequency of the expected rated frequency should be used, as well as a current value close to the rated current value. The inductance per phase at 1kHz was 12.35 H, 12.20 H and 13.9 H. The inductance per phase at 100 Hz was 14.6 H, 14.4 H and 16.7 H. When the rotor position was varied, the change in inductance was clearly observed. The values differed between 12.2-13.8 H for phase U, 12.44-13.31 H for phase V, and between 13.9-14.2 H for phase W. The measurements at different rotor positions were performed at a frequency of 1 kHz.

Temperature
Temperature tests were performed after the load was maintained at a value close to some expected continuous rating until the temperature no longer increased. The following data was recorded; input power to the motor, motor speed, output torque, stator and ambient temperatures. This allows a possibility to calculate the thermal resistance of the motor. Also the outer temperatures of the core and the clamping plate were measured.

Weight
The weight of the motor parts was measured to be 745-750 g/stator stack, 1982 g for the whole rotor (including the ball bearings), and 2050 g for the clamping plates. Thus the active parts of the motor weighed about 4.25 kg.

Load tests
The torque output capability was tested while observing the winding temperature to ensure that thermal limits were not exceeded. A synchronous generator was used to load the claw-pole motor. The generator was connected to a torque reaction arm with a possibility to place certain weights on predefined positions on the arm. The load torque was varied until the torque reaction arm is in a horizontal position. At such positions, the load torque equals the applied torque produced by the weight on the reaction arm. The motor was powered from a voltage-source inverter which phase commutation control was according to the rotor angle position feedback from the motor. The input current, voltage and power were measured, as well as the speed.

If the winding temperature became too high the applied load torque was reduced, or a lower speed was chosen. The first run with a load of 1 Nm gave a quick rise of winding temperature and the run was stopped. Then two different load torques were applied; 0.5 Nm and 0.7 Nm. The voltages, currents, speed and power were recorded, and the power factor, efficiency, output power and power losses were calculated.

The recorded values are given in Table 3.1 together with the calculated copper losses in the stator winding, P_{Cu} and the rotational losses $P_{rot} = P_{core} + P_{mech}$, where P_{core} is

the core losses in the stator and rotor cores, and P_{mech} is the mechanical losses (such as ventilation and friction loss). From Table 3.1, the loss components at no load are plotted against speed as per Fig 3.19. It is seen that the rotational losses, of which the core losses are the major part, are increasing rapidly with speed. This is due to the solid rotor core.

One can also observe the poor efficiency, which also has to do with the solid rotor but also with the low rotor flux and other design features. Another observation is that the power factor is decreasing with higher speeds and currents. This is because the leakage flux and the saturation are increasing at higher currents, and the frequency dependent losses, such as core losses and mechanical losses, increase at higher speeds (and thus higher frequencies).

U (V)	I (A)	Pin (W)	cosφ	T (Nm)	n (rpm)	Pout (W)	η %	Ploss (W)	R (Ω)	Pcu (W)	Prot (W)
13,0	3,05	59,0	0,86	0,50	146	8	13	51	2,49	35	17
23,2	3,25	103,0	0,79	0,50	500	26	25	77	2,49	39	37
39,0	3,40	160,0	0,70	0,50	996	52	33	108	2,49	43	65
77,0	3,80	305,0	0,60	0,50	1999	105	34	200	2,49	54	146
16,0	3,78	90,0	0,86	0,70	146	11	12	79	3,212	69	10
26,5	3,84	132,0	0,75	0,70	497	36	28	96	3,3	73	23
45,5	4,07	210,0	0,65	0,70	996	73	35	137	3,4	84	53
80,5	4,15	345,0	0,60	0,70	1999	147	42	198	3,5	90	108
127,0	4,85	600,0	0,56	0,70	2996	220	37	380	3,57	126	254

Table 3.1: Measurement recordings

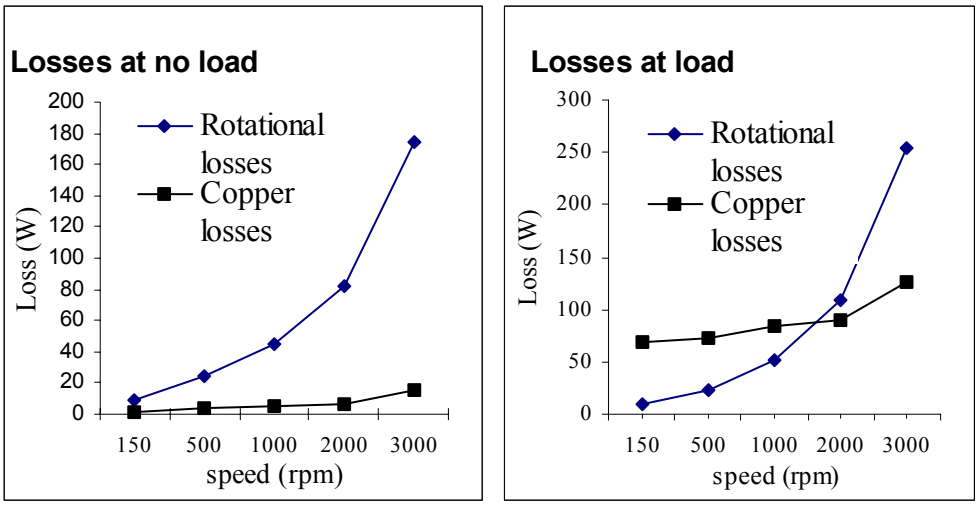

Figure 3.19: Copper loss and rotational loss as a function of speed.

To be able to compare the measured values with the finite element calculations, the torque and current values at low speed are the most interesting. This is because the finite element calculations are not considering the effects of eddy currents. At low speeds, the eddy currents may be assumed small enough not to affect the magnetic

fields in the motor. However, they still give rise to a loss component, and should be considered in the loss calculations. The torque values at the different speeds are plotted in Fig. 3.20 for different currents. As can be seen, there is a linear dependency.

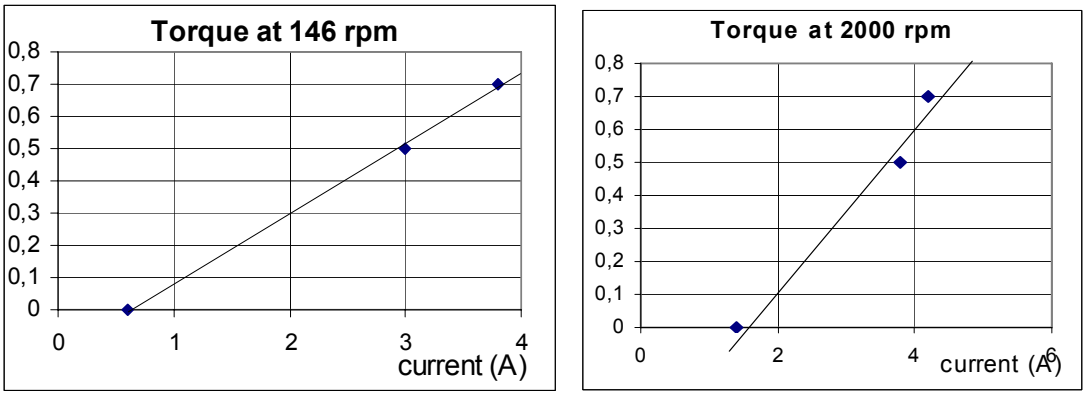

Figure 3.20: Torque-current values at the speed of 146 rpm and 2000 rpm.

3.3.3 Finite element computation and validation

A model of the whole motor, including the two rotor core parts, the magnet, the shaft, the three coils, and the six stator core parts were modelled with the aid of the finite element package (Infolytica 2004). The model is shown in Fig. 3.21. The dimensions are the same as in the built experimental model (given in Appendix 1) apart for some details: The claw-shape is more rounded off in the built machine than in the model, as the drawing tool in combination with the scripting facilities did not allow the circular lines in some directions. This also applies to the coil model that was simulated having a rectangular cross section. Furthermore, the magnetisation curve of the used steel in the rotor was approximated to be the same as the magnetisation curve of the soft magnetic composite material. This was because the true magnetisation curve for the used steel was not found and all the simulations prior to the measurements were with a rotor of soft magnetic composite, thus using the same magnetisation curve simplified comparison with expected results. (Using the laminated steels defined in the finite element program gave only slightly higher torque and emf values.) Natural boundary conditions were set with an air box surrounding the whole model. The size of the air box was deliberately kept small (even though this is believed to introduce some faults) in order to keep the solution time down. The small air gaps between stator core parts that appeared due to the glue could not be modelled without significantly increasing the solution time. However, the motor air gap could be increased 0,1 mm without affecting the solution time. This would give a total air gap of 0,51 mm. Thus the increasing of the air gap is used to consider the increased air gap between core parts. The effect, in both the motor and the model is lower torque and emf values. However, the air gaps in the experimental motor might give other effects than the increased air gap in the model due to the different paths of the magnet flux in the aligned position and in the unaligned position, respectively.

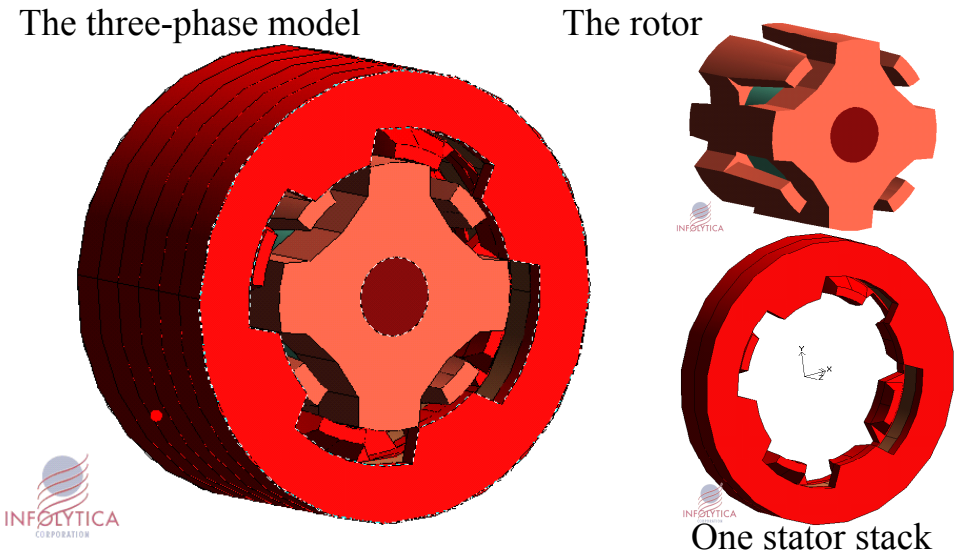

Figure 3.21: The finite element model of Mark 0.

Scripting was used, thus the model parameters were given in Microsoft Excel, and the finite element program was opened and run through the Visual Basic code within the Excel-program. In this way, the building of the model, the setting of the boundary conditions, the modelling of the rotor rotation, and the visualisation of the results were easily done in Excel. However, due to the size of the model, the solving time of the finite element solver was long. Therefore, the accuracy of the finite element calculations must be chosen carefully. Also the step angle must be carefully selected, when the torque is calculated, as the torque changes abruptly at some rotor positions (for instance when the claws are about to approach each other). In Fig. 3.22 two solutions of the same problem is solved with different tolerance and different step angles. The motor is a one-stack claw-pole motor of eight poles at no load. The torque and flux linkage is solved when the rotor position is varied over one pole pitch. The high accuracy solution is solved with an adaption tolerance of 1% and a mechanical step angle of 1.25 degrees, whereas the low accuracy solution is solved with an adaption tolerance of 5% and a mechanical step angle of 2.5 degrees. It is clearly shown the difference in the torque! Even with the higher accuracy, the torque values may be uncertain, as can be seen from the high peaks in Fig. 3.22. Increasing the accuracy, those peaks will diminish.

Winding temperatures were only measured and are not compared with calculations. Comparison is now made between the following measured and computed values:

1. Induced electromotive force (emf) in the stator windings as a function of time/ rotor position and rms values.
2. Stator winding resistance
3. Stator winding inductance
4. Weight of active parts
5. Core losses
6. Torque for different stator currents and speeds

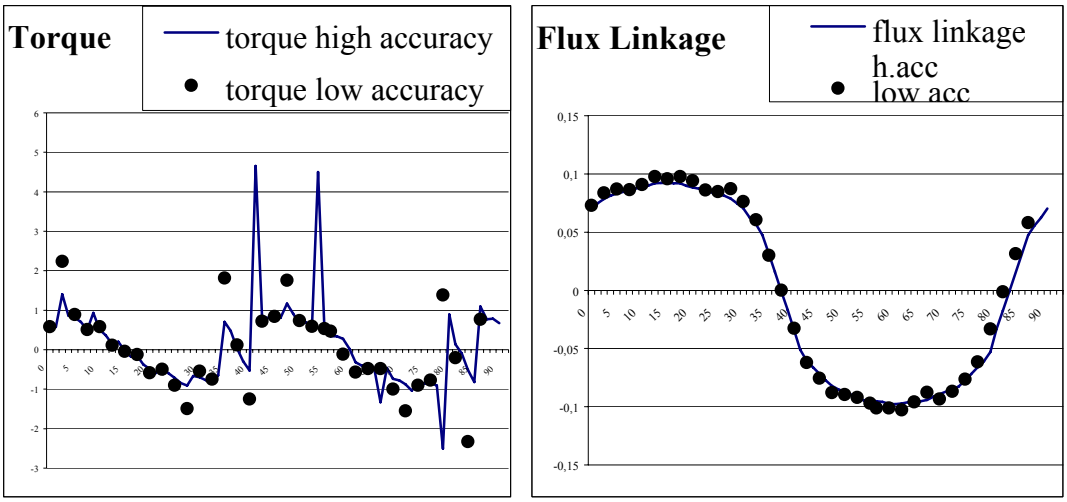

Figure 3.22: The torque and flux linkage is solved when the rotor position is varied over one pole pitch with different tolerances and different step angles. The motor is a one-stack claw-pole motor of eight poles at no load.

Back emf

To calculate the emf, the stator windings' flux linkage is calculated for several rotor positions, at no load. As the rotor rotates, the flux linking the stator winding, ψ, varies and an emf is induced. The frequency of the generated emf depends on the rotor speed, ω_m. The emf waveform is determined by the waveform of the flux, ϕ. The number of turns, N, will affect the induced emf, as follows:

$$emf = \frac{\partial \psi}{\partial t} = N \frac{\partial \phi}{\partial t} \tag{3.1}$$

To obtain the time derivative of the flux linkage, Eq. 3.1 is transformed to a derivative of the position. As the rotor position can be expressed as $\alpha = \omega t$, where ω is the mechanical angular frequency, $\omega_m = \frac{2}{p}\omega_e$, the emf can be found from Eq. 3.2.

$$emf = \frac{\partial \psi}{\partial t} = \frac{\partial \alpha}{\partial t}\frac{\partial \psi}{\partial \alpha} = \omega_m \frac{\partial \psi}{\partial \alpha} = 2\pi f \frac{2}{p}\frac{\partial \psi}{\partial \alpha}. \tag{3.2}$$

Calculating the derivative of the flux linkage will introduce some errors due to the differentiation (a process that inherently magnifies errors). Therefore, inaccuracies in the computation of the flux linkage will be exaggerated. In order to minimise this effect, the harmonic components of the flux linkage are first calculated and then used to derive the emf. A rotor step angle of 1,25 mechanical degrees allows the computation of the first seven harmonics. The resulting emf for one phase is shown in Fig 3.23. In fact, the flux linkage waveform is nearly sinusoidal as can be seen in Fig. 3.24.

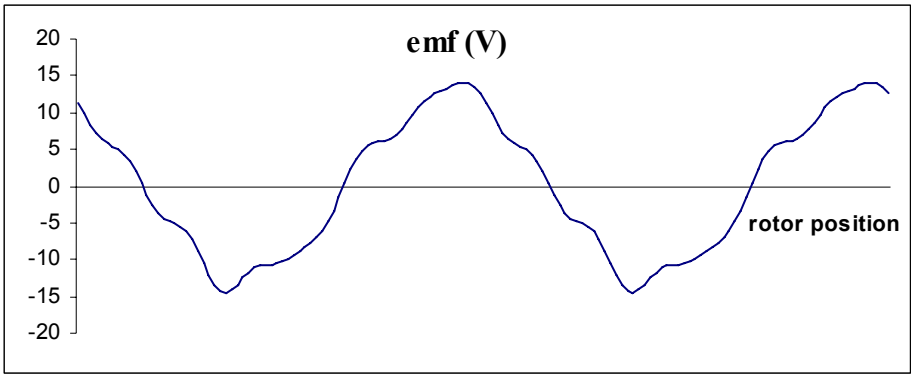

Figure 3.23: Calculated emf as a function of rotor position with rotor step angle 1,25 degrees.

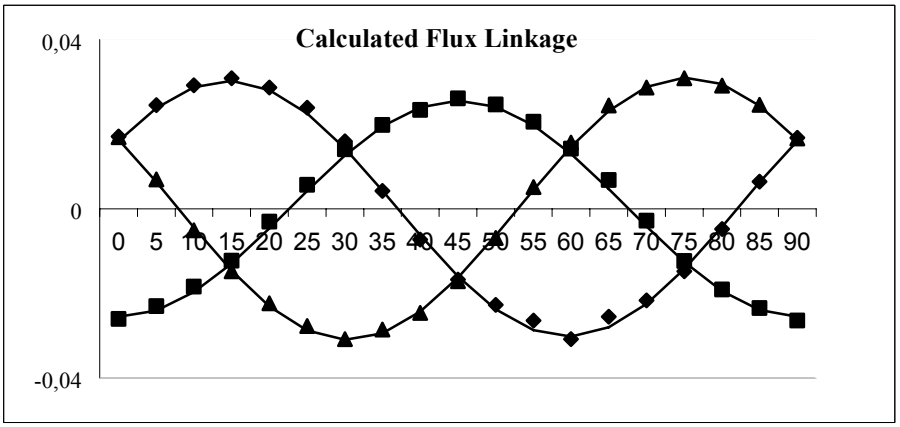

Figure 3.24: Calculated flux linkages as a function of rotor position with rotor step angle 5 degrees. The markers show the calculated values at each rotor position and the solid lines show the fundamental components.

From the fundamental component of the flux linkage curves and from Eq. 3.2, the emfs of different speeds can be found. This is done for the same speeds as used in the measurements (503 rpm and 1022 rpm). The results are as below.

503 rpm		1022 rpm	
phase 1:	4.50 V	phase 1:	9.15 V
phase 2:	3.81 V	phase 2:	7.74 V
phase 3:	4,62 V	phase 3:	9.38 V

Comparing these values with the measured values give a maximum discrepancy of 8%. In both the measured and the calculated curves, the phase voltages are non-symmetric and contain harmonics.

The major reason for the non-symmetric curves is the magnetic flux leakage between stator stacks. This is the reason why the voltage in the middle stack is lower. The leakage flux is partly a consequence of the magnetization of the magnet. As the magnet is magnetized axially, the flux in the rotor claws has a large axial component, and the normal component (the radial component passing the air gap) is not constant on the claw surface. This can be seen in Fig. 3.25, where the normal component of the flux density along the air gap is shown, at an axial position above a saturated rotor claw (at a current of 3.8 A).

Another reason for the harmonics is the non-symmetry between the overlapping areas of the stator and rotor claws at the different rotor positions. The harmonics of the measured values can partly be explained with the dimensional changes of the stator claws, that is a result of the machining of the SMC material. If only a small number of claws are deformed due to machining, then the resulting flux density will only be lower than with perfect claws. However, if all stator claws are smaller than the rotor claws, then the flux density will cease to be sinusoidal, and thus be more like trapezoidal. Also, the phase angle displacement of the three-stator stacks was not as exact as the calculated displacements. This, however, only affects the phase displacements between the phase voltages and not the forms of the curve. There is also some saturation mainly in the rotor claws.

Stator resistance

The resistance can be calculated from

$$R = \frac{\rho l}{A_c} N \tag{3.3}$$

where ρ is the resistivity ($1{,}67*10^{-8}$ Ω m for copper), l is the mean length of one turn, N is the number of turns, and A_c is the conductor area. For Mark 0, the number of turns is 100, and the conductor diameter is 0.71 mm, and the mean length of one turn is 93.4π mm. With the given winding data R=1.24 Ω. As the measured stator phase-to-phase resistance was about 2,5 Ω the computed phase value at 1.24 correlates very well with measurements.

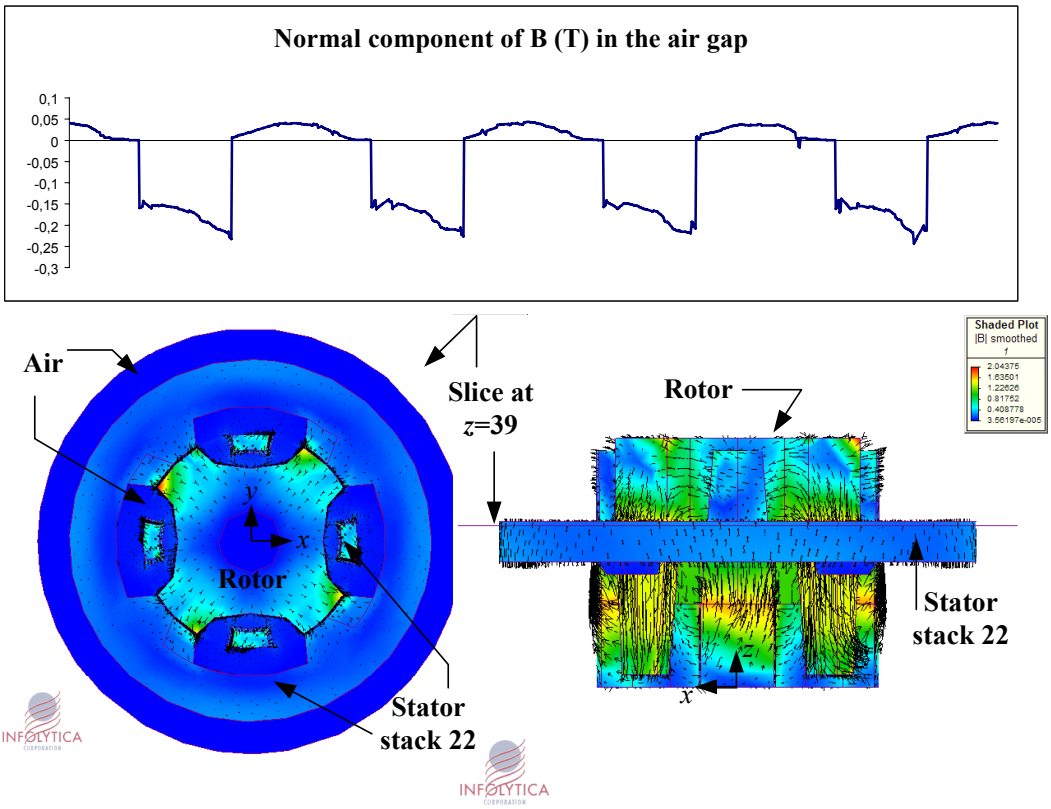

Figure 3.25: The normal component of the flux density in the air gap at z=39 mm. This is on the edge of the second part of the middle stack (named stack 22). (Stack 11 would be at z=0, if shown.)

Inductance

The synchronous self-inductance of the stator winding, L_1, can be calculated by

$$L_1 = \frac{\psi_1}{I_1} \tag{3.4}$$

ψ_1 is the flux linkage in the stator winding due to the stator current I_1. It can be obtained from the results of the FE calculations with only the stator current I_1 as a source for the flux, thus no permanent magnets (they can be replaced with air). The inductance can also be calculated from the value of the energy, as

$$W = \frac{L_1 I_1^2}{2} \tag{3.5}$$

The two calculation methods yield the same result. As the motor has salient poles the inductance vary with rotor position. The calculated inductance values are between 14 and 18 mH. The expected rated speed is about 2000-3000 rpm, which gives a rated frequency of about 100-200 Hz. The measured inductance per phase at 100 Hz was between 14 and 17 mH, thus a good correlation with the calculated values is evident. As different current values will give different inductance values due to saturation, then if the inductance value is to be used in further calculations (not only for validation as is the case here) inductance values for each current value should be calculated.

Weight

The weight of the motor active parts where calculated to 3.64 kg. The bearings were not included, and the weight of the winding was calculated as the volume of the winding times the density of copper times a factor of 0.7. This factor is to account for the insulation of the winding, giving the weight of one stator stack to be 750 g, which is similar to the measured weight.

Output performance

The average electromagnetic torque for a given sinusoidal current is found with the finite element program. The static torque for different rotor positions and different currents, were solved. An example is shown in Fig. 3.26, where the current is set at 4.15 A, the step angle 5 mechanical degrees, and the adaption tolerance is 1%. The shown 90 degrees thus cover the rotation of the rotor over two pole pitches. A mean torque for each current value was calculated. No losses were considered in this calculation (except for the iron losses but they did not significantly affect the torque calculations) and the computed torque values should indeed be higher than the measured ones.

The result of the comparison can be seen in Table 3.2. The discrepancy between measured output torque and calculated electromagnetic torque, at increasing speed, is also shown in Fig. 3.27. The discrepancy is clearly increasing with speed due to the frequency dependant loss components. The discrepancy is about 25% for the low speed values. For the high-speed values, the losses are too high to warrant any comparison. Still, the experimental machine has provided data for comparison with computation, giving confidence in the general correctness of the numerical modelling rather than to vindicate its absolute accuracy. In order to get more accurate comparison between calculated and measured torque, all loss values should be

calculated. Also the measurements should be refined, so that the mechanical losses and the core losses could be separated, as well as the rotor and stator core losses.

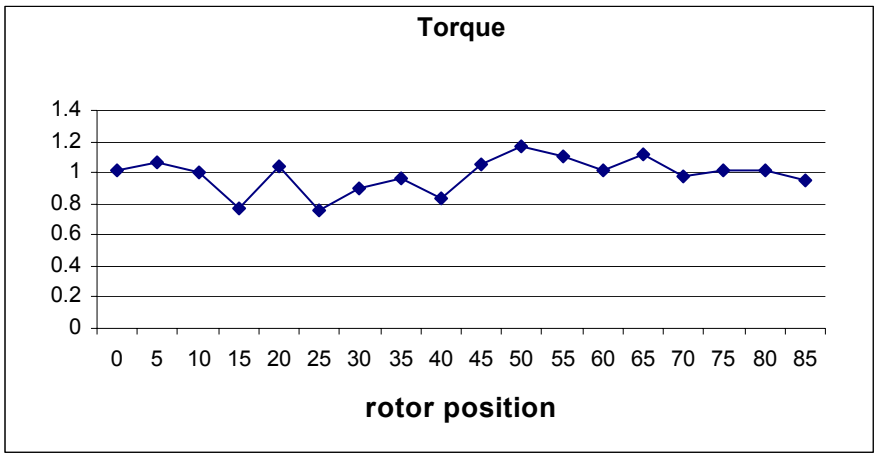

Figure 3.26: The calculated static torque when rotating the rotor 90 degrees, thus two pole-pitches, at a current of 4.15 A.

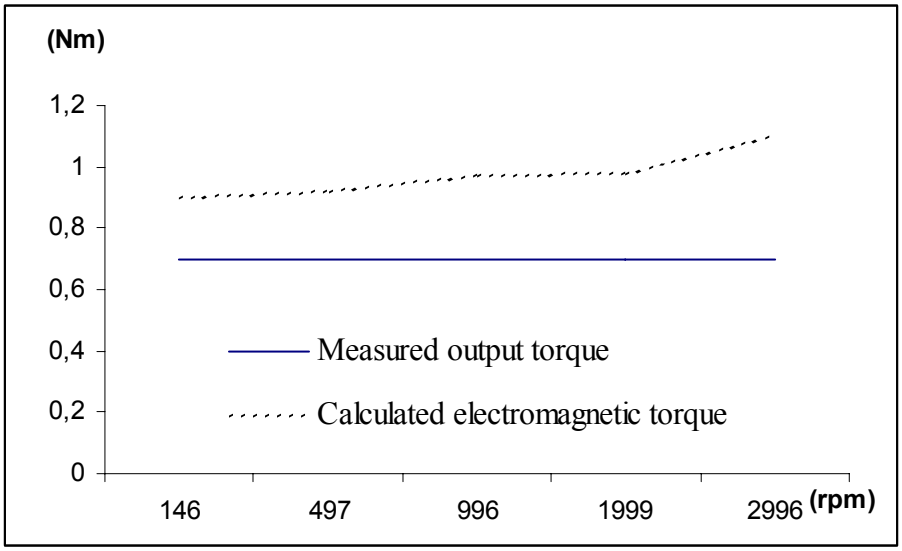

Figure 3.27: The calculated and measured torque at varying speeds (and currents).

The same equivalent circuit of the synchronous motor can be used for the claw-pole motor to predict the performance, and it turns out that a phasor diagram essentially identical to that of a conventional synchronous machine can represent the performance (see section 3.5). With the closed-loop control of position feedback it can operate in brushless dc mode where the current and the induced open-circuit back emf (induced by the magnets) are in phase, to achieve a maximum electromagnetic power at a given speed. Under these circumstances, the power factor can be estimated as the simple ratio of (reactive voltage drop on full load)/(open circuit back emf)=*IX/E=(the top flux linkage due to armature current acting alone)/(the top flux linkage due to magnet flux acting alone)*. This means that the voltage drop over the stator resistance and the saliency is neglected. Then, the power factor is found as cos(arctan(*IX/E*)). However, the operating power factor may be significantly below this value if appreciable saturation is present on full load. (Harris, Pajooman et al. 1997)

Calculating the power factor of Mark 0 turns out to be difficult, using the method of (Harris, Pajooman et al. 1997). This is because of the large inter-phase leakage. Still, the power factor in one phase ($\cos\varphi_1$) was calculated and given in Table 3.2.

The power factor was also calculated using the equivalent circuit of Fig 3.61 and Eq. 3.13. Then the resistance is included in the calculations, as well as the value of the inductance. The saliency is considered giving a value of the phase inductance of 14 mH, which is the assumed (unsaturated) inductance in the unaligned positions. The measured resistance values are used since they are corrected for the measuring temperatures. The result of this calculation is also given in Table 3.2 as $\cos\varphi_2$. The major errors in the calculation of $\cos\varphi_2$ accrue from the approximation of the inductance, as no adjustments are made for varying currents (thus no consideration of saturation). Still, this second method of calculating the power factor is the better one of the two. The main reason to the deviations between $\cos\varphi_1$ and the measured power factor seems to be the neglecting of the resistance, as it is for the low speed values, that the largest faults arise, when the reactance is comparable in size to the resistance. The reason to use the first approximate method is to get a quick idea of how the power factor change during the initial design procedure.

		Measured values			Calculated values			
I (A)	n (rpm)	cosφ	Tout (Nm)	Pfe+ Pμ (W)	$\cos\varphi_1$	$\cos\varphi_2$	Tem (Nm)	Pfe,stator (W)
3,05	146	0,86	0,5	16,61	0,67	0,96	0,73	0,36
3,25	500	0,79	0,5	37,37	0,65	0,80	0,78	1,3
3,40	996	0,70	0,5	64,68	0,64	0,66	0,81	2,7
3,80	1999	0,60	0,5	146,41	0,61	0,52	0,91	6,0
3,78	146	0,86	0,7	10,46	0,61	0,97	0,90	0,44
3,84	497	0,75	0,7	22,58	0,62	0,84	0,92	1,5
4,07	996	0,65	0,7	52,51	0,59	0,69	0,97	3,2
4,15	1999	0,60	0,7	108,06	0,59	0,55	0,98	6,5
4,85	2996	0,56	0,7	254,43	0,54	0,46	1,1	11

Table 3.2: Results of torque calculations.

Concerning the calculations of the losses, the core losses can be separated into two components; hysteresis loss and eddy current loss. Sometimes the losses are also expressed as anomalous (excess) losses. This last loss component considers the fact that the behaviour of the core losses is yet not fully understood. Traditionally, the core losses are expressed with an equation like the following:

$$P_{core} = P_h + P_e = C_h f B_p^{\ n} + C_e \left(f B_p\right)^2 \tag{3.6}$$

where C_h and C_e are constants depending on the material characteristics, f is the excitation frequency, and B_p is the peak flux density. Moreover, these losses are mostly considering the effect of alternating time varying magnetic fields. A more exact description of the time-varying fields would include the rotation of the fields, as rotation of the field would most certainly appear in the claw-pole construction (Reinap 2005). As the experimental machine did not allow a good comparison of

calculated and measured loss values, the refined methods of loss calculation in the SMC-core were not used at this stage. The losses in the stator core were instead calculated only considering the fundamental component of the alternating magnetic flux and only considering the hysterisis losses, as described below. This is recognised as a coarse approximation; performed in order to give an indication of the size of the losses in the experimental machine and to allow comparison between losses for different designs during the design process of the prototype (Mark 1) as explained in Section 3.4. The loss calculation method should definitely be improved in any future design work.

Thus, the core loss in each finite element could be calculated with the formula above if the constants in Eq. 3.6 could be specified, or a valid curve could be imported to the material databases. The latter is the used procedure in the finite element package. The curve should show iron losses (W/kg) as a function of the flux density (one curve for each frequency). Then, the loss per element can be calculated, together with the mass density to give a loss value per element (W/m^3). From that the total iron loss (W) can be calculated by integrating over the volume of the component where the iron losses occur. This should be done for different rotor positions, and then the core loss is found as the mean value of these results. According to (Infolytica 2004) this is a correct procedure for laminated materials, when using a static solver, if the effect of the eddy currents is negligible. That is, if the core losses consist mainly of hysteresis losses. This is since eddy currents are usually negligible in the manufacurers' measurement set up (for laminated materials), in which case the static B field corresponds to that of the time-harmonic solver with B replacing B_{rms}. Iron losses can also be obtained using the time-harmonic solver. However, the solver cannot handle non-linear materials as rigorously as the static solver. Iron losses cannot be calculated like this in the transient solver, as the manufacturers' data is valid at a specific frequency only.(Infolytica 2004)

When it comes to the SMC material, the same type of loss curve as is used for laminations, can be used in order to calculate the hysteresis loss. Data from the manufacturer regarding a ring with OD 55 mm/ID 45 mm and H 5 mm is used. However, to calculate the eddy current loss, the time variation of the magnetic field needs to be considered as the core losses depend also on the shape of the specimen. This is not possible with a static solver.

For the solid steel rotor, the eddy currents will be huge, and the second order effects cannot be neglected. Kuppers and Henneberger determined the iron losses in the solid claws of a claw-pole alternator. They found that the iron losses were about twice that of the iron losses in the armature. They mean that the slotting harmonics of the air gap field induce eddy currents into the claws, and that those currents must be calculated with a time step calculation procedure. (Kuppers and Henneberger 1997)

According to (Chalmers 1965), the assumption that the field is not modified by the eddy currents, is only valid when the depth of penetration, d, is much larger than the half length, b, of the conducting material. For a solid claw in Mark 0; $5.5<b<9$mm (the claw is tapered), and d is found from Eq. (3.7) with the result given in Table 3.3. The frequencies correspond to the speeds of the measured points (146, 500, 1000, 2000, and 3000 rpm). The permeability values are 500 and 2000 for SMC and steel, respectively. The resistivity values are 50 μΩm and 0.16 μΩm for SMC and steel,

respectively. From Table 3.3 it is clear that $d<<b$ for the solid steel, and thus the second order effect of the eddy currents cannot be neglected, not even for the lowest frequency value. For the SMC material though, b is not the width of the claw, but rather the width of the powder particles, which is about 5-200μm. Thus the simple method of using measured loss curves is applicable but only for all investigated frequency values.

$$d = \sqrt{\frac{\rho}{\mu\mu_0\omega}} \tag{3.7}$$

	f	9.7	33	67	133	200
SMC	d	36	20	14	10	8
Steel	d	1.0	0.55	0.39	0.28	0.23

Table 3.3: Calculated depths of penetration

Considering the lack of measured data of the loss components, and the difficulty to estimate the losses in the solid steel rotor, the loss calculations could not be validated.

Observe that the measured torque density at rated speed (3000 rpm and 200 Hz) was only 0,7 Nm/3,64 kg=0,19 Nm/kg. The calculated torque density at that speed was 1,1 Nm/3,64 kg=0,302 Nm/kg. The difference is explained with the large losses. There will be a difference of torque density between measured and calculated values also when SMC is used in the rotor, but the difference is expected to be markedly smaller.

3.4 Internal design of claw-pole motors

After establishing the reliability of the 3-D finite element model and computation, a theoretical investigation into the internal design of claw-pole motors is carried out. The work focused on one motor topology, having claws in both rotor and stator. This topology is chosen because it provides the possibility of changing a large number of geometrical values, and to study the effect these changes may have on performance.

3.4.1 Leakage flux

Both in the stator and in the rotor there will be quite high flux leakage. The leakage may be as high as 60% of the magnet-produced flux. There are three major leakage paths:

- Leakage around the coil in the stator, and around the magnet in the rotor
- Leakage between adjacent claws in the same stack
- Leakage between phases

Leakage around the coil in the stator, and around the magnet in the rotor

These leakage paths are illustrated in Fig. 3.28, where the flux density is shown on a slice in the radial-axial plane. Stator flux leaks through the air gap between the stator claws and the stator core, and, similarly, rotor flux leaks through the air gap between the rotor claws and the rotor core. This leakage can be minimised by increasing the air

gap of the flux path. Hollowing the core as shown in Fig. 3.29 does this as well as the radially tapered claw construction.

The hollowing of the cores should be as large as possible, as this does not only prevent leakage but also reduce weight. However, sharp corners should be avoided, as this will give a smoother path for the flux.

The claws' base (the structure from which the claws emerge) must be thick enough to withstand the strain of the magnetic pull forces on the claws (due to forces of attraction between the magnetised stator and rotor). These forces will be felt during the assembly of the motor. During normal operation (after assembly) only the effect of forces due to magnetic unbalance would exist.

The leakage in the rotor is higher than in the stator because of the large magnet that is needed when using a ring magnet. Also, the armature mmf is quite small compared to the magnet mmf, which is chosen in order to get a high power factor. In both the unaligned and the aligned positions, the flux in the rotor claw is large and consequently the rotor leakage is also large. This can be seen in Fig. 3.30.

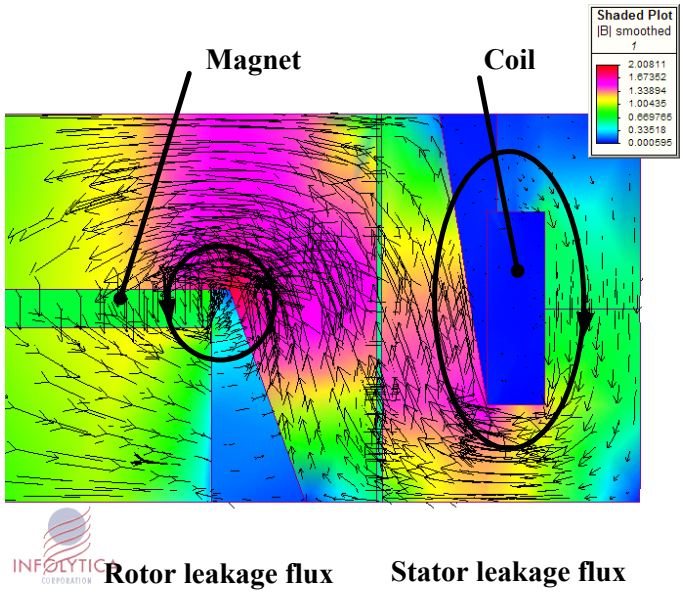

Figure 3.28: Stator flux leaks through the air gap between the stator claw and the stator core. The rotor flux leaks through the air gap between the rotor claw and the rotor core.

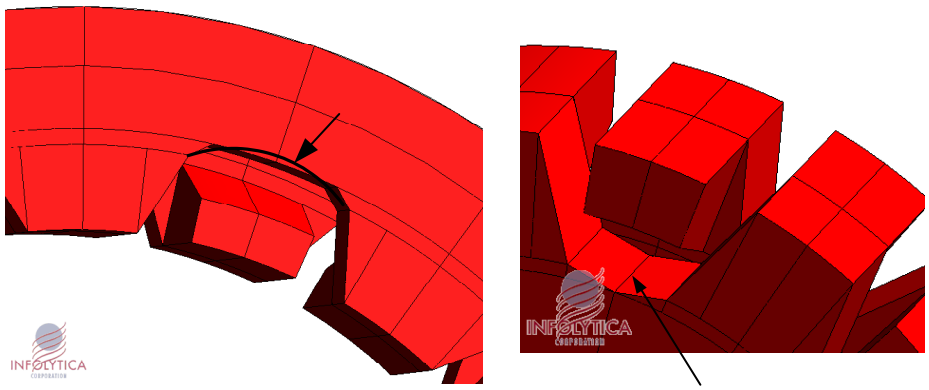

Figure 3.29: Hollowing of the core to minimise stator and rotor flux leakage.

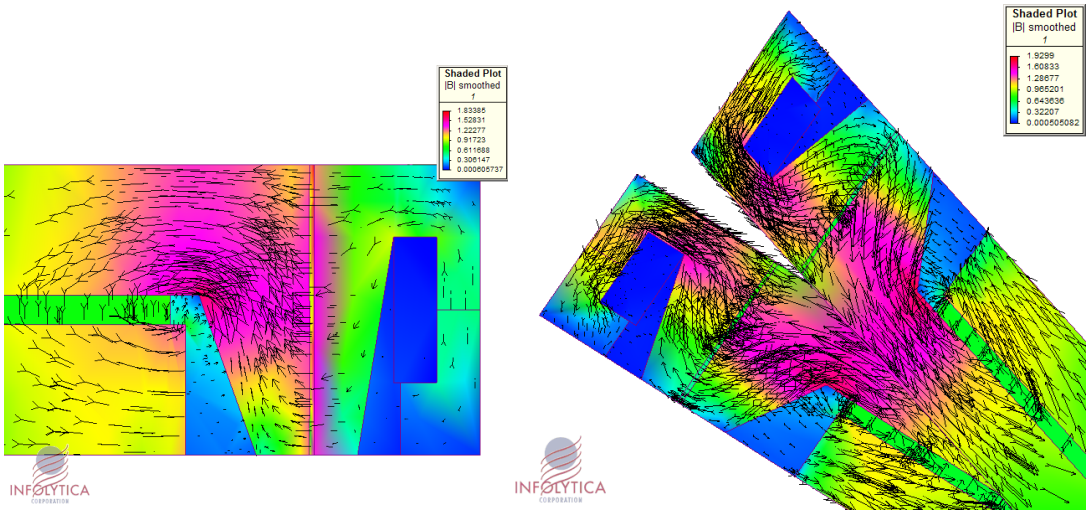

a) Unaligned position (flux density on a slice on the claw edges)

b) Aligned position (flux density on two slices through the middle of the claws)

Figure 3.30: Flux leakage between the claw and the core at the unaligned position (left) and the aligned position (right).

Leakage between adjacent claws in the same stack

The space between neighbouring claws must be much larger (an order of magnitude) than the effective air gap between the stator and the rotor otherwise the main flux will bridge through the claws, and not pass the air gap, as illustrated in Fig. 3.31. This would result in low torque production (the stator flux linkage will however not change just by this stator leakage). This leakage may be limited by lowering the number of poles and by decreasing the claw arc relative to the pole-pitch. In both cases, the air gap between the claws would be increased. However, if the claws are made thin, relative to the pole-pitch, they may become saturated. Also, the reluctance at the aligned position will increase and the stator flux linkage will consequently decrease. Thin claws will also become mechanically weak and, in extreme cases, it may not be possible to press the iron powder into the required shape.

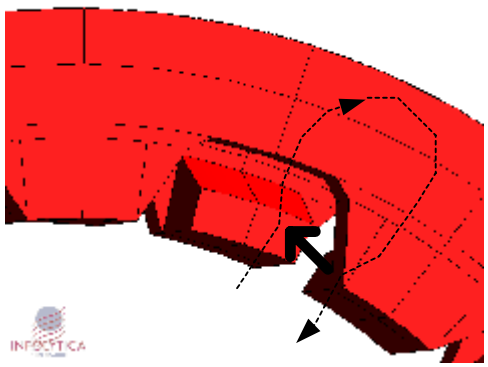

Figure 3.31: Leakage between claws (thick arrow)

Leakage between phases

The one-phase claw-pole motor will give a positive torque for all rotor positions if the armature mmf is large enough to overcome the cogging torque. The torque from such a one-phase motor is shown in Fig. 3.11 for rotor-rotation during a pole-pitch. If m

such one-phase modules are stacked together in the axial direction the result is an *m*-phase motor. If *m*=3, the stator (or rotor) stacks (phases) should be rotated 120 electrical degrees in order to get a smooth output torque. The torque-components from the stacks and the resulting torque are shown in Fig. 3.32 where the stator stacks are rotated and the three rotor stacks are aligned. In the computation the stacks are separated by non-magnetic barriers of 3 mm.

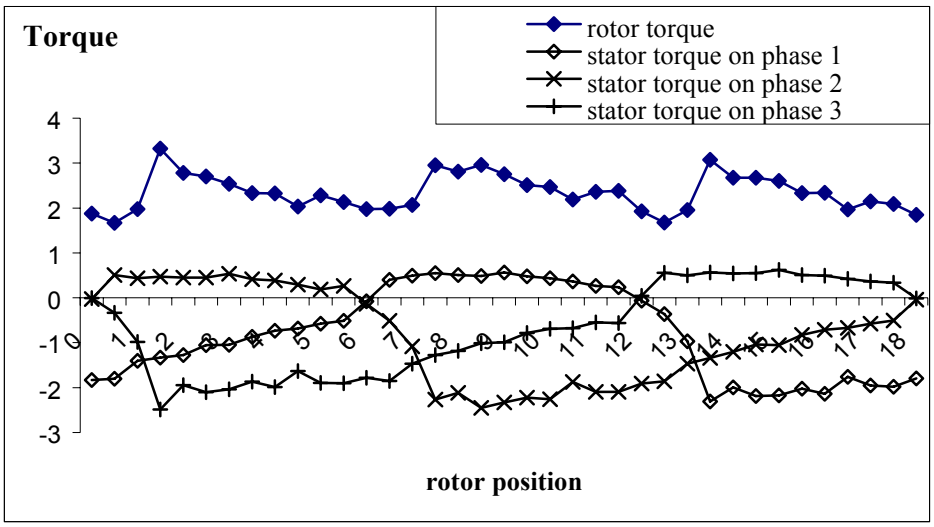

Fig. 3.32: Torque in the three phases as well as the resulting three-phase torque.

For poly-phase motors, there will be leakage between phases and a barrier (of air, aluminium or any other non-magnetic material) is necessary. It is especially obvious that the flux leakage between phases is large, when only one rotor core is used (for a three-phase motor) and when the magnet(s) is/are magnetised in the axial direction. The lowest value of phase-to-phase leakage was found in motors with surface mounted magnets in the rotor. The effect of the leakage between phases can be seen in the resulting non-symmetric emf and lower torque values. Even with 1 mm barriers, the leakage between phases is apparent. This can be seen in Fig. 3.33 where the stator-flux linkage at no-load is shown for a three-phase motor with 1mm barriers and compared to the stator-flux linkage at no-load for a one-phase motor.

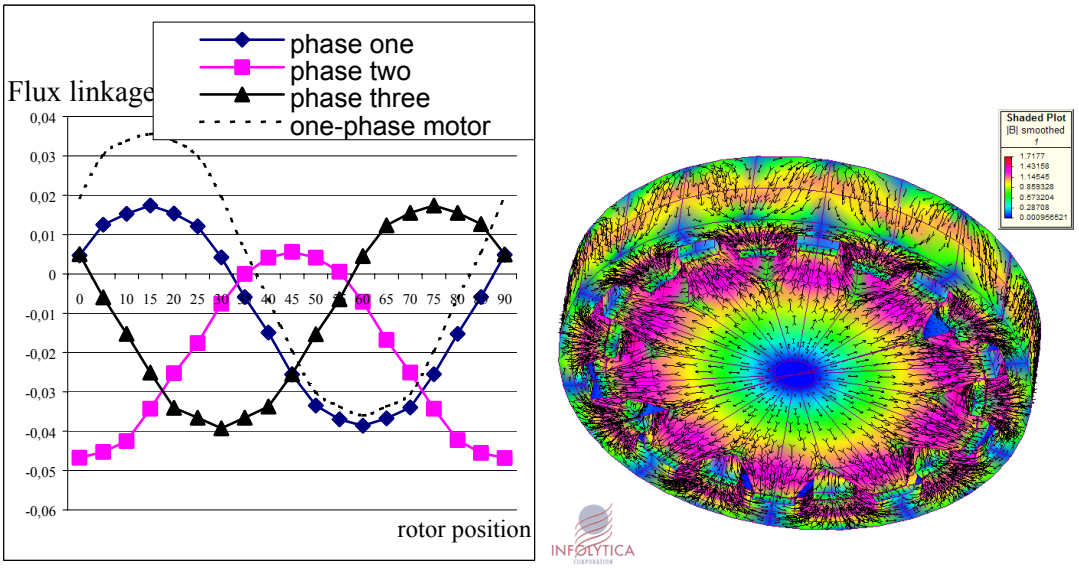

Figure 3.33: Stator flux linkage at no-load for a three-phase motor with 1 mm barriers, compared to a one-phase motor (left) and the flux density in a one-stack-motor (right)

The leakage between phases can also be seen in detail in Fig. 3.34. It may be seen that flux from the rotor core leaks into the closest rotor core in the nearest phase and then returns through the stator cores to the opposite rotor claw in the phase where the flux originated. The leakage path in the stator differs depending on the rotor position; the main leakage path will be through the closest stator claws. If the barriers between claws are increased, the reluctance of this leakage flux path would obviously increase, and the barrier between the rotor core parts can remain small. This implies that a model with rounded off claws, as explained in Section 3.4.5 will be a better solution than a model with long straight claws.

The influence of the length of inter-phase air barriers is investigated. A three-phase motor built with three stator-stacks and three rotor-stacks is considered. The three stator-stacks are shifted (rotated) 120 electrical degrees, whereas the rotor-stacks are aligned. A barrier of air separates the stacks (both rotor and stator stacks), as shown in Fig. 3.34. The claws in the investigated motor are, however, rounded off, giving shorter claws than those in Fig. 3.34 (a rounded claw construction is shown in Fig. 3.6). Only one rotor position is considered, namely when the middle stack is aligned (giving the peak flux linkage in the corresponding phase). The same adaption tolerance (of 5%) is chosen for all solutions, giving the solution time to about 1.5 hours. (Choosing an adaption tolerance of 1% instead of 5% gives a change in flux linkage below 7% and looking at the results below shows that the tolerance is not the major factor in the results.) The result of the flux linkage in the aligned phase is seen in Fig. 3.35 when the barrier length varies. The result is compared with the calculated flux linkage that results of a single phase in the aligned position (when no leakage from other phases exists). The results show, again, the significance of the influence of leakage between phases, even with large inter-phase barriers.

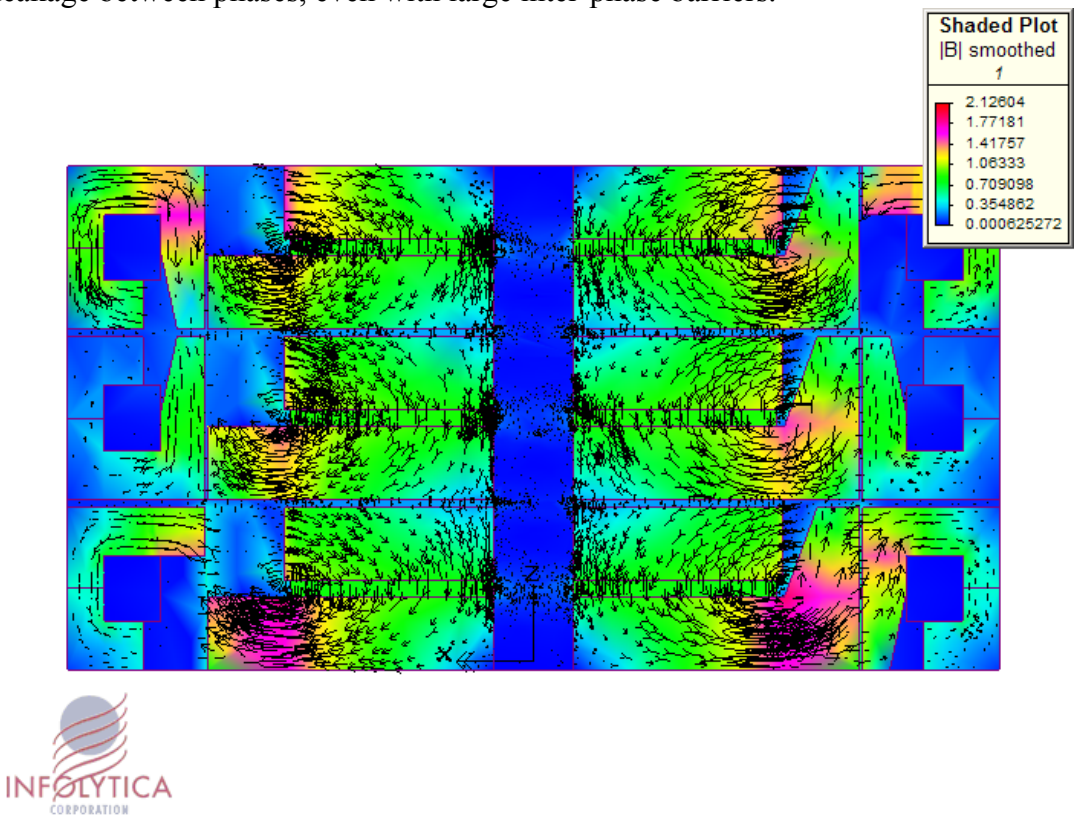

Figure 3.34: Leakage between phases in a three-phase claw-pole motor.

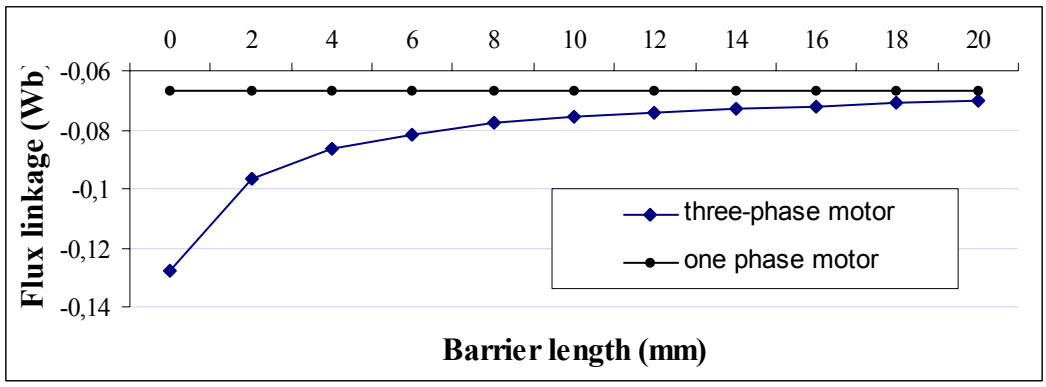

Figure 3.35: Flux linkage in one single (aligned) stack (one-phase motor) compared to flux linkage in an (aligned) stack surrounded by two other stacks, and with the barrier length between the stacks varying (three-phase motor).

There is another way to limit leakage between phases (other than the use of non-magnetic barriers between phases). This is to reverse the direction of magnetisation of the magnet in the middle phase and rotate the middle rotor stack 180 electrical degrees relative to the other two rotor stacks, as shown in Fig. 3.36 (when originally all three rotor stacks are in phase with each other as are stack 1 and 3). This way of assembly (called the +z assembly for short) results in the same torque production from the middle stack (phase) but now the rotor fluxes of the different phases will oppose each other, and the leakage between phases will therefore decrease drastically. In fact the existing leakage seems to add to the torque production, as can be seen in Fig. 3.37 where the three-phase torques of the different rotor assemblies are compared (the original assembly and the +z assembly). The induced flux linkage will also be more symmetric, as shown in Fig. 3.38, as well as the cogging torque, as shown in Fig. 3.39. In fact, with this way of assembly, there is no longer any need for barriers between phases and the middle rotor parts can be attached directly to each other, or even be made as one part already at the manufacturing stage. If so, the rotor core would be built of four parts, where the two end parts are identical, and the two middle parts are also identical. Probably, the advantage of having six identical parts are greater though, as the cost of the tool of the pressing of the core parts is a large part of the manufacturing cost. Of course, there are drawbacks: The assembly of the rotor is made more difficult and the load on the bearings will be higher.

It should be noted that the results shown in Figs. 3.37 to 3.39 are calculated with an adaption tolerance of 5%, as the models are rather large. Because of this, the torque curves show some peaks that would be lower with an improved adaption tolerance. The results are however deemed adequate for the purpose of comparative study.

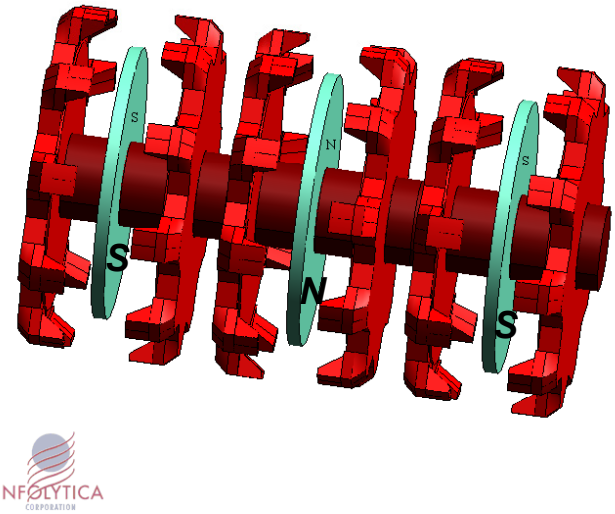

Figure 3.36: The middle rotor is rotated 180 electrical degrees relative to the other two rotors and the direction of magnetisation in stack 2 is the opposite of the magnetisation in phase 1 and 3. (The parts are separated in order to show the magnets clearly.)

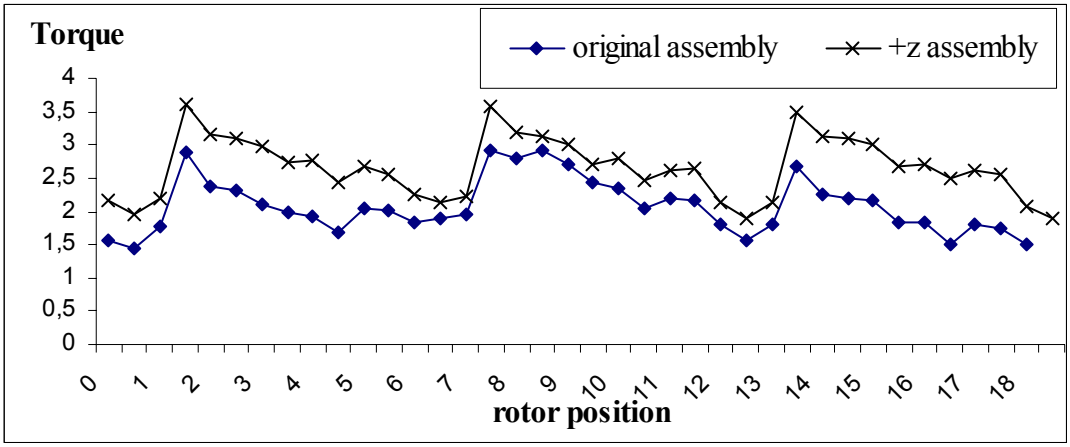

Figure 3.37: Calculated torque with two different rotor assemblies

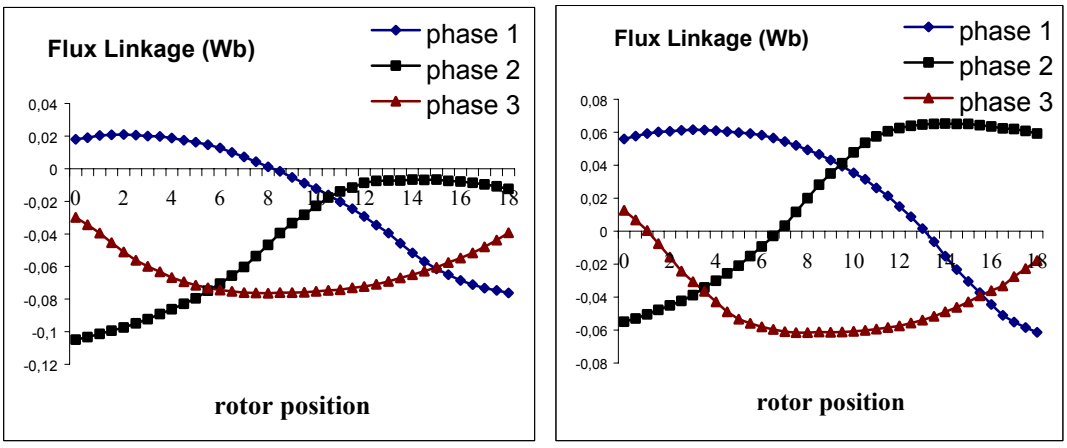

a) original assembly b) +z assembly

Figure 3.38: Calculated flux linkage with two different rotor assemblies.

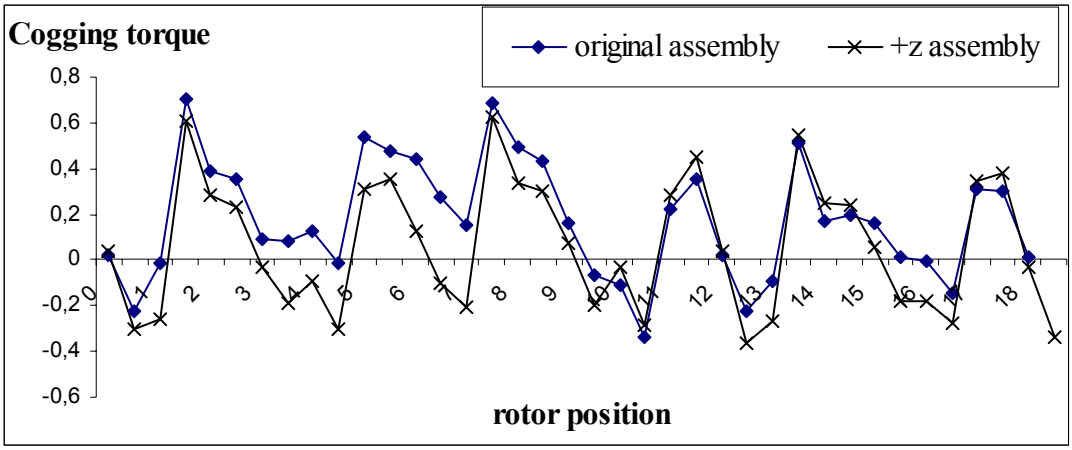

Figure 3.39: Calculated cogging torque with two different rotor assemblies.

3.4.2 D and L

Both the specific electric loadings and the output coefficient are proportional to the air-gap diameter, *D*. Therefore, in most cases; significant advantages accrue from designing for large diameter and small core length, *L*. In conventional, radial-flux, machines the pole-pitch (and the length of the end-connections) increases as the diameter increases but for claw-pole machines we do not have the problem of end-windings. One fact is true for all machines, the peripheral speed increases with increasing *D* but according to (Hamdi 1994), for small machines this should not cause any mechanical problems. Another fact is that the inertia will increase with D^4L. This might be a limiting factor for *D,* as machines for control system applications should have the smallest possible diameter (Hamdi 1994).

One limit on the stator core back is set by the materials' brittleness (when using soft magnetic composite) and not by risk of saturation. Similarly, the minimum magnet length and the maximum magnet radius are not only set by the required magnet mmf but also by the materials' brittleness.

3.4.3 Number of poles

As is stated earlier, a characteristic of claw-pole machines is that the number of poles can be increased, without decreasing the conductor volume, resulting in a high torque density. This is because the armature mmf remains constant when the number of poles is changed, as the full winding mmf appears across every pole (which is not the case in conventional motors). The problem with conventional motors is that the teeth and the slot cross sections are in the same plane. When the pole numbers increase, the teeth and the slot cross-section decrease. In a claw-pole motor, only the teeth (claw) cross section is affected (decreased) and the coil cross section is the same as for the lower pole number. Therefore, the pole number can be increased without decreasing the armature mmf. High pole number, however, gives less space between the stator- and rotor-claws at the rotor-positions where the rotor claws are approaching (or leaving) the stator claws. As these positions are the ones where the highest torque is developed, high pole number would result in high torque density. The upper limit of the number of poles is set by the leakage flux as a high number of poles leads to a smaller distance between the claws of opposite polarity and hence higher leakage flux. An optimum value of pole pitch exists and it depends on the stator design (Henneberger and Bork 1998).

A low pole number gives a high synchronous speed but this can be regulated with the frequency converter. More important is to keep the power factor at an acceptable value. This is because a low power factor demands a large, more expensive converter. Also, a large number of poles will give core constructions with long thin claws, which is not good because the SMC material is brittle. (The tensile strength of Somaloy^{TM}500 is 50 MPa (Höganäs) which can be compared to about 400 MPa for carbon steel (MPIF 1999)). A high speed gives a high output torque for a small volume of the active material. Therefore it is good with a high speed. However, a too high speed gives mechanical stresses in the rotor and higher iron losses.

Low working power factor seems to be the price that must be paid for the high specific output (at high pole number). The lowest power factor (about 0.35) is found in machines with surface mounted permanent magnets, whereas the machines with flux concentration have a power factor of about 0.55 (Harris, Pajooman et al. 1997). This is because the flux concentrated rotor has a superior magnetic circuit as the use of surface mounted magnets implies a larger effective air gap. A low number of poles would give low torque values but also a higher power factor. This is illustrated in Fig. 3.40, where the average torque and estimated power factor are shown for different pole numbers and excitation currents. In computing the results of Fig. 3.40, the pole phase profile and the claw angle/pole pitch ratio were kept constant as well as the frequency (with decreasing speed for higher pole numbers). Also, the volume of the cores is kept constant as the pole number is increased.

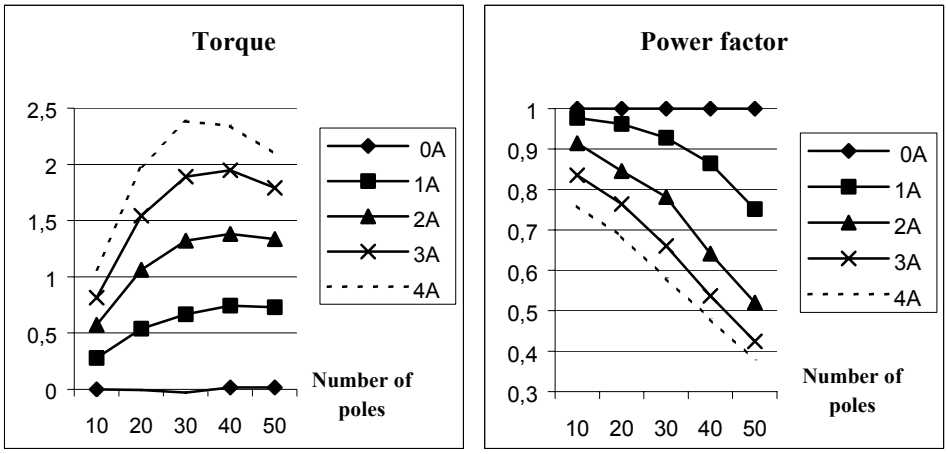

Figure 3.40: Average torque and power factor for different pole numbers and excitations.

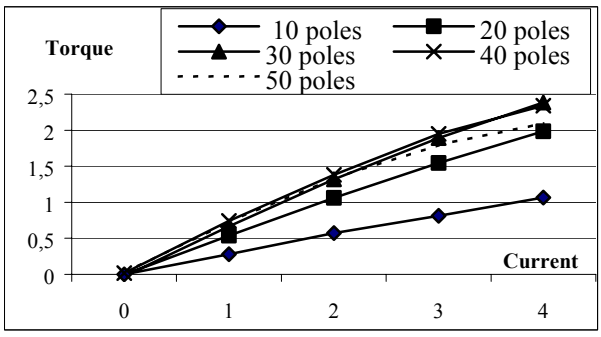

Figure 3.41: Average torque for different pole numbers and excitations.

In Fig. 3.40, it is seen that the power factor decreases and the torque initially increases and then stays constant or even decreases for increasing pole numbers. Two effects must be considered here: saturation and flux leakage. For higher excitations, there are saturation effects but only for higher pole numbers. Considering Fig. 3.41 where the ampere-turns are increased for constant pole numbers, the effect of saturation is clear. The saturation is noticeable for higher pole numbers even though the flux density in the core parts should be the same for all pole numbers (because of the equal core volumes and the equal mmfs). This can only be explained by the increased leakage between claws for the higher pole numbers. Thus the saturation in the claws enhances the claw-to-claw leakage. Hence, the reason to why the torque-increase stops for higher pole numbers at constant excitation current (in Fig. 3.40) is mainly due to the higher flux leakage between claws. However, when the saturation is worse, then the claw leakage is higher and this is the reason to the torque-decrease at high pole numbers in combination with high ampere-turns.

The power factor can be estimated by the ratio of *(the top flux linkage due to armature current acting alone)/(the top flux linkage due to magnet flux acting alone)* as is done in (Harris, Pajooman et al. 1997). A small ratio gives a better (higher) power factor. High leakage between claws will give less flux linkage due to magnet flux, because the magnet leakage flux will stay in the rotor and not link with the stator coil. Studying the armature flux, however, it is obvious that the leakage between claws in the stator only improves the flux linkage. Thus, the armature flux at peak current (when the claws are out of alignment) will increase with the pole number, and consequently, the power factor will decrease.

Fig. 3.42 shows core loss versus armature current characteristics as the number of poles is changed. These results are computed at a fixed frequency of 100 Hz. In the absence of stator excitation, the flux will be due to the magnet flux only, so when the pole number increases, the leakage between the rotor claws increases, increasing the rotor flux density and decreasing the flux linkage. Therefore, the value of the flux in the stator will become lower (and also the loss in the stator will be reduced) as the pole number is increased. However, at high excitation values, the larger number of poles implies a high claw-to-claw leakage in the *stator*, which improves the flux linkage. Around the unaligned positions (where the current is high and the influence of the magnet flux is low), the flux linkage is higher for higher pole numbers, and thus increases the stator losses (at those positions). The rotor claw-to-claw leakage still reduces the flux linkage due to magnet flux. So, in fact, the losses in the stator core will still decrease for higher pole numbers, as seen in Fig. 3.42, but the reduction is not so large as for zero excitation. Thus, as the pole numbers is increased, the stator loss will be reduced, for high excitation currents.

The cogging torque for different pole numbers is shown in Fig. 3.43. Reduction in the cogging torque values is observed. This can be explained by remembering that the cogging torque is calculated with stator excitation set to zero. As the claw-to-claw leakage in the rotor increases with pole numbers, the flux linkage (which is only due to the magnet) and the cogging torque decrease.

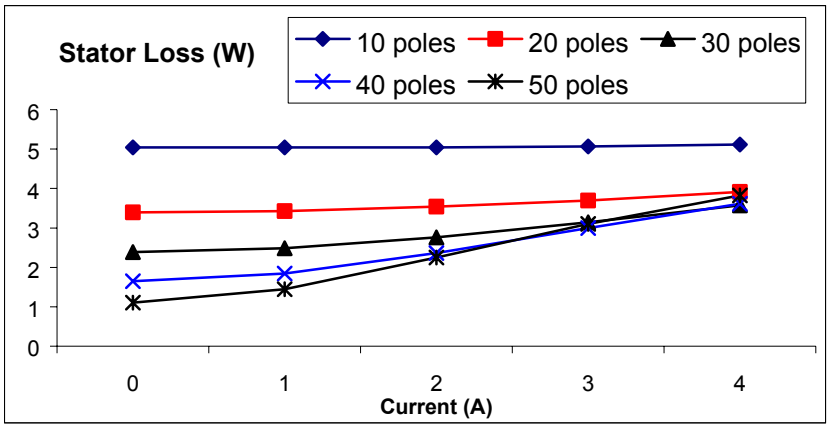

Figure 3.42: Loss data for different pole numbers and excitations.

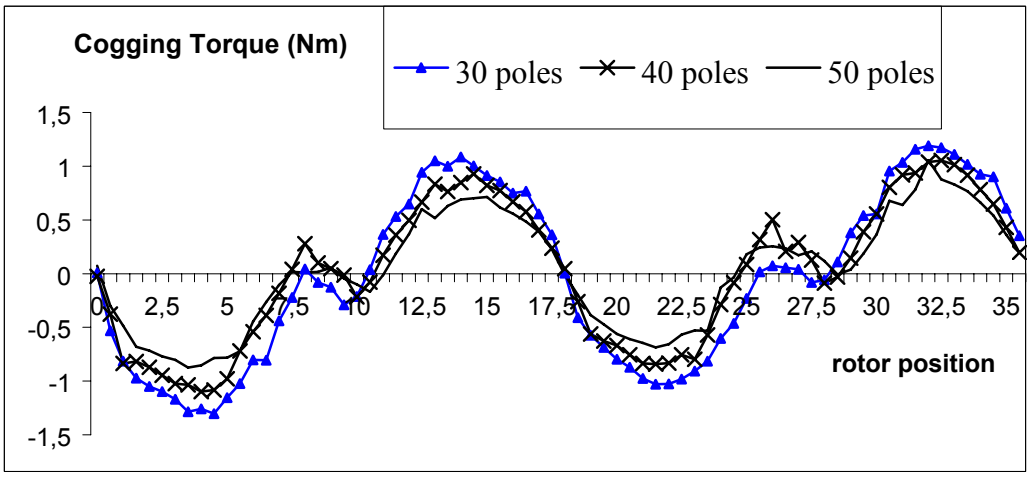

Figure 3.43: Cogging torque at no load for different pole numbers.

3.4.4 Magnet design

When the magnet is a ring magnet, axially magnetized, the remanence must be high. This is because the area of the magnet, A_m, cannot be so large compared to the air gap area, as the rotor is an inner rotor. The power factor would increase as the magnet radius is increased. This is because the magnet flux will be larger relative to the flux due to the stator coil, for a given current value. In order to achieve high torque density, a design value for the flux density in the air gap was set at about 1 T. This would necessitate the use of a high-energy permanent magnet material, such as NdFeB.

For a given air gap diameter, the magnet area, A_m, can be increased by reducing the shaft diameter. The shaft should be made as thin as possible (having enough mechanical strength to transmit the load torque). However, the magnet area (of a ring-shaped magnet) is more sensitive to changes in its outer diameter. If the magnet area is increased, the core parts need to be modified to be able to accommodate the increased flux without being saturated. Thus, for a given air gap flux, and a given magnet length, the minimum claw size and the minimum length of the core parts enclosing the magnet can be set. The length of the magnet can be varied to vary the working point (slope of static load line). The minimum magnet length is decided by the needed magnet mmf, and by manufacturing limitations.

As the rotor is of the inner type, the magnet area, $A_{m,}$ will be

$$A_m = \pi\left(r_o^2 - r_i^2\right), \tag{3.8}$$

where r_o is the outer radius of the magnet and r_i is the inner radius which is equal to the shaft radius.

For a one-phase stack, the air-gap area per pole is

$$A_g = l_{sc} r_s \beta \tag{3.9}$$

where l_{sc} is the stator claw length, r_s is the inner radius of the stator and β is the overlapping angle of the claws.

From Gauss' law of the magnetic flux (div **B**=0), and from Ampere's law of circulation (curl **B**=μ_0 **J**), the following two equations can be used for the magnet design:

$$B_m A_m = B_g A_g K_l \tag{3.10}$$

$$H_m l_m = H_g l_g K_r \tag{3.11}$$

where the magnet flux B_mA_m is the product of the flux density and the area of the magnet. The air gap flux B_gA_g is the product of the flux density and the area of the air gap, and K_l represents the leakage flux. The magnet mmf H_ml_m is the product of the field intensity and the length of the magnet. The air gap mmf H_gl_g is the product of the field intensity and the effective length of the air gap, and K_r is the reluctance factor, representing the mmf drop in the core.

The magnet's working point is determined, mainly, by its dimensions together with the air gap dimensions. In Fig. 3.44 two operating points are shown and their meaning is now discussed.

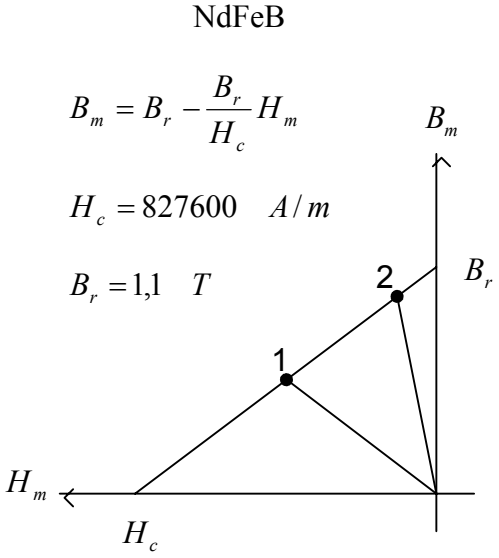

Figure 3.44: Magnet characteristics. The magnet length in point 1 is less than in point 2.

If, for example, we consider a one-phase motor with 20 poles with a claw angle of 10 mechanical degrees, a claw length of 20 mm, and the inner radius of the stator is 45 mm then the air-gap area at the aligned position will be 3141.6 mm^2. Assume 0.8 T in the air gap and a reluctance factor of 1.2, then H_m can be calculated from: $H_m = \frac{H_g l_g K_r}{l_m}$. If we aim for an operating point that gives H_m a value at about half the coercivity (as this yields minimum magnet volume), then l_m would be 1.1 mm for a 0.3 mm air gap. The magnet operating flux density, B_m, would be 0.55 T (working point 1 in Fig. 3.44).

If we now assume a leakage factor of 2 (50% leakage), and a shaft radius of 5 mm, we will need the outer radius of the magnet to be $r_o = \sqrt{\frac{B_g A_g K_l}{\pi B_m} + r_i^2}$ =54 mm. This is not realistic for two reasons; l_m is too small (giving a brittle magnet), and the outer radius of the magnet is too large (larger than the inner radius of the stator). With the more reasonable value of the magnet length of 4 mm (B_m=0.95 T), the outer radius of the magnet needs to be 41 mm (working point 2 in Fig. 3.44).

The performance can be improved by increasing the air gap between the rotor claws and the rotor core (at the expense of the outer radius of the magnet). As this decreases the rotor leakage, the magnet area can be made smaller without loosing performance.

To demonstrate the effect of varying the magnet length on performance, the magnet length and the rotor core were varied and while keeping all other parameters constant, the motor's performance (torque and power factor) was computed at rated current. The results are shown in Fig. 3.45. For a short magnet (l_m=0.5 mm), the flux linkage is nearly sinusoidal (yielding a sinusoidal back emf) but for all other magnet lengths, saturation occur in the rotor core side parts and in the claws. It can be seen that increasing the magnet length more than l_m=1.5 mm will give little change in torque and power factor due to saturation, for this specific design. If it were not for manufacturing reasons, the choice might be l_m=1.5 mm instead of l_m=2.0 mm (at this value of ampere turns). Of course, at higher currents the saturation will be more severe. Also, the core losses increase with magnet length, due to the increased mmf in the core.

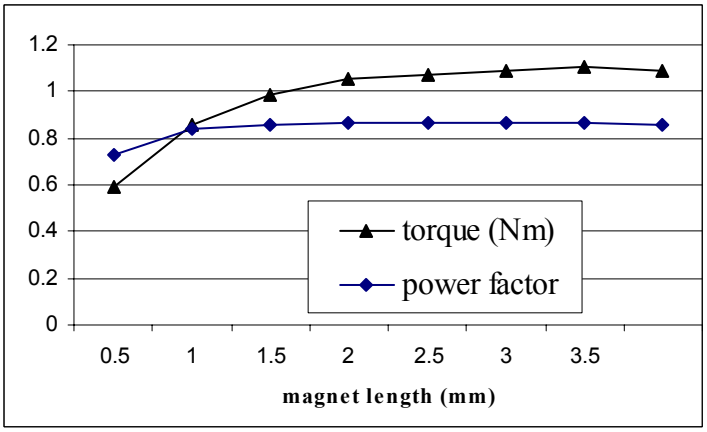

Figure 3.45: Effect of varying the magnet length on the torque and power factor.

If the length, L, is increased, the rotor parts can be made thicker, avoiding saturation in those parts. This increases the torque. Consequently, if L is decreased, the torque is also decreased. This is true for small (reasonable) values of l_m. However, for large values of l_m, saturation will occur just as is illustrated in Fig. 3.45. Additionally, increasing L and l_m may give larger torque but also less torque density due to the increased volume. Additionally, the power factor decreases as the length of the active parts L, is increased. This is due to the relatively larger air gap area, A_g, compared to the magnet area, A_m. Because of this, rounded-off claws could be advantageous, as is discussed in Section 3.4.5. Thicker claws (in the radial direction or in the circumferential direction) also allow a larger magnet length, l_m, to be used without causing saturation.

The result above is applicable to the design in which there is one rotor with one ring magnet to give flux to three stator stacks. With such a design, the magnet can be made longer, but not longer than necessary. However, this design has some major disadvantages, namely, its long thin (brittle) rotor claws (the length of the rotor claws must be enough to lead flux to the stator claw furthest away), and the inter-phase leakage.

The magnet relative permeability is close to 1 and it thus acts as a large air gap in the rotor. However, most of the armature flux only passes the rotor claw and never enters the back core, thus never crosses the magnet. The demagnetising effect of the armature field does not cause a problem if the magnet is a ring magnet inside the rotor as the rotor will rotate at synchronous speed and there will only be high eddy currents on the rotor surface, depending on the rotor core material. At the aligned position, when most of the stator-induced flux would be lead through the magnet, the current is zero, and at the out of alignment position all flux pass through the rotor claws only. (This is comparable with the magnet flux that only passes through the stator claws around the unaligned positions.) Therefore, the only time the stator flux may pass through the magnet is when the claws are in between the aligned and the unaligned positions (at about 45 and 135 electrical degrees in Fig. 3.46).

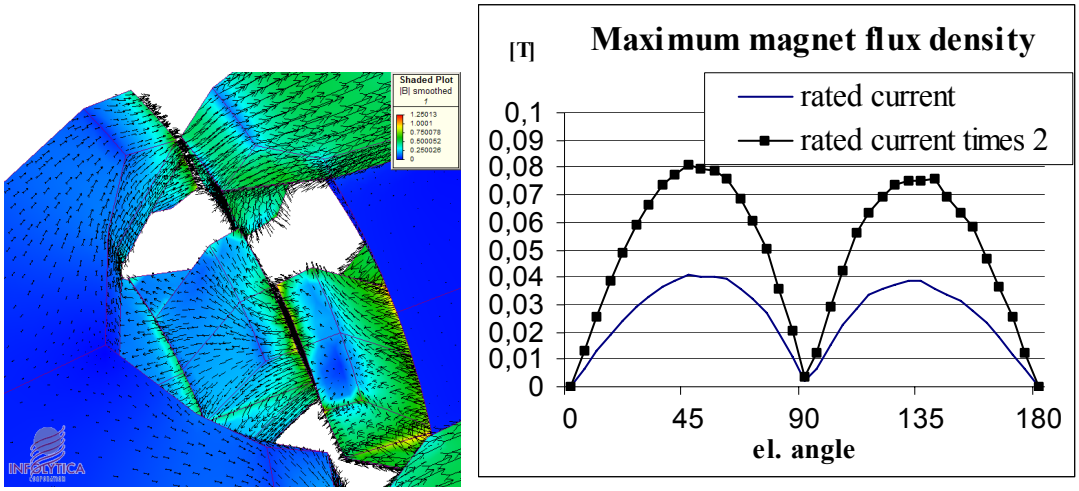

Figure 3.46: Armature reaction. Left picture showing the armature flux from one stator claw to the opposite stator claw mainly through the rotor claw in between the stator claws (only a small part of the flux enters the magnet). The rotor position is that of 45 electrical degrees. The graph (to the right) shows maximum flux density in the magnet for rated current, and rated current times 2.

In fact, as the magnet is thicker than the air gap between stator and rotor claws, even at the positions between alignment and non-alignment, only a fraction of the armature-induced flux will pass the magnet. This can be seen in Fig. 3.46 (left), showing such a rotor position, and the armature flux when the magnet is replaced by air (from a two-pole-pitches model).

In Fig. 3.46 (right), the maximum value of the flux density within the magnet due to armature reaction are shown, both at rated and twice the rated current. It is seen that only a small part of the armature flux will reach the magnet. This means that there is no risk of demagnetisation of the magnets due to the armature reaction field.

If only the magnet radius, r_m is varied with all other dimensions kept constant, it can be said that changing r_m to as low as 28 mm (from 34 mm) does not give a large change in the power factor or of the torque, as shown in Fig. 3.47. This implies presence of saturation in the core parts. To investigate this further, the rotor radius is varied just like the magnet radius. Thus, if the magnet radius is set to 40 mm instead of 34 mm, then the other radiuses (all but the shaft) also are made 6 mm larger. This obviously means a larger motor (with a larger diameter) and larger core parts. However, if the torque density is compared instead of the torque, the investigation would be meaningful. The result is shown in Fig. 3.48 for a 30-pole motor.

It is seen that there is no increase in the torque density beyond a magnet radius of about 32 mm. This is due to saturation in the cores. In order to avoid this, the cores should be made even thicker as the diameter is increased (for instance by increasing the axial lengths of the core parts). However, it should also be noted that the stator core volume increases more than the rotor core volume as the radius is increased. Also, the stator winding needs to be longer, for the same cross section of the coil. Therefore, the material is better used for the designs with smaller radiuses.

Fig. 3.48 also shows that the power factor increases with increasing magnet radius. This is because the magnet flux will be larger relative to the flux induced by the stator coil.

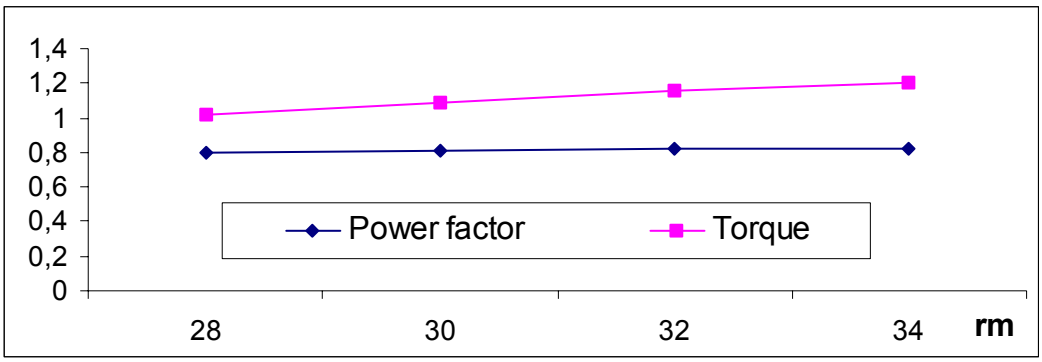

Figure 3.47: Torque and power factor in a 30-pole motor with rounded claws and different magnet radius (at 2 A).

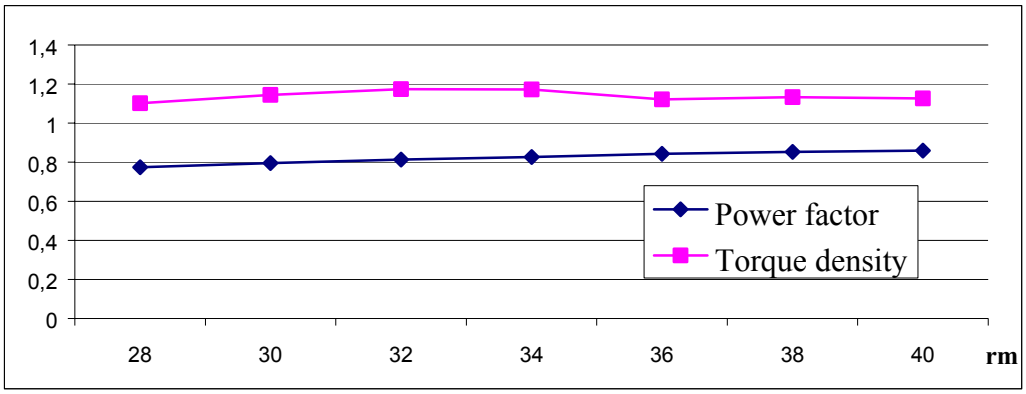

Figure 3.48: Torque density and power factor at rated current in a motor with rounded claws and different magnet radius and other radiuses. The number of poles is 30.

3.4.5 Pole-face profile

Claw shape

The overlapping regions between the stator and rotor claws must be independent of rotor position in order to ensure symmetry of the flux linkage. In Fig. 3.49, claw shapes that do not give the same overlapping regions for all rotor positions are shown (stator claw at top). When the rotor claws (bottom) are aligned with the stator claws at the same side of the stack, then the overlapping area is larger than when claws on opposite sides are aligned. The claw shape should be so chosen that the highest flux linkage (and thus emf) and the highest average torque are obtained. Some of the claw designs are shown in Fig. 3.50.

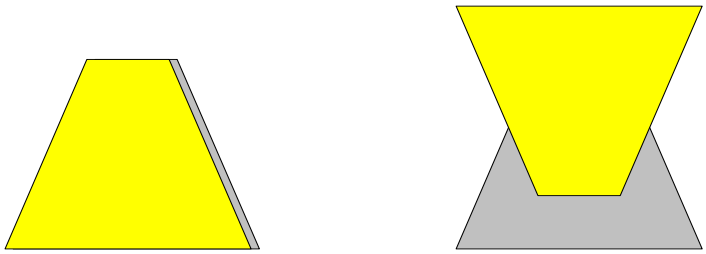

Figure 3.49: Claws on the same side aligned (left) and claws on opposite side aligned (right).

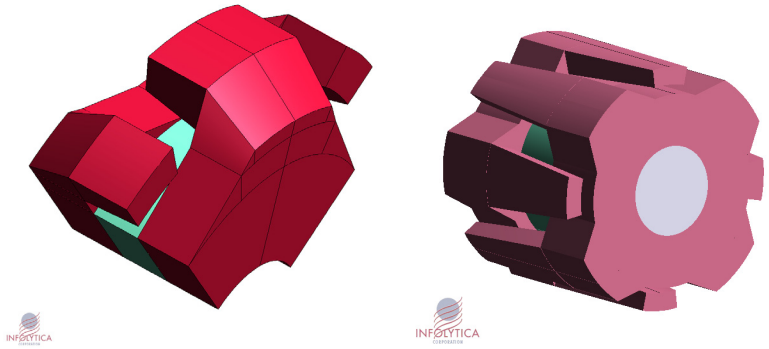

Figure 3.50: Short straight rounded claws (left) and long tapered claws (right).

Four different designs, based on the topology of Fig. 3.50, are investigated. In the absence of stator excitation, the magnetic flux distribution due to the rotor permanent

magnet is obtained, in each case, by solving the non-linear magneto-static field problem.

The waveform of the flux linking the stator winding is then determined and plotted, for the different designs, as shown Fig. 3.51. It is seen that the designs that have the same overlapping areas of claws yield symmetrical flux linkage waveforms. The two designs are short, straight rounded claws and long, straight claws. If the claws are tapered and rounded, a slight change in flux linkage can be seen, and a larger cogging torque is obtained. The results are even worse if the claws are short and tapered (and not rounded).

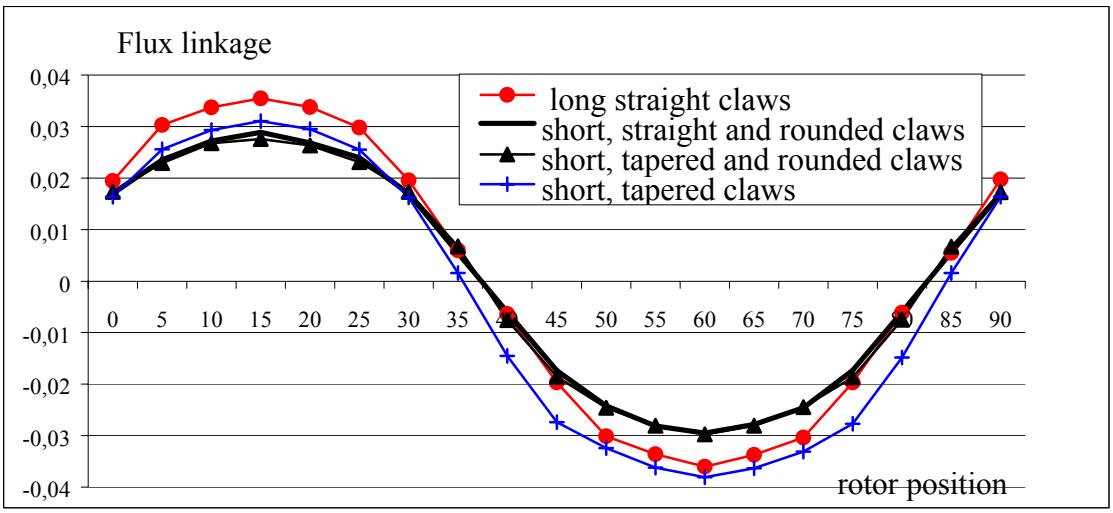

Figure 3.51: Stator flux linkage at no-load for different rotor claws

The two best designs of the pole face profile are investigated further, and compared to each other. These are designs with short, straight rounded claws and long, straight claws. For simplicity, these designs are referred to, here, as *rounded claws* and *long claws* (the two designs are also illustrated in Fig. 3.6). The long claw designs offer the advantage of large area, avoiding saturation, but the three phases will be close to each other and the phase-to-phase leakage will be larger than in the rounded claw designs. The rounded claw shape allows the use of coils with circular cross sections and it avoids sharp corners in the core. This also increases the air space between the claws of different phases (and for the stator core parts if the stator is made shorter than the rotor). The extra barriers lead to less leakage between phases, less core material, and better cooling. Shorter claws also give a better, stronger, design, which is important when using SMC material.

Of course, the design of the soft magnetic core affects the dimensions of other motor parts. For example, the case of a single-phase motor is considered. The number of poles is assumed to be 20, with a claw angle of 10 mechanical degrees. For an air gap radius of 45 mm, a long claw design (not rounded) having a claw length of 20 mm would yield an air-gap area at the aligned position of 3142 mm^2. With shorter claws (rounded) with a claw length of 10 mm, the air gap area would only be half as much. This means that the magnet area can be halved, compared to the long claws design, and still give the same flux density in the air gap. However, this would only be true if the leakage factor is the same for both cases, which is not probable. More likely, the leakage (and saturation) is larger for the rounded claw version, implying that the

magnet area would be smaller but not as much as half the value of the magnet area for the long claws.

Even if short claws and small magnet radius give about the same flux density in the air gap (as long claws and large magnet radius), the torque values will not be the same. This is because the active air gap area will be smaller for the short-claw case. Even so, the smaller design would give a reasonable torque density due to the smaller volume.

To investigate the torque values, the claw length and the magnet radius are varied. The claw length is varied between 8 mm and 20 mm, where 20 mm is the stack length. When the magnet radius is varied, the other radiuses are varied accordingly. Thus, a design with a large magnet area has a larger volume than a design with a small magnet area. The outer diameter is allowed to exceed the value of 115 mm, which is the value of the SMC blanks that are used to build the experimental and prototype machines. The aim of such a study is just to provide a clearer picture of the variations in torque. In this study, other dimensions are kept constant. However, the dimensions assumed are not exactly as assumed in other investigations in this chapter, as the magnet length is 4 mm and the claws are thicker to allow the use of such a long magnet without causing saturation.

The results are shown in Fig. 3.52 for a 20-pole motor. It can be seen that short claws give less torque density than long claws. The best value seems to be a claw length of about 16 mm, which is 80% of the stack length. Longer claws than that only add material that is not so useful. When it comes to the choice of magnet radius, the results are not so easy to translate into firm conclusions. Different magnet radiuses seem to give similar results of the torque density. However, for the claw length of 16 mm, the magnet radius of 32 mm seems to give the best torque density but choosing a magnet radius of 28 mm only decreases the torque density by about 4%.

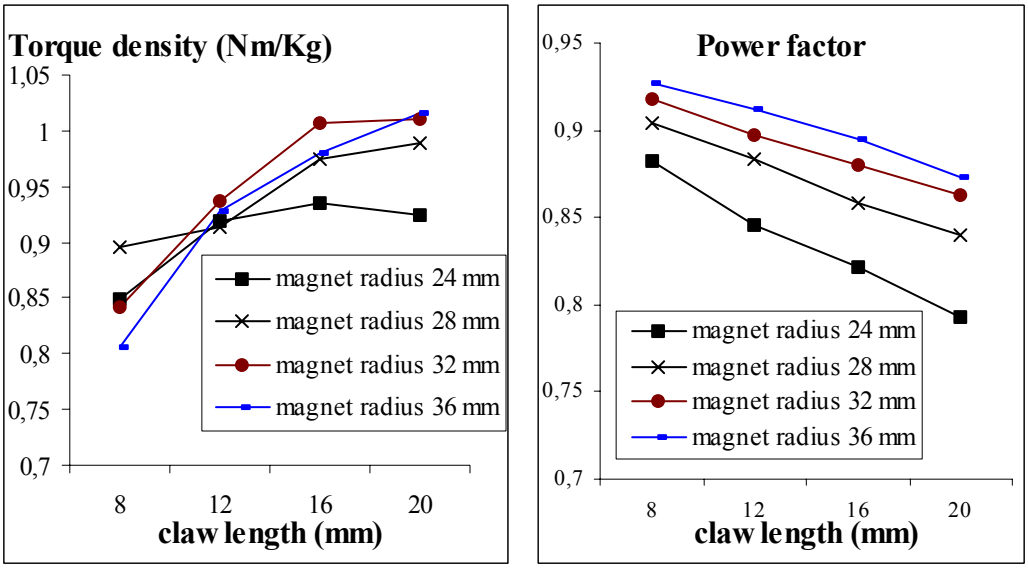

Figure 3.52: Torque density and power factor in a motor with rounded claws and different magnet radius (and other radiuses). The number of poles is 20. The claw length varies from 8 mm to 20mm (where 20 mm equals the stack length).

As seen in Fig. 3.52, the highest power factor is obtained when short claws are assumed. This is reasonable as the air gap area will be smaller for smaller claws, giving a relatively larger magnet area (and air gap flux density). Additionally, if the claws are made short, relative to the stack length, the cores would carry more flux and may become saturated. The reluctance of the claws would also increase, due to a smaller cross section area, and there will be more leakage, so the flux linkage will consequently decrease for shorter claws. Therefore, the peak flux linkage due to armature current acting alone, $\hat{\psi}_s$, and the peak flux linkage due to magnet flux acting alone, $\hat{\psi}_m$, would both be lower for short claws (due to the increasing reluctance), which may imply a lower power factor (than for long claws). However, the decrease of $\hat{\psi}_s$ is relatively larger than the decrease of $\hat{\psi}_m$, and the power factor would be increased (for shorter claws).

Considering the power factor alone, the claws should be short and the magnet radius large, in order to get the best power factor (in case shown in Fig. 3.52, a claw length of 8 mm and a magnet radius of 36 mm yield a power factor of 0.93). However, this is the condition that gives the lowest torque density.

Improving the torque density by reduction of material

Some parts of the core carry very little flux, as shown in Fig. 3.53 (the dark (blue) parts). In order to improve the torque density, these core parts can be removed. One suggestion to achieve this is shown in Fig. 3.54. A solution assuming 30 poles, 2A, and a magnet radius of 32 mm, gives a torque density of 1.15 Nm/kg at a power factor of 0.81. This is a small improvement compared to the same model but without taking away any core material (which gave 1.10 Nm/kg at the same power factor of 0.81). Examination of Figs. 3.53 and 3.54 shows that the core parts could be further improved. For instance, the rotor core should be made thicker close to the claw and thinner (in steps) close to the shaft. Obviously, the shaping of the core parts also depends on the limitations of the production of the core material. This is further discussed in Chapter 4.

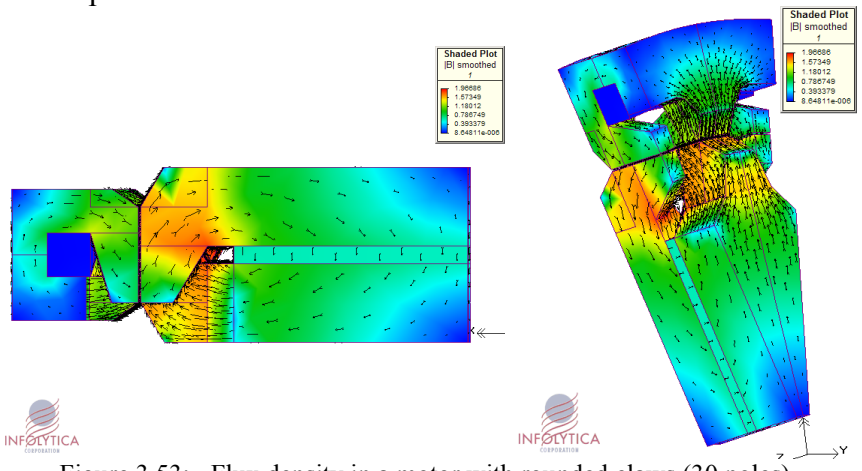

Figure 3.53: Flux density in a motor with rounded claws (30 poles).

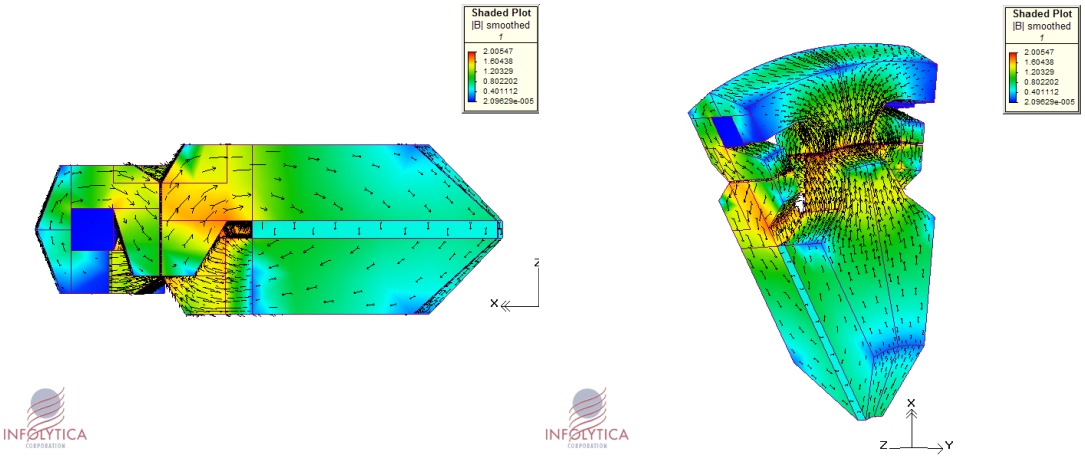

Figure 3.54 Flux density in a motor with rounded claws and rounded core parts (20 poles).

The effect of the spacing between the claws

The effect of the spacing between the claws on the leakage flux is investigated. This is achieved, here, by varying the claw angle relative to the pole pitch. The angles are varied from 44% to 78% of the pole pitch (cases 1 to 7). The pole phase profile is kept constant apart from the claw smoothing angles (see Fig. 3.7). The claw smoothing angles are varied as the claw angle varies, keeping the sum of the claw angle and the claw smoothing angle constant. This is done in order to get an acceptable claw smooth for all claw angles at all pole numbers. (Otherwise, if the claw-smoothing angle is too large at large claw angles, the claws will coincide, and if the claw-smoothing angle is too small at small claw angles, there will be problems with the model accuracy.)

The results of the torque, power factor and loss are given in Fig. 3.55, where the results are shown for a 20-pole one-phase motor with long claws. Just as when the number of poles was decreased, the larger air gap between claws gives less torque and less leakage. Thus, a smaller air gap (thicker claws) gives more torque up to where the leakage becomes too high and the torque again starts to decrease. There is definitely an optimum value at which the torque is at a maximum.

As seen in Fig. 3.55, case 3 (a claw angle that is 56% of the pole pitch, or 10 mechanical degrees) seems to be a good choice for the investigated motor. The same results are found for other pole numbers as seen in Fig. 3.56. However, the peak torque value occurs at different claw angles, depending on the assumed pole number. It can be said that relatively smaller claw angles are better choices for the high pole numbers.

Considering the power factor, the claw angle should be small for all investigated pole numbers and it is found that, for a given design, it is only the 10-pole motor and the 20-pole motor that can give a power factor as high as 0.9. If a power factor of 0.8 is acceptable, then the number of poles could be increased to 30, and the claw angle should be as in case 2 (namely, 6 mechanical degrees which is half the pole pitch). There is little to be gained from designing with higher pole numbers than 30 (for the topology examined here). This is because with higher pole number, the torque would only increase slightly, or even decrease, and the power factor would be significantly reduced.

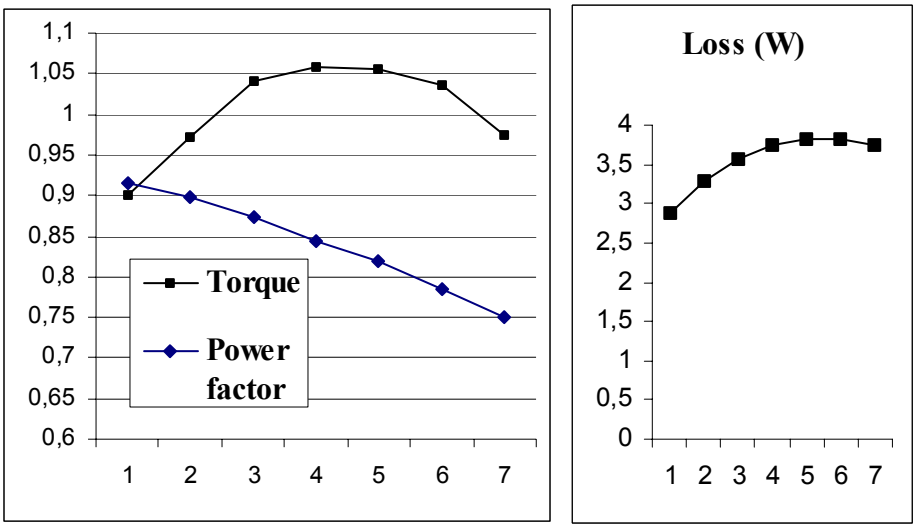

Figure 3.55: Average torque and stator core loss per phase and power factor as the claw angle varies.

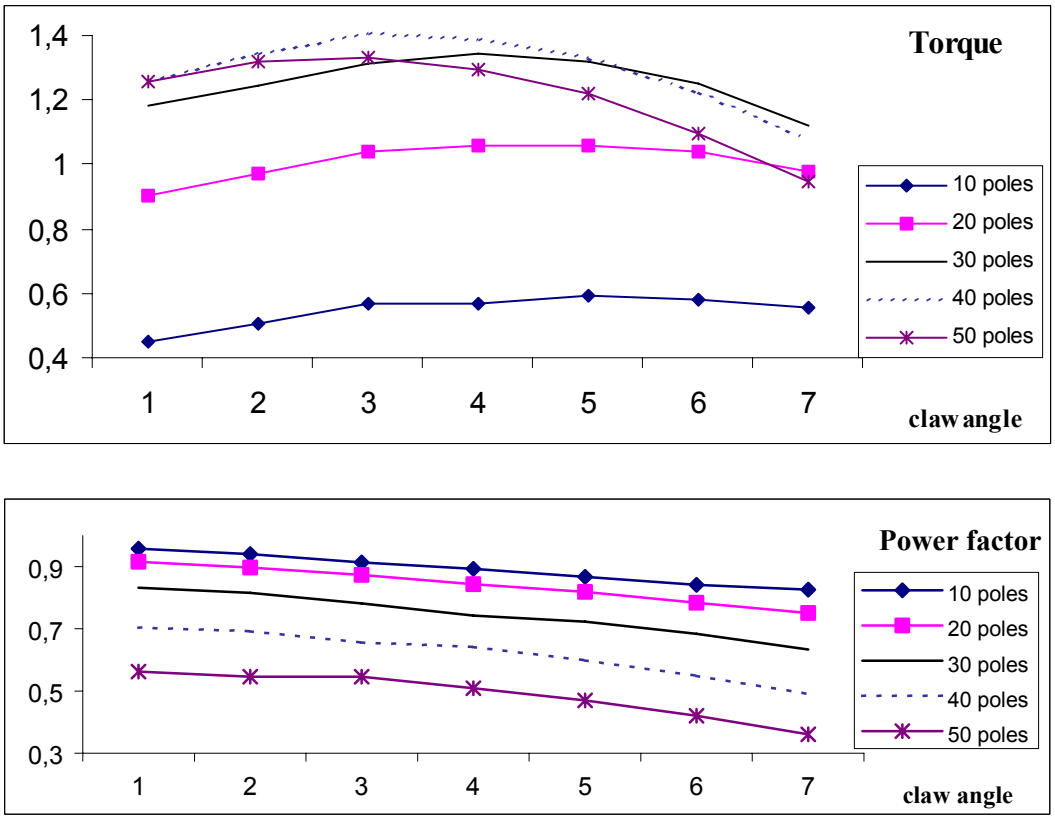

Figure 3.56: Average torque per phase and power factor as the claw angle and pole number varies. The current is 2A.

For a 20-pole design, the distance between claws would be about 8 mm (depending on the thickness of the claws). This distance is much larger than the air gap (0.3 mm). Because of this, the leakage effect would not be so dominant, even for thicker claws. For instance the claw angle of 14 degrees (the thickest possible) with 20 poles give a distance between claws of 3.14 mm which is ten times the air gap. The power factor improves for smaller claw angles, just as it does with smaller claw lengths.

Claw smoothing angles

The claw angles can also be varied (smoothed) in the radial position. This gives a possibility to avoid the sharp corners of the claw, thus the torque can be increased. It is found that there is an optimum value of the claw smoothing angles concerning the developed average torque just as there is an optimum value of the claw angles. The same reasoning applies. If the air gap between the claws is made too small, the leakage between claws increases, and the torque decreases. If the claw smoothing angles are made too small (giving a large air gap between the claws), the sharp corners of the claws restrict the main flux, and the torque decreases. Somewhere in between, the maximum torque is obtained. Two examples of this are given in Fig. 3.57, for a case with 20 poles and claw angles of 10 (the trace labelled claw angle 3) and 12 (the trace labelled claw angle 5) mechanical degrees. It is evident that claw smoothening has an advantageous effect on torque production, and that there is an optimum value of the claw smoothening (as far as the power factor and the produced electromechanical average torque are concerned). It is seen in Fig. 3.57 that the power factor improves with claw smoothing but it does not vary much as the smoothing angle is changed. The low power factor, in the absence of claw smoothening, is due to the increased reluctance of the magnet induced flux path.

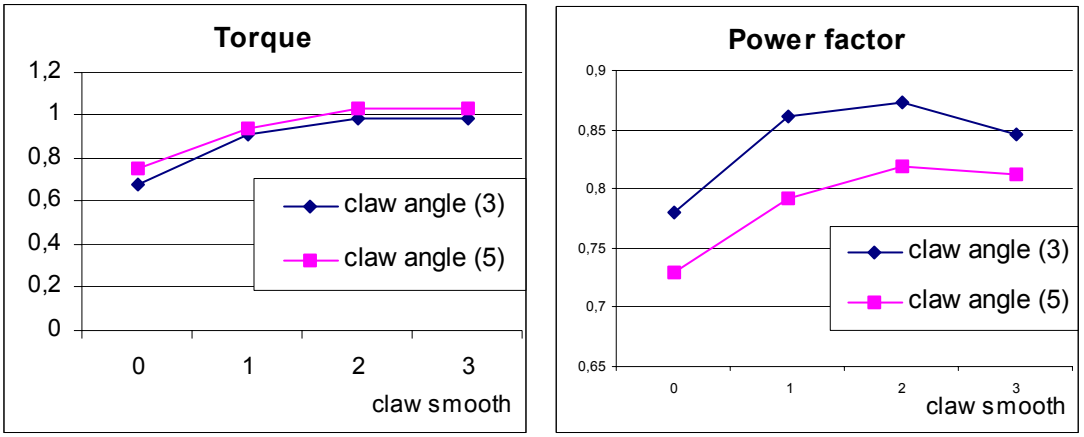

Figure 3.57: Claw smoothing is varied (for a 20 pole motor). Point 0 shows the torque and the power factor at no claw smoothening, and then the claw smoothening angles are increased up to point 3, which have the highest possible claw smoothening angles (avoiding that the claws coincide).

3.4.6 Air gap length

A small air gap demands high tolerances on the rotor and stator parts. With a rotor with surface mounted magnets, using a large air gap is not so detrimental. This is because the magnets appear as an additional air gap for the stator flux, so the effective air gap that the stator flux has to pass is the sum of the mechanical air gap and the radial magnet length. With flux concentration, it is more important to have a small air gap. However, also in such a topology, the magnets appear as an additional air gap for some of the stator flux but only a small fraction, as shown in field plot of Fig. 3.46.

The torque is expected to increase when the air gap decreases, and this effect can be seen in Fig 3.58. (Increasing all stator radiuses accordingly, increases the air gap.) The power factor decreases slightly for the decreasing air gaps, but the change is so small that no certain conclusions should be drawn from this fact. However, it could be noted that when the air gap decreases, the reluctance of the main flux path decreases,

and the linked flux increases. For the investigated air gap lengths, the increase of the peak stator flux, $\hat{\psi}_s$, is relatively larger than the increase of the peak magnet flux, $\hat{\psi}_m$, resulting in a small reduction of the power factor.

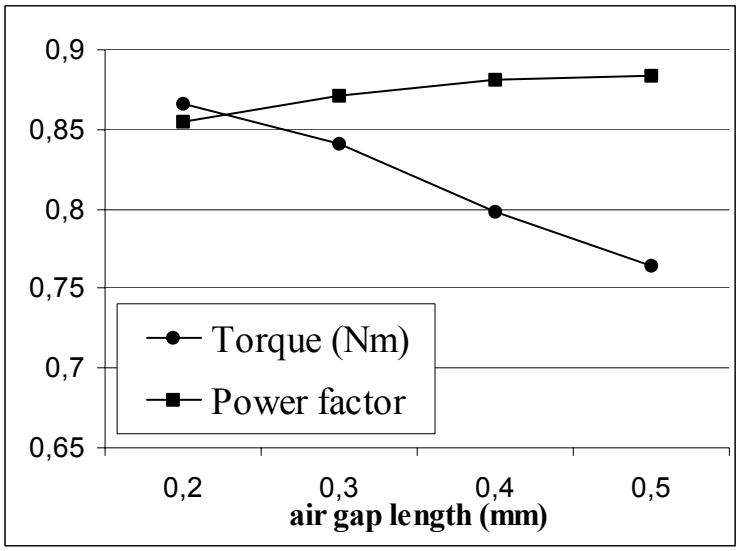

Fig 3.58: The average torque and the power factor as the air gap change for a one-phase motor with 20 poles.

3.5 Equivalent circuit

In normal operation, the TFM is driven as a brushless drive. For the claw-pole motor with salient rotor poles, the motor should be designed to give sinusoidal flux linkage, and consequently it can be excited with sinusoidal voltages. There is also the option to feed the motor with square-shaped currents, which could actually give a higher torque, but this is not investigated in this thesis.

The same equivalent circuit of the synchronous motor can be used for the claw-pole motor to predict the performance, according to (Guo, Zhu et al. 2002) and (Harris, Pajooman et al. 1997); see Fig. 3.59.

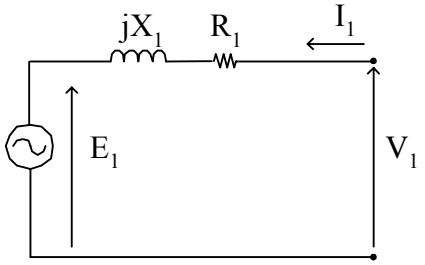

Figure 3.59: Simple equivalent circuit of a claw-pole motor (Guo, Zhu et al. 2002).

E_1 and X_1 can be determined from FE calculations. R_1 can be calculated from material data and winding details. When surface magnets are used, there will be no rotor saliency, so that $X_d=X_q=X$. However, if the motor has salient poles the reactance will vary with rotor position. Also, as the current is increased, saturation will eventually occur, and the reactance will decrease. There will also be deviations as the leakage reactance varies with current. Therefore, the reactance value must be

calculated for each current (and frequency) value. A more detailed equivalent circuit (for a transverse flux motor) is proposed in (Rang, Gu et al. 2002), where the resistance due to the core losses, and the leakage reactance are included. This is illustrated in Fig. 3.60.

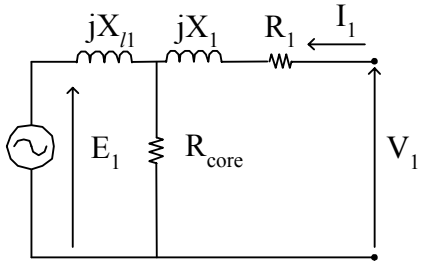

Figure 3.60: Equivalent circuit of a transverse flux motor (Rang, Gu et al. 2002).

In normal operation, position controlled switching of the inverter is employed, so that the phase of the stator current in relation to open-circuit back emf (induced by the magnets) may be adjusted as required. The phase advance angle, γ (the angle between I and I_q) can then be varied to obtain a phase current in phase with the back emf (γ=0). This will give maximum torque for a given current, as illustrated by the phasor diagram of Fig. 3.61.

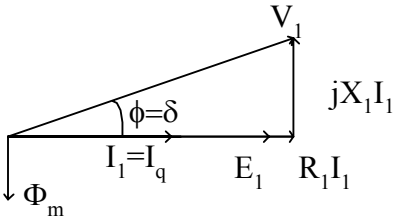

Figure 3.61: Equivalent circuit of a transverse flux motor driven as a brushless drive with phase advance angle, γ=0.

The rated line-to-neutral rms voltage is found from

$$V_1 = \sqrt{\left(E_1 + I_1 R_1\right)^2 + \left(I_1 X_1\right)^2} \tag{3.12}$$

The power factor is found from

$$\cos\phi = \left(E_1 + I_1 R_1\right)/V_1 = \cos\left(\arctan\left(I_1 X_1 / \left(E_1 + I_1 R_1\right)\right)\right) \tag{3.13}$$

In (Harris, Pajooman et al. 1997) they show that the power factor can be estimated by the simple ratio of *(reactive voltage drop on full load)/(open circuit back emf)* or I_1X_1/E_1. This is equal to *(the peak flux linkage due to armature current acting alone)/(the peak flux linkage due to magnet flux acting alone)*= $\hat{\psi}_s / \hat{\psi}_m$. Then, the power factor is found as cos (arctan ($\hat{\psi}_s / \hat{\psi}_m$)). They neglect the voltage drop due to the stator resistance and the saliency effect. They also state that the operating power factor may be significantly below this value if appreciable saturation is present at full load.

To obtain a power factor of 0.9, the I_1X_1/E_1 ratio should be 0.5, thus the magnet flux should be twice that of the armature flux. For small values of the reactance (at low speeds), neglecting of the resistance will lead to large errors, as was seen in Section

3.3. A more accurate value could then be obtained with the aid of Eq. 3.13. Both methods of calculations, however, neglect the saliency. This of course introduces errors when considering claw-pole motors, especially those with salient rotors. However, considering the saliency effect does not complicate the calculations, as the current in the direct position, I_d, is zero (when the rotor and stator are aligned). Because of this the reactance value $X = X_q$ should be used in the calculations. In fact, the method of (Harris, Pajooman et al. 1997), use $\hat{\psi}_s$ instead of X, and as $\hat{\psi}_s$ is calculated at the unaligned position (where $X = X_q$), it can be said, therefore, that this method do take the saliency into account.

According to (Harris, Pajooman et al. 1997) there is a way to improve the power factor. Employing a phase advance angle, for a given current, I_1, the torque producing current, I_q, will be smaller but the power factor may be higher (although this does not work well for motors with already low power factors). The phasor diagram illustrating this is shown in Fig. 3.62.

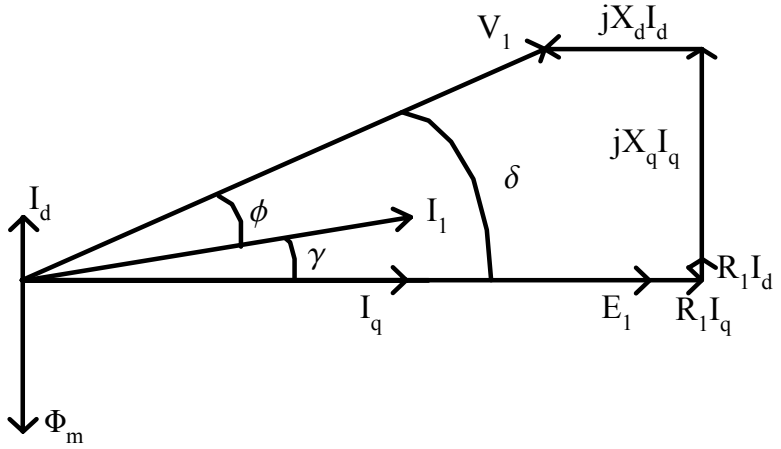

Figure 3.62: Equivalent circuit of a transverse flux motor driven as a brushless drive with phase advance angle, $\gamma > 0$.

With an open loop control, the motor can operate in the normal synchronous mode. Then, the phase advance angle cannot be controlled, and the electromagnetic power and torque versus the load angle can be derived as described in (Guo, Zhu et al. 2002) as follows:

$$P_{em} = m_1 E_1 I_1 \cos\gamma = \frac{m_1 E_1 \left[V_1 \left(R_1 \cos\delta + X_1 \sin\delta \right) - R_1 E_1 \right]}{R_1^2 + X_1^2} \tag{3.14}$$

$$T_{em} = \frac{P_{em}}{\omega_r} \tag{3.15}$$

where m_1 is the number of phases, γ the phase advance angle between E_1 and I_1, ω_r the rotor angular speed in mechanical radians per seconds, and δ is the load angle.

With closed-loop control of position feedback it can also operate in the brushless DC mode where the current I_1 and the induced emf, E_1 in the stator winding are in phase, to achieve a maximum electromagnetic power P_{em} at a given speed, then:

$$P_{em} = m_1 E_1 I_1 \tag{3.16}$$

The output power is $P_{out} = P_{em} - P_{core,rotor} - P_{mech}$ (3.17)

The input power is $P_{in} = P_{em} + P_{cu} + P_{core,stator}$ (3.18)

$$T_{out} = \frac{P_{out}}{\omega_r} \tag{3.19}$$

At a given voltage input, the steady state characteristics can be predicted by:

$$\omega_r = \frac{V_1}{K_e} - \frac{R_1}{K_e K_T} T_{em} \tag{3.20}$$

where K_e is the back emf constant. K_T is the torque constant. And T_{em} is the electromagnetic torque (Guo, Zhu et al. 2003).

4 Design of a claw-pole servomotor

4.1 Introduction

The objective here is to design a motor (Mark 1) that is comparable in performance to a brushless dc machine, but less expensive to manufacture. The power factor should not be below 0.9, so that a standard drive can be used. Due to this, it is accepted, from the outset, that the torque most likely will have to be lower than otherwise obtainable from TFMs (reported figures for TFMs are about 20 Nm/kg according to (Maddison, Mecrow et al. 1998), (Harris, Pajooman et al. 1997) and (Henneberger and Bork 1998) compared to 2 Nm/kg of a servo machine of the same size).

The intended application is as a standard servomotor to operate at 3000 rpm or, if possible, higher, with a frequency of about 400 Hz. The target efficiency is about 0.8 pu, which is normal for a brushless dc machine of a comparable size. The air gap can be as small as 0.3 mm considering the manufacturing method, using an inner rotor construction. The shaft must be nonmagnetic and the outer diameter should not exceed 115 mm because this is the size of the available SMC blanks to be used for the building of the prototype.

A thorough investigation of the internal design features of claw-pole motors was carried out and described in the previous chapter. In this chapter, the conclusions of Chapter 3 are used to design a motor with the specifications described above. The design that was finally chosen should give the best torque density at a high power factor. However, the design was not optimised in a general sense, where most design parameters were varied until the best result is found. This was not possible due to the large complicated model, including too many design parameters. Because of this, the design described below, which is arrived at by direct application of the conclusions of Chapter 3 above, is first presented, then some further improvements are sought.

4.2 Design

The first decision to be made is regarding the topology to be considered in the design. The single rotor stack topology, which was used in the experimental machine (Mark 0), was shown to suffer from large inter-phase leakage (and this will have an adverse effect on the power factor). Additionally, the construction required long, thin, rotor claws. Such claws would be very difficult, if not impossible, to manufacture by pressing the SMC iron powder. (A solid steel rotor had to be used in the experimental machine.) Therefore, the single rotor stack topology is not considered in designing the prototype servomotor, Mark 1. The rotor is instead designed with three individual stacks. One stator phase consists of the claws, the core and the coil while a ring magnet and the surrounding claw construction forms one rotor stack (phase). In this way, the relative orientation of the rotor stacks (phases) can be adjusted to give favourable conditions that could result in reduction of inter-phase leakage, and cogging torque. The Mark 1 motor topology is illustrated in Fig. 4.1.

4.2.1 Number of poles and claw angles

The experimental machine (Mark 0) was built with 8 poles. This was believed to give a relatively high power factor considering that it is a claw-pole motor, which is known

to give low power factors, and considering that the power factor decreases as the number of poles is increased, as is seen in Fig. 3.40.

As the work progressed, the investigations described in Chapter 3 indicated that a higher pole number could be used, without decreasing the power factor below 0.9, if the magnet design and the core shape were altered. In order to increase the possibility of achieving the specified torque density value, a 20-pole design was chosen. At 500 Hz, the rated speed will be 3000 rpm; the rated value. The best claw angle and claw smoothing angles were selected, with the aid of Figs. 3.55 and 3.57, to be 10 degrees for the claw angle, and 3.2, 5.2, and 4.2 degrees, for the stator and rotor claw smoothing angles (as defined in Fig. 3.7).

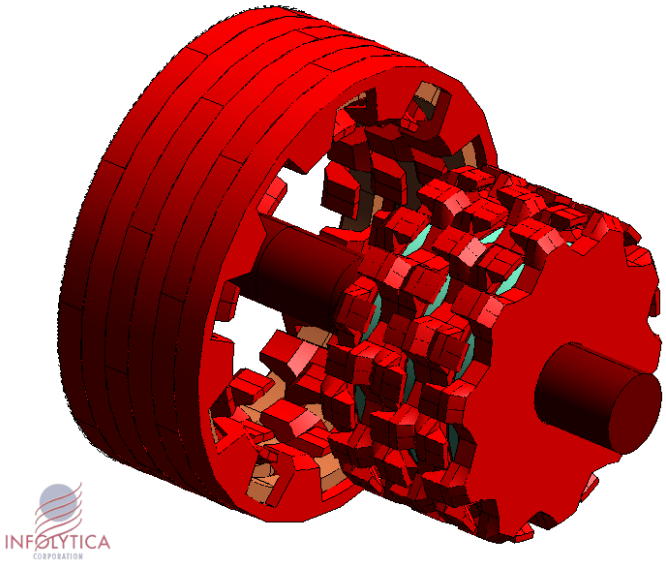

Figure 4.1: Model of the prototype 3-phase claw-pole motor (Mark 1).

4.2.2 D and L, control, and air gap length

The air gap was set to 0.3 mm, the smallest allowable, in order to get the highest torque (accepting the small decrease in power factor). The outer diameter as well as the stack length, and thus the motor length, were set after the diameter of the magnet was decided, as described below.

The standard drive that was used in testing the Mark 0 motor is also assumed. It feeds the motor with sinusoidal voltages, keeping the *d*-axis current to zero. Thus, the claw-pole motor is driven as a brushless drive.

4.2.3 Magnet design

The magnet needed to be large enough to achieve a power factor of 0.9. According to Fig. 3.52, the best choice is a magnet radius of 32 mm. The length of the magnet was set to 3 mm. This is longer than the best value of 1.5 mm found in Fig. 3.45 (no improvement in power factor and torque above this value). However, the magnets must not be too thin, because of the brittleness, and a longer magnet will give better results provided that the core is modified so that it can accommodate larger flux. Another consideration is the cost, as a magnet of about 2.5 mm is the most cost effective. The shaft diameter was increased to 20 mm when originally the shaft was intended to be smaller (in order to obtain the largest magnet area possible). However, the reduction in magnet area due to the larger shaft is only 7.5 %, and the larger shaft

adds stability as well as contributing to the weight reduction of the motor (the shaft material has a mass density of 2707 kg/m^3 compared to the mass density of SMC, which is 7350 kg/m^3). Thus three identical ring magnets are used, each having an outer diameter of 64 mm and an inner diameter of 20 mm, and the length of 3 mm. The material is sintered NeFeB with a maximum working temperature of not less than 120 °C. One magnet piece is shown in Fig. 4.2.

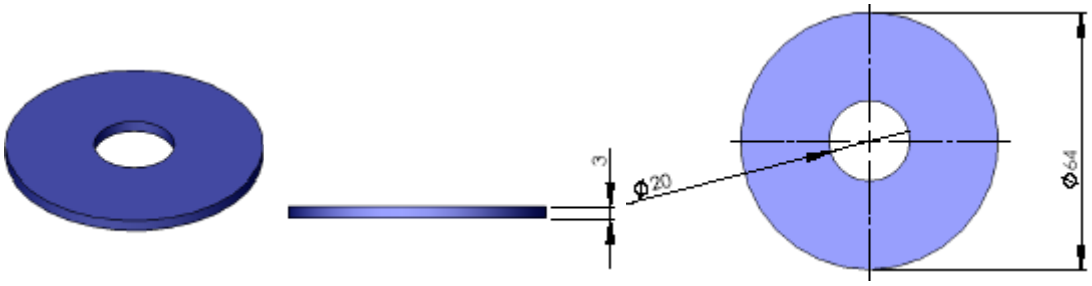

Figure 4.2: Magnet drawing.

4.2.4 Pole phase profile and coil design

The rounded claw construction is preferred, with a claw length of 11 mm. As the total length of one stack is 14 mm, the claw length is 80% of the total stack length. In Fig. 3.52 this relative length value is shown to be a good choice, as far as torque production is concerned (although the data in Fig. 3.52 is obtained for a longer stack length). The rounded claw construction is believed to yield lower inter-phase leakage than the long claw construction although this was not quantified.

The thickness of the core parts (and thus the stack length) was found following additional investigations, after the magnet shape and the pole number and angles were selected. The main goal of this additional investigation was to increase the torque density, by reducing the active material, without impairing the power factor.

The round-claw construction of the stator core, as well as providing a geometry that follows the expected natural flux path, it makes it possible to use a coil with a circular cross-section, as is illustrated in Fig. 4.3. While it may be possible to realise the geometry of Fig. 4.3 in mass production (when SMC powder will be pressed into the required shape), it would be rather difficult to produce by machining of a block of SMC material, as is the case in the manufacture of the prototype Mark 1. Therefore, for the prototype motor, the claw shape of Fig. 4.4 is considered.

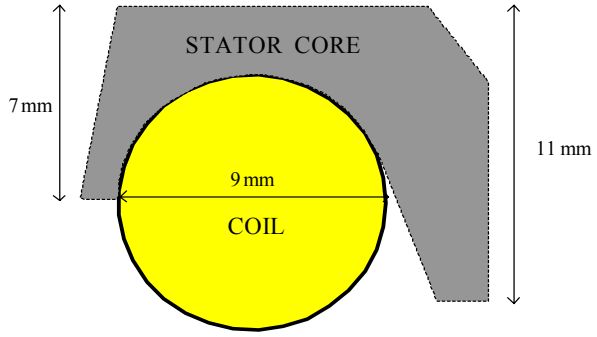

Figure 4.3: Cross section of a stator core part with a circular coil cross section.

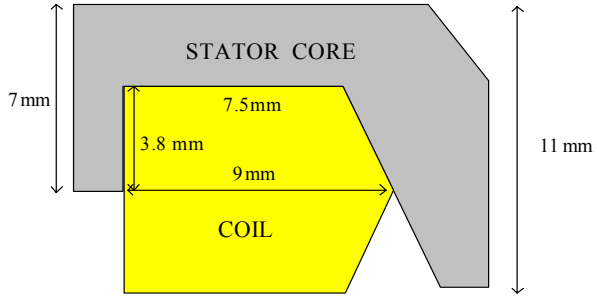

Figure 4.4: Cross section of a stator core part with a pentagonal coil cross section.

With reference to Fig. 4.4, in order to make use of all the available space between stator core back and the stator claws, a suitably shaped pentagonal coil is considered. In Figs. 4.3 and 4.4, the area of the coil cross section is approximately 63 mm^2 in both cases. The pentagonal coil shape of Fig. 4.4 allows a slightly larger stator claw, but this is not the main reason why such a shape is used in the prototype.

The winding with a pentagonal cross section, as shown in Fig. 4.4, needs a special type of wire. The shaping can be realised with DAMIDBOND from Dahréntråd (www.dahrentrad.se). The coil can be made in a tool and then heated with an appropriate current, so that part of the wire insulation bonds with the other wires yielding the required shape. The coil can then be retrieved from the tool and assembled between the stator stacks.

Irrespective of the coil shape, the assembly process does not put any strain on the winding thus no destruction of the wire insulation is to be expected (as is usually the case when the windings are pressed into the slots in normal radial motors). Because of this, depending on how the phase winding is prepared and insulated it may be possible to achieve reliable operation without using *slot* liners. This of course would improve the *slot* fill factor. There is another way as to improve the fill factor (and the cooling), according to (Pennander 2005), and that is to press the winding with high pressure, allowing the fill factor to improve to 75-80%. This technique is said to be advantageous especially for machines with SMC cores. In the current claw-pole design, the coil can be pressed in the axial direction.

The excitation voltage should not exceed 240 V, which is the rated voltage of the 3-phase inverter used to supply the brushless motor to be replaced. The back emf per turn is calculated from the flux linkage at no load (according to Eq. 3.2). This shows an expected back emf of 237 V for a coil having 100 turns at a speed of 3000 rpm. (i.e. a flux factor of 0.75 Vs/rad). The wire diameter is then found from:

$$A_{Cu} = \frac{\pi d^2}{4} = \frac{A_{coil} f_c}{N} \tag{4.1}$$

where A_{Cu} is the area of the bare copper wire, with diameter d, and A_{coil} is the area of the coil cross-section, and f_c, is the fill factor.

A reasonable value of the fill factor is 0.5, allowing for the wire insulation and the slot insulation. If, however, slot insulation can be avoided, then the fill factor of 0.5 is no longer relevant, and the fill factor, f_{cm}, given by the wire manufacturer (giving the

number of insulated wires per cm^2) is more relevant. An example of f_{cm} is 190 (depending on the wire diameter), and this gives f_c =0.67 (just allowing for not using a slot insulation, not considering a pressed coil).

4.2.5 Assembly and materials

The two-stator core parts can be made identical. However, the parts can also be made with a recess for easier mounting. The recess can be made in the circumferential direction (like a lid on a jar) or in both the circumferential and the axial direction (like claws locking each other or like taps and tap holes). In both cases, the connection area is larger than with no recess, and in the first case, the two parts are no longer identical. For practical reasons, the identical parts alternative was chosen for the prototype.

The cogging torque reduction is not considered in detail. However, the parts can be assembled in such a way that cogging torque is reduced. The three stator stacks will be shifted two thirds of a pole pitch. The middle rotor stack will be shifted one pole pitch relative to the other two stacks and the magnet in the middle stack will be oriented in the positive z-direction, whereas the other two magnets are magnetised in the negative z-direction (referred to as the +z assembly in Chapter 3). This way of assembly is believed to give the smoothest torque and emf, as well as the smallest cogging torque, as is seen in Figs. 3.37 to 3.39.

The temperature sensors will be fitted to the windings between the claws. The mounting of the shaft on the rotor might be a problem because the core material (SMC) is brittle. One possibility is to make the shaft with a smaller diameter at the end where the machine is not connected to the load, because at that side (non-drive end), the stress on the shaft is not so large, and like that the shaft can be pressed into the core and fixated at the end. Another option is to make a recess in the core and in the shaft of the same size and put a flat wedge in the recess, as is done on Mark 0. The magnet and the rotor core parts can also be assembled with a shrink fit. In this, the shaft is frozen (and will shrink) before mounting the parts on the shaft. When the shaft assumes normal temperature, it will become firmly attached to the rest of the rotor. This last method will, however, put too much strain to the SMC core parts, and, therefore, using a flat wedge is preferred.

The SMC core parts are to be manufactured using injection moulding. The geometry that is suggested for mass production is shown in Fig. 4.5, together with the computed field values. However, the pressing of the parts requires specially made tools that are far too expensive to justify for the building of one prototype. Because of this, the prototype machine (Mark 1) has to be made by machine tooling SMC parts, giving a design such as shown in Fig. 4.6. It is seen that the shaping of the rotor core, and the thin stator back are avoided in Fig. 4.6.

In the prototype, the minimum thickness of the core parts is not only determined by magnetic considerations. Mechanical considerations (namely the material stress introduced by machining and the brittleness of the SMC) set the minimum thickness. Such constraints are removed when the parts are pressed, as would be the case for mass production. The design of the machine-tooled prototype is further described below, in Section 4.3.2. Drawings of the machine-tooled prototype are given in Figs. 4.7 and 4.8. Dimension differences between the prototype and the design for mass productions are given in Section 4.3.

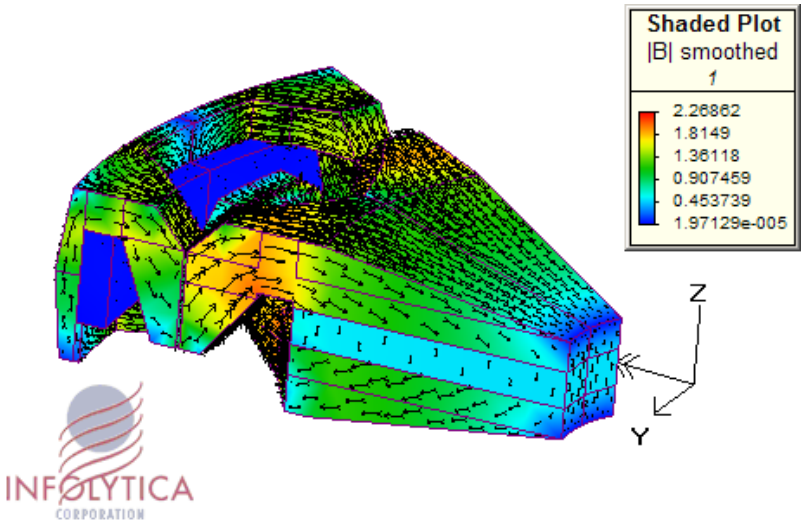

Figure 4.5: Core parts when the SMC parts are made with a pressing tool.

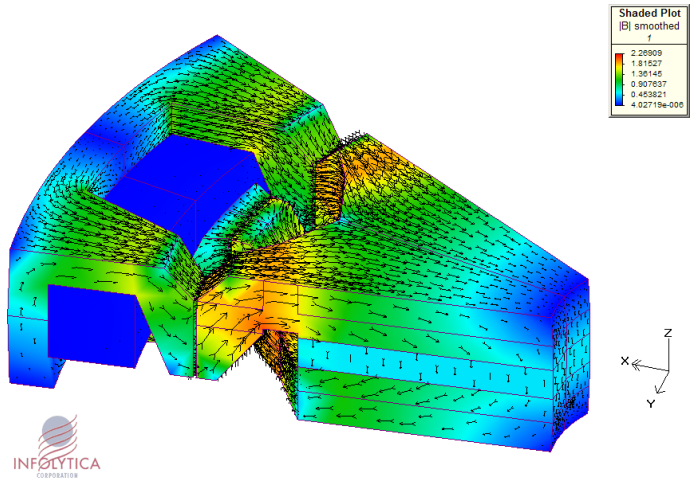

Figure 4.6: Core parts when the SMC parts are made with machine tooling.

4.2.6 Cost considerations

The cost of the used parts is found from (Martinez-Munos 2005) and (Dubois and Polinder 2004). The estimated cost of the iron powder is about 2 Euro/kg. The price of copper is approximated as 6 Euro/kg. The cost of the shaft non-magnetic steel was estimated by (Laszlo) to be 5.5 Euro/kg (compared to ordinary steel 1.4 euro/kg). The price of the magnet material is strongly dependant on the size of the magnets and the quantity ordered. An approximate figure, based on an order of 1 million pieces, was obtained from Sura Magnets AB at 2.2 Euro/magnet ring.

4.3 Predicted results

4.3.1 Performance

In order to predict the best performance possible (for a motor with pressed core parts), the highest possible winding fill factor (0.8) is assumed. This would allow minimisation of the space required to accommodate the coil and would, obviously, yield a slimmer motor with the highest possible torque density. The design is as

shown in Fig. 4.5 and the actual dimensions are similar to those given in Figs. 4.7 and 4.8. The differences are in the rounding off of the stator core back and the rotor part close to the shaft, as well as the smaller coil cross section. The effect of reducing the coil cross section is simply to reduce the inner radius of the stator core back. The pentagonal shape of the coil cross section is thus maintained. With these assumptions, the coil area is 39 mm^2, and the bare wire diameter is 0.65 mm, giving a current density of 6 A/mm^2 (which is within the acceptable range for an air-cooled motor).

The results are predicted with the finite element method. 36 magneto-static 3-D problems, covering the rotation of one pole-pitch, were solved. First, the performance from one phase was calculated with a model of two pole-pitches with periodic boundaries. The adaption tolerance was set at 1.5%, and the frequency was fixed to 500Hz, which corresponds to the rated speed of 3000 rpm.

The computed torque density at rated current (2A) for a one-phase model is 1.4 Nm/kg at a power factor of 0.87. The 3-phase stator hysterises loss at 500 Hz is 7W. The torque density for a three-phase model with a +z assembly is 1.6 Nm/kg. The electromagnetic torque is then 2.6 Nm. The total cost of the active parts of the Mark 1 prototype would be about 3.5 Euro/phase where the major cost is due to the magnets, as shown in Table 4.1. The cost per unit torque is, therefore, 4 Euro/Nm and the torque per unit volume is 7.2 kNm/m^3. The material cost is rather high but the cost of production (of the parts and the assembly) is expected to be lower than that of a conventional brushless motor, due to the simple construction with fewer parts.

Stator	0.25 Euro
Winding	0.43 Euro
Rotor	0.56 Euro
Magnet	2.2 Euro
Shaft	0.02 Euro

Table 4.1 Cost of the parts in one phase of Mark 1

4.3.2 Prototype modifications

As the prototype will have to be built with machine-tooled core parts, some design modifications are necessary and these are described below. Of course, further calculated results (allowing for the design modifications) will be needed for future comparisons and these are presented in the following subsection.

Due to manufacturing reasons, the prototype is to be based on the geometry of Fig. 4.1. The strict objective to reduce materials to achieve a better torque density was relaxed, due to the brittleness of the SMC and due to the stress on the material when machine tooling the parts. The circular cross section was difficult to realise both for the machine tooled SMC parts and for the pressed SMC parts. It can be pressed but it would need extra tools, and as the pentagonal shape uses the natural space between the claws in a more efficient way, this shape was chosen. The coil area is chosen to be larger than necessary so that the coils need not to be pressed, and a current above rated current can be used for the testing, and there will even be some space for slot insulation, if preferred.

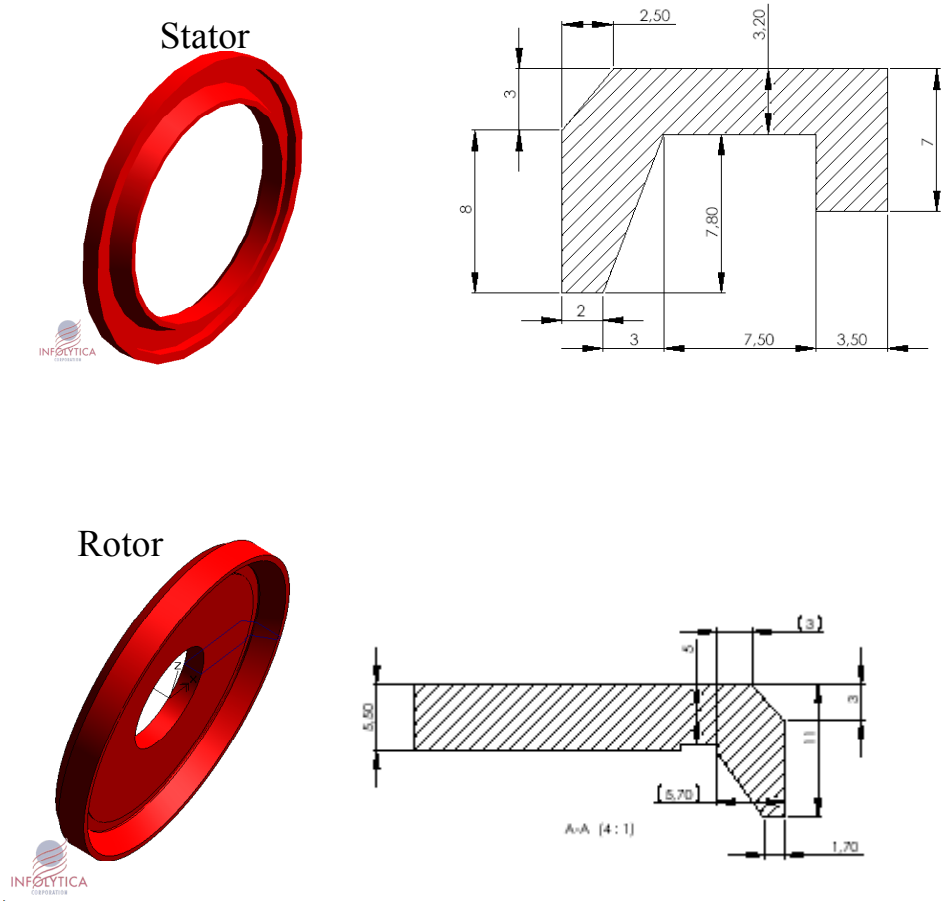

Figure 4.7: The turned core parts and the cross sections of the parts.

The machine-tooled prototype is made out of pre-pressed blanks. First the stator and rotor is turned, according to the dimensions in the radial-axial plane, giving parts as shown in Fig. 4.7. After the parts are heat-treated, wire cutting techniques are utilised to make the remaining intricate details.

The rotor is wire-cut in two planes, allowing the claw-tips to be thinner than the claw-backs, as shown in Fig. 4.8, whereas the stator claws may only be wire-cut in one plane. This restriction in the wire cutting of the stator is due to the stator core back being in the way of the wire when the stator claw-tips are cut. Thus, the thin rotor and stator in Fig. 4.5 is avoided due to the stress while turning and the smaller stator claw-tips is avoided due to the restrictions in the wire cutting. The last restriction will lead to more leakage between stator claws but using thicker rotor and stator core will not lead to lower performance, apart from the lower torque density (due to the increased weight).

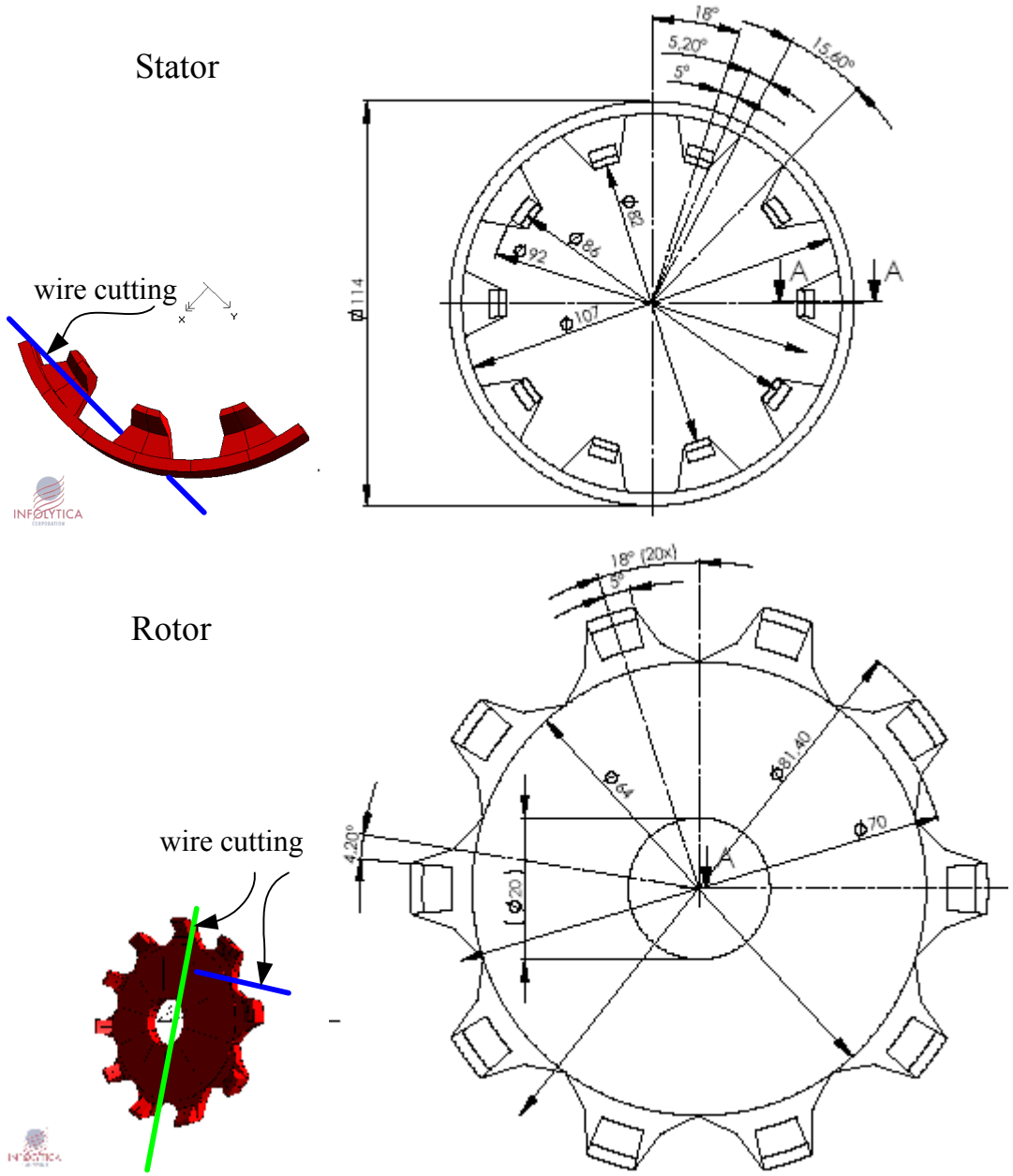

Figure 4.8: The wire-cut core parts and the cross sections of the parts.

4.3.3 Prototype machine predicted results

The expected results are calculated with the aid of the 3-D finite element program with the magneto-static solver for 36 rotor positions within the rotation of one pole-pitch. First, the performance from one phase was calculated with a model of two pole-pitches with periodic boundaries. The adaption tolerance was 1.5%, and the frequency was set to 500Hz, which corresponds to the rated speed of 3000 rpm. The results of the torque density, power factor and stator hysteresis loss at different current loadings are shown in Fig. 4.9. The rated current is 2 A, and the number of turns is 100. The dimensions are shown in Figs. 4.7 and 4.8. The torque density is rather low (calculated on the electromagnetic torque, not the shaft output torque); at rated current only 1.1 Nm/kg. This however can be improved with reduction of material, which is possible if the core parts are pressed and not machine tooled, and if the full advantage of not using slot insulation is taken, as discussed in section 4.3.1.

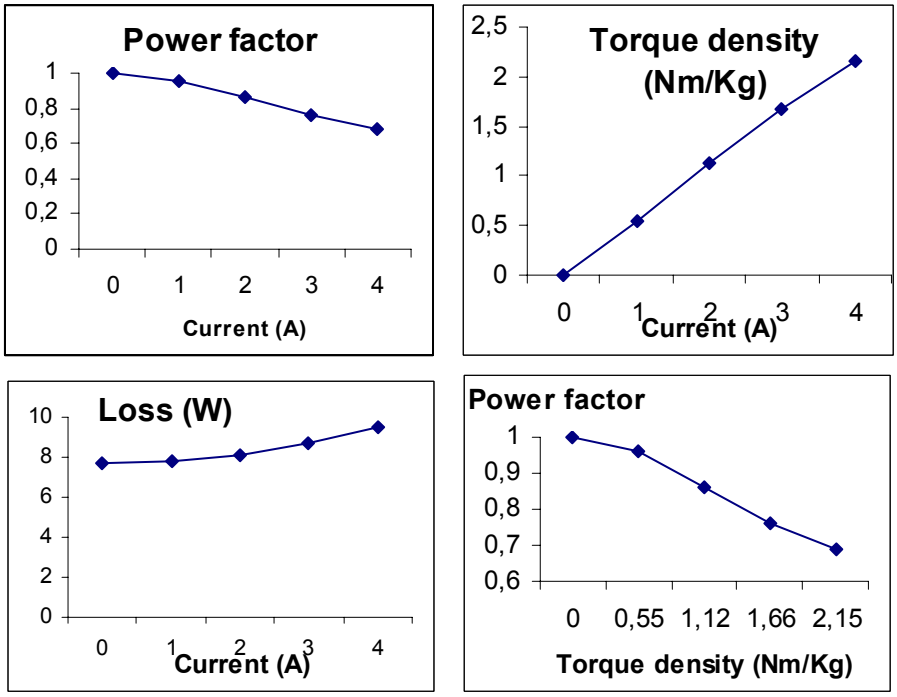

Figure 4.9: Torque density, power factor and stator hysteresis loss at different current loadings in a one-phase model of the machine tooled prototype.

At no-load, the rotation of two pole-pitches (360 electrical degrees) was modelled, as this allows the calculation of one period of the flux linkage and the induced back emf. To get the emf, the first seven harmonics of the flux linkage were calculated, and then differentiated with respect to the rotor position according to Eq. 3.2. The results are shown in Figs. 4.10 and 4.11. The flux linkage contains harmonics, mostly of third and fifth order, giving the shape of the emf waveform of Fig. 4.11.

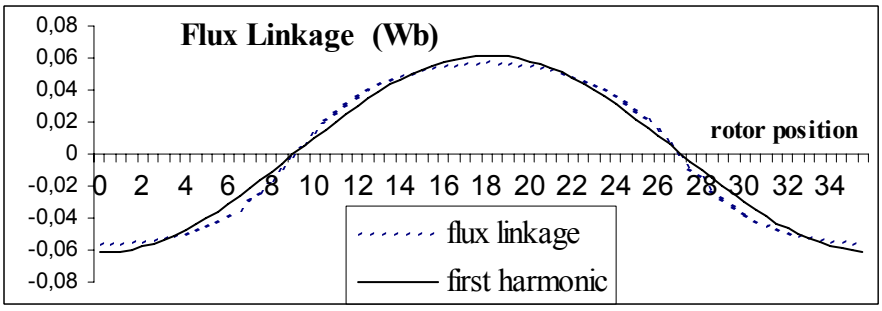

Figure 4.10: Induced flux linkage at no load in a one-phase model of the machine tooled prototype.

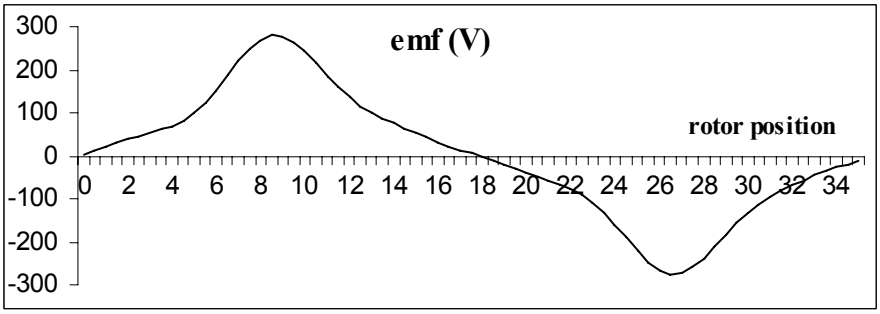

Figure 4.11: Induced emf at no load in a one-phase model of the machine tooled prototype.

In order to investigate inter-phase leakage, a model for the whole three-phase motor was developed. The three stator stacks were shifted two thirds of a pole pitch with respect to each other. The +z assembly is assumed with no barriers between phases. The middle rotor stack was shifted one pole pitch relative to the other two stacks and the magnet in the middle stack is magnetised in the positive *z*-direction, whereas the other two magnets are magnetised in the negative *z*-direction.

At rated current (2 A) the torque density was 1.25 Nm/kg, slightly higher than what was calculated in the two-pole pitch-model. The power factor was not properly solved, as that would require a too long solution time but the loss at 500 Hz was found to be 29W, similar to the results of the one phase model. The cogging torque of the three-phase motor has a peak value of 0.4 Nm (15% of the rated torque of 2.7 Nm) at a frequency of 6 kHz but the accuracy of this calculation should be improved in order to obtain a more reliable value.

The weight of the active parts (cores, shaft, magnet, and coil) was calculated to be 2.2 kg. The resistance of the armature is 1.46 Ω/phase, and the unsaturated inductance/phase was calculated to be about 14 mH, at a rated current of 2A (thus a reactance of 0.63 pu at rated speed).

The finite element calculations give an air gap flux density value, B_g, of about 0.8 T at the aligned position, and B_g about 1.3 T at the unaligned position. B_m is about 0.64 T (H_m is about 366000 A/m). The reluctance factor is thus K_r=2.9. This high value implies that there is saturation in the core. However, the core material is SMC and the reluctance factor is expected to be slightly higher than the reluctance factor of a machine with laminated core material (a common figure is 1.2). In fact, calculating the inductance at different rotor positions and at different current values shows that the saturation occurs only above the rated current (2 A). This is seen in Fig. 4.12.

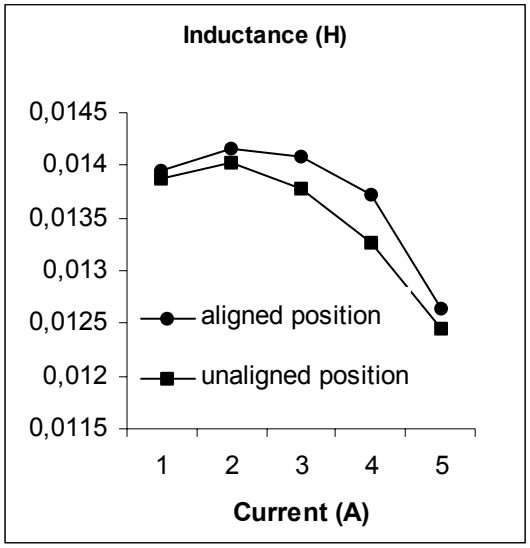

Figure 4.12: Inductance per phase in the machine tooled prototype.

It should be noted that the magnet mmf is much higher than the armature mmf, thus the saturation occurs mainly in the rotor claws due to the large magnet mmf. This does not show in the inductance calculations where the magnet material is set to air.

(In order to calculate the reluctance factor in the absence of rotor saturation, the magnet length is set to 1 mm, yielding a reluctance factor of 1.7.) Further, at the aligned position (and with zero current), the magnet flux is compared to the flux linking with the coil giving a flux leakage of 57% of magnet flux. This position of the rotor (aligned rotor and stator claws) is the position showing the most saturation. At the unaligned position, the leakage flux cannot be measured in a similar fashion, as no magnet flux links with the coil.

The normal component of the flux density is investigated, both for the three-phase motor and for one phase (the middle phase). The flux density is obtained along a line in the air gap in the middle of the motor, thus under stator 2 (the middle stator). The results are given in Fig. 4.13. Here it is clearly seen that the (small) leakage of the outer phases actually improves the air gap flux density in the middle phase.

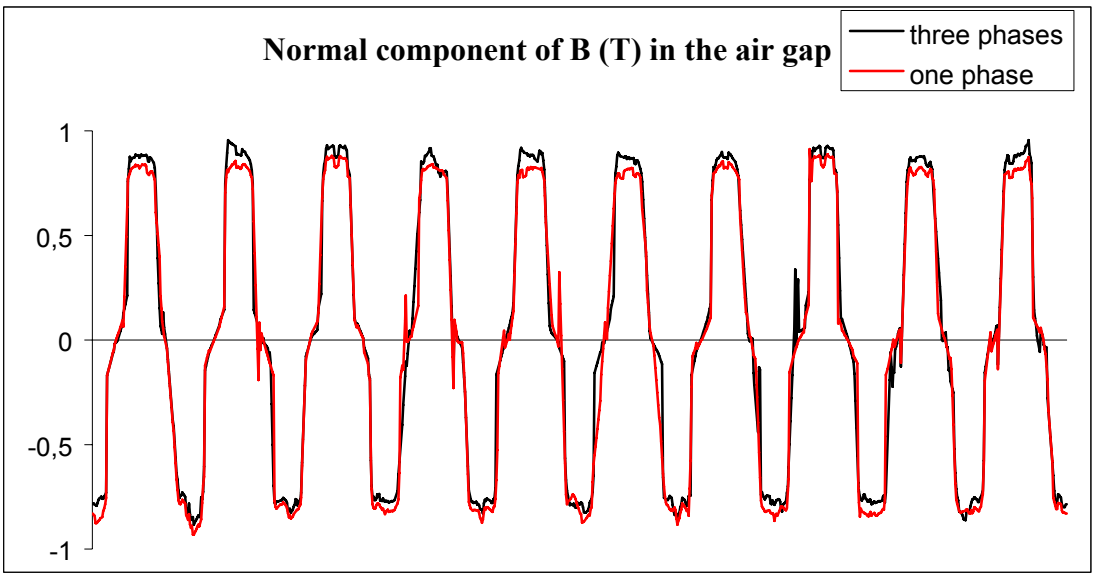

Figure 4.13: The normal component of the flux density in the air gap at z=21 mm. This is in the middle of the motor.

4.3.4 Possible improvements

There are still several means of reducing the active material in the motor in order to improve the torque density and cost. As the first priority when choosing a design was to achieve a high power factor at a reasonable torque density, the cost reduction measures were only limited to achieving a simple design that is easy to assemble. However, as seen in Section 4.2.6, there can be large reductions in the cost if the magnet volume could be reduced. This was not exploited in the design of Mark 1. In fact, the magnet length can be further decreased without impairing the performance much. This is evident in the results shown in Fig. 3.45. The smaller magnet length will also give less saturation (with less leakage as a result) and a slightly more sinusoidal back emf. Preliminary investigations along this line show that a magnet length of 2 mm (instead of 3 mm) gives a three-phase torque of 2.5 Nm and a power factor of 0.86 at rated current (compared to 2.6 Nm and a power factor of 0.87 for the motor with a 3 mm magnet). The magnet cost would be reduced by about 20% (the core volume will change as the magnet length is decreased).

Also, the control can be improved: if feeding the stator windings with square currents instead of sinusoidal currents, the torque can be improved with about 10%. There is also the possibility to use a longer rotor than stator, in order to decrease the rotor saturation, and still get a large magnet mmf.

Another improvement may be achieved if the shaping of the rotor core could be improved by using solid steel close to the shaft. This would allow a thinner shaft and thus a larger magnet area (giving a higher power factor). The solid steel would not mean higher core losses, as the core losses in the rotor are due to armature reaction and this is restricted to the surface of the rotor close to the air gap. The design of the rotor with this steel ring is shown in Fig. 4.14, which can be compared with the structure of Fig. 4.5. However, it is not sure that this design will be advantageous as it would add yet another component (totally 6 steel rings) with extra cost of assembly. Also there might be mechanical problems when fixing the steel to the shaft and the SMC part. An additional disadvantage is that the steel weighs more than SMC (7350 kg/m^3 for SMC and 7800 kg/m^3 for steel).

When the general design parameters, such as outer diameter, number of poles, air gap etc are decided, the design could be further optimised for torque density, power factor and cost, by allowing the other variables (such as claw length and width, and magnet dimensions etc) to vary in preset intervals. This way of optimisation is very time demanding, and it could give unrealistic results. Therefore, this should only be done at the final stage of the design procedure.

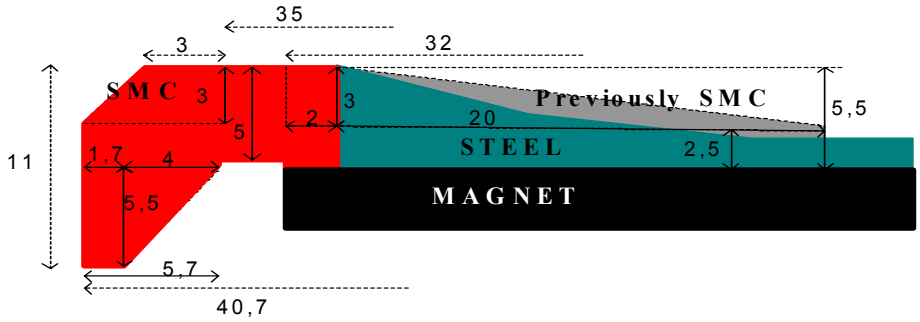

Figure 4.14: Cross section of a rotor part with a steel ring.

5 Conclusions

The general aim of the work was to investigate designs of claw-pole motors in order to find out if there is such a design that can meet requirements of reasonably high torque density and a power factor comparable to conventional topologies. This claw-pole topology was investigated because it is believed to yield reduction in manufacturing cost.

After critically reviewing previously proposed designs of Transverse-flux and Claw-pole machines, a special type of claw-pole motor having claws in both the stator and the rotor was chosen. The choice is based on the number of parts required for the motor's construction, and also because of the flux concentrated construction (which was found preferable compared to surface mounted magnets). Only three ring magnets are needed for a three-phase motor. The magnets, the shaft and six identical rotor core parts (or four parts with two different layouts) build up the rotor. The stator is equally simple with three ring coils and six identical core parts (or four parts with two different layouts). The core parts are made of Soft Magnetic Composites (SMC); consisting of iron powder particles that are individually insulated and can be readily pressed into complex geometries.

The internal design of the claw-pole motor was investigated with the aid of three-dimensional finite-element field computation. In particular, the effect of the following parameters on the motor's performance has been investigated: number of poles, main dimensions, magnet material and dimensions, pole-face profile, air gap length and claw angle. This theoretical work was verified, to some extent, against measurements obtained from an experimental machine especially constructed for this purpose.

The investigation focused on a motor with an outer diameter of 115 mm. It shows that, for the given size, a pole number of 20 yields a good balanced performance. Higher pole numbers would give too low power factor (due to increased leakage) and require too high frequencies at the specified rated speed of 3000 rpm. Lower pole numbers would give too low torque with little improvement in power factor. The work also demonstrates the negative effect of magnetic saturation, which amplifies the leakage and has an adverse effect on the torque production.

The inter-phase leakage in the three-phase machine was found to be too large if the phases were stacked in the axial direction, in the traditional way; that is to shift either the rotor phases or the stator phases 120 electrical degrees. The inter-phase leakage of course is present in all claw-pole motors but in this particular design with axially magnetised magnets, this leakage component was found to be particularly large. In order to minimise this leakage, without having to use large non-magnetic barriers between the phases, it was found that if a phase shift of the stator phases (120 electrical degrees) is combined with a special mounting of the rotor, the inter-phase leakage could in fact be used to add to the torque production. The mounting of the rotor is such that the claws of middle rotor phase are shifted 180 electrical degrees from the original position (when all rotor phases are aligned) and the middle phase magnet has its magnetisation in the opposite axial direction compared to the other two magnets. With this assembly, the combined three-phase torque was found to be larger than three times the torque produced by one-phase.

The investigation of the internal design of the claw-pole motors presented in this thesis as well as providing a physical insight into their operation, it can be utilised for their general design. Indeed, this work enabled realisation of a claw-pole servomotor that is capable of achieving a torque density of about 1.5 Nm/kg at a power factor of 0.9. The torque per volume is 7.2 kNm/m^3. The number of poles and the pole face profile were selected according to the conclusions of the internal design investigation. The magnet dimensions were chosen so that the target power factor could be achieved. The core parts were then modified to being able to carry this magnet flux, and so that the leakage could be minimised.

Throughout the design procedure, there was a conflict between the achievable torque and the power factor, and this is a special feature of these types of machines. It was also shown that there is little risk of demagnetisation of the magnets, as only a negligible part of the stator-induced flux passes the magnet.

The material cost of the proposed design is about 3.5 Euro/phase where the major cost is due to the magnet. Further improvements in the design are suggested. For instance, it is shown that a 20% reduction in magnet cost (by reducing the magnet length) is possible without much loss in performance. Even if the material cost is rather high, the cost of production of the parts and the assembly is expected to be lower than usual due to the simple construction with few parts.

The advantages of the soft magnetic composites can be exploited in claw-pole machines. The core can be shaped according to the expected flux path and the SMC can be pressed into complex geometrical shapes. Thus no excess material is needed except for support, considering that the soft magnetic composites are more brittle than steel.

Future work

The prototype described in Chapter 4 with the tooled SMC parts is in the process of being built. When this is completed, it will be tested and a comparison will be made with predictions. It is regretted that logistical difficulties in building the prototype prevented this comparison to be presented in the thesis.

Stress calculations should be done in order to achieve the thinnest SMC core parts without risk of damage during assembly or during normal operation. Modelling of the temperature distribution would also add to the knowledge, especially useful when designing the winding and the cooling system. Further optimisation with respect to the torque density and power factor and magnet size could probably lead to an even better design, as discussed in Section 4.3.4.

Other alternative applications for claw-pole machines should be investigated, for example, a large motor for direct-drive traction applications. A high power factor would still be important but for such an application the number of poles could be higher (28-48 number of poles) as the frequency (and speed) would be much lower (about 150 rpm). As the interesting construction would be an inside out motor, the magnet area would be large and the use of NdFeB magnets might not be necessary.

Appendix 1 Mark 0 drawings

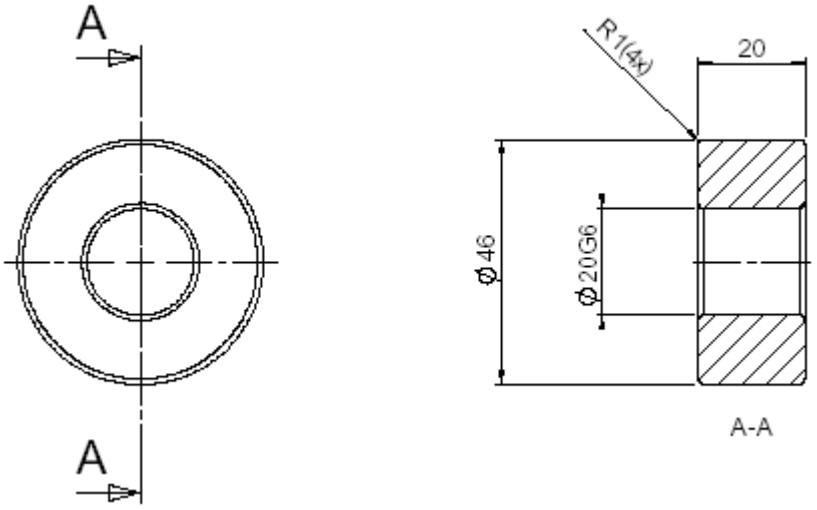

Figure A1.1 Magnet

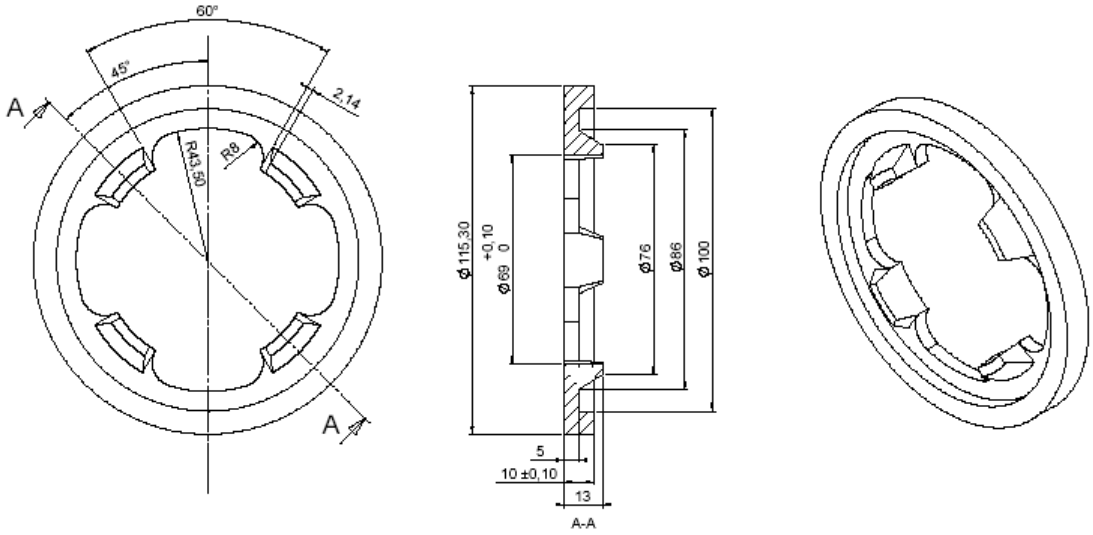

Figure A1.2 Stator

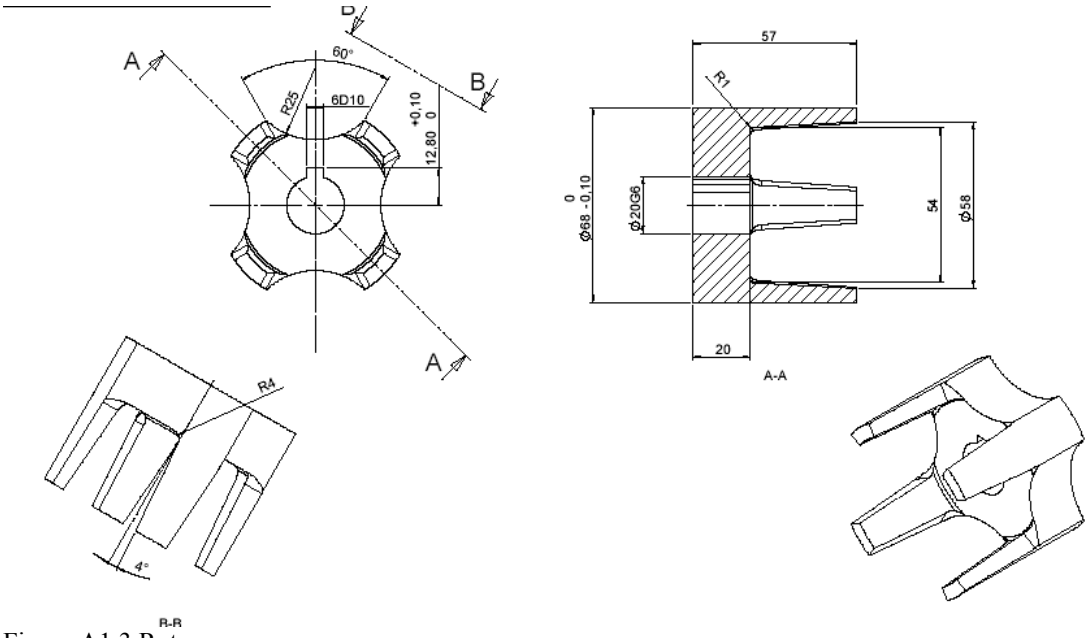

Figure A1.3 Rotor

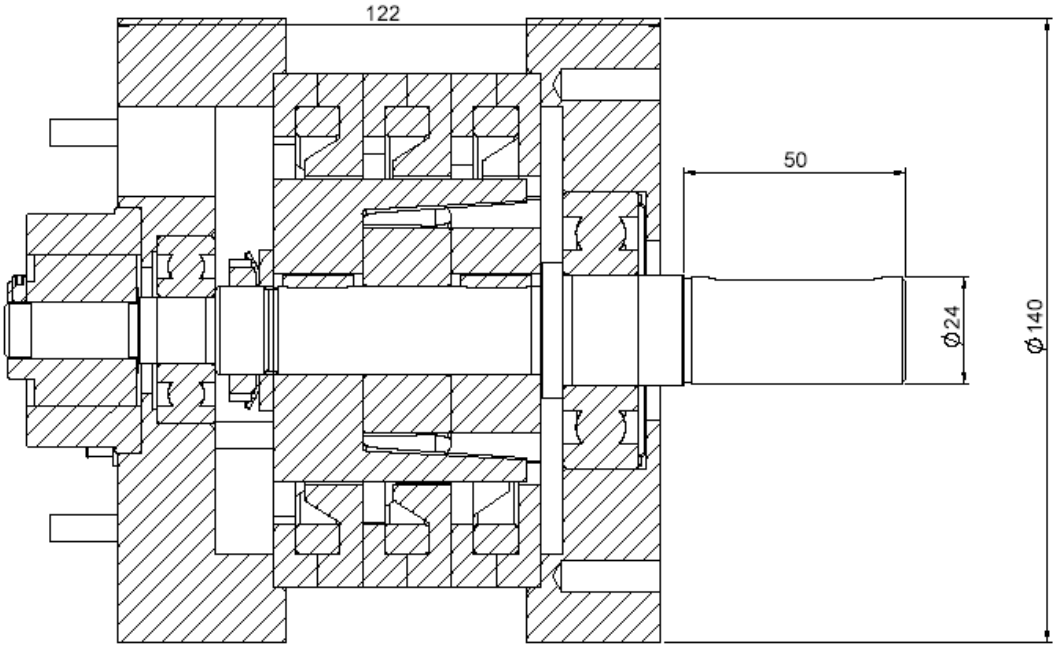

Figure A1.4 Motor

Appendix 2 Published papers

Paper A

Lundmark, S. T., et al. (2004). Effect of Pole Face Profile on Performance of a Class of Claw-pole Motors. Norfa Summer Seminar, Tallinn, Estonia.

Paper B

Lundmark, S. T. and Hamdi, E. S. (2004). "Construction, Operation and Internal Design of Transverse-Flux Machines." WSEAS Transactions on Circuits and Systems **3**(8): 1724-1728.

Paper C

Lundmark, S. T. and Hamdi, E.S. (2004). "Design of Claw-Pole Machines Using SMC Cores." WSEAS Transactions on Circuits and Systems **3**(8): 1729-1734.

Appendix 3 Submitted paper

Paper D

Lundmark, S. T. and E. S. Hamdi (2005). "Construction, Operation and Internal Design of a Claw-Pole Servo Motor." Submitted for publication in *Electromotion* Journal.

References

Anpalaham, P. (2001). "*Design of transverse flux machines using analytical calculations and finite element analysis*." Tech. Licenciate Thesis, Stockholm, Sweden, Royal Institute of Technology.

Arshad, W. M., T. Backstrom, et al. (2002). "*Investigating a transverse flux machine with intermediate poles*." Proceedings of International Conference on Power Electronics Machines and Drives, p. 325-8, 16-18 April 2002, Bath, UK, IEE.

Arshad, W. M., P. Thelin, et al. (2003). "*Use of transverse-flux machines in a free-piston generator."* Electric Machines and Drives Conference, 2003.Vol.3, IEMDC'03. IEEE International.

Chalmers, B. J., Ed. (1965). "*Electromagnetic problems of A.C. Machines*." Modern Electrical Studies. London, 102 p.

Chen, Y. and P. Pillay (2002). "*An improved formula for lamination core loss calculations in machines operating with high frequency and high flux density excitation*." Industry Applications Conference, 2002, 37th IAS Annual Meeting, p. 759-766, Vol.2.

Collins, G. C. (1966). "*Rotor assembly*." Patent 3,271,606. United States.

Cros, J. and P. Viarouge (2004). "*New Structures of Polyphase Claw-Pole Machines*." Industry Applications, IEEE Transactions on 40(1): 113-120.

Cros, J., P. Viarouge, et al. (2001). "*A new structure of universal motor using soft magnetic composites*." Proceedings of 2001 IEEE Industry Applications Society 36th Annual Meeting - IAS'01, Vol. 1, p.75-82, 30 Sept.-4 Oct. 2001, Chicago, IL, USA, IEEE.

Deliege, G., H. Vande Sande, et al. (2002). "*3D finite element computation of a linear transverse flux actuator*." International Conference on: Power Electronics, Machines and Drives, Vol. 487, p.315-319, Apr 16-18 2002, Bath, United Kingdom, Institution of Electrical Engineers.

Dubois, M. R. and H. Polinder (2004). "*Study of TFPM Machines with toothed rotor applied to direct-drive generators for wind turbines*." paper ref: 071, p. 1-9, Nordic Workshop on Power and Industrial Electronics NORPIE / 2004, Trondheim, Norway.

Dubois, M. R., H. Polinder, et al. (2002). "*Prototype of a new transverse-flux permanent magnet (TFPM) machine with toothed rotor*." 15th International Conference on Electrical Machines, paper ref: 635, p. 1-6.

Dubois, M. R., H. Polinder, et al. (2002). "*Transverse-Flux Permanent Magnet (TFPM) machine with Toothed Rotor*." International Conference on: Power Electronics, Machines and Drives, Vol. 487, p.309-314, Apr 16-18 2002, Bath, United Kingdom, Institution of Electrical Engineers.

Felicetti, R. and I. Ramesohl (2003). *"Design of a mass production low-cost claw-pole motor for an automotive application."* COMPEL - The International Journal for Computation and Mathematics in Electrical and Electronic Engineering 22(4): 937-952.

Guo, Y. G., J. G. Zhu, et al. (2002). "*Comparative study of 3D flux electrical machines with soft magnetic composite cores*." 37th IAS Annual Meeting and World Conference on Industrial applications of Electrical Energy, Vol. 2, p.1147-1154, Oct 13-18 2002, Pittsburgh, PA, United States, Institute of Electrical and Electronics Engineers Inc.

Guo, Y. G., J. G. Zhu, et al. (2003). "*Design and analysis of a three-phase three-stack claw pole permanent magnet motor with SMC stator*." Paper 85, Proceedings of Australasian Universities Power Engineering Conference (AUPEC 2003).
Hamdi, E. S. (1994). "*Design of small electrical machines*." UK, John Wiley & Sons.

Hamdi, E. S., A. F. Licariao-Nogueira, et al. (1993). "*Torque computation by mean and difference potentials [PM motors]*." Science, Measurement and Technology, IEE Proceedings A 140(2): 151-154.
Harris, M. R. and B. C. Mecrow (1993). "*Variable reluctance permanent magnet motors for high specific output*." Electrical Machines and Drives, 1993. Sixth International Conference on (Conf. Publ. No. 376)**:** 437-442.
Harris, M. R., G. H. Pajooman, et al. (1997). "*The problem of power factor in VRPM (transverse-flux) machines*." Electric Machines and Drives, 1997 Eighth International Conference on (Conf. Publ. No. 444), p.386-390.
Harris, M. R., G. H. Pajooman, et al. (1996). "*Comparison of alternative topologies for VRPM (transverse-flux) electrical machines*." Proceedings of the 1997 IEE Colloquium on New Topologies for Permanent Magnet Machines, Jun 18 1997, No. 090, p.2-1, London, UK, IEE, Stevenage, Engl.
Hasubek, B. E. and E. P. Nowicki (2000). "*Design limitations of reduced magnet material passive rotor transverse flux motors investigated using 3D finite element analysis*." CCECE 2000-Canadian Conference on Electrical and Computer Engineering, Vol. 1, p.365-369, May 7-May 10, Nova Scotia, NS, Can, Institute of Electrical and Electronics Engineers Inc., Piscataway, NJ, USA.
Henneberger, G. and M. Bork (1998). "*Development of a new transverse-flux motor*." Electromotion 5(1): 1-7.
Hultman, L. and Z. Ye (2002). "*Soft Magnetic Composites-Properties and Applications*." Powder Metallurgy Word Congress 2002, Orlando, USA.
Hultman, L. O. and A. G. Jack (2003). "*Soft magnetic composites-materials and applications*." International Electric Machines & Drives Conference, Vol. 1, p.512-522, 1-4 June 2003, Madison, WI, USA, IEEE.
Höganäs "*Soft Magnetic Composites from Höganäs Metal Powders (SOMALOY^{TM}500)*." 11p.
Höganäs (2005). "*SMC Update*." Issue 1.

Ichimura, H. (1994). "*Stepping motor*". United States Patent No. 5,331,237.

Infolytica (2004). Documentation Center.

Ishikawa, T., M. Matsuda, et al. (1998). "*Finite element analysis of permanent magnet type stepping motors*." Magnetics, IEEE Transactions on 34(5): 3503-3506.
Ishikawa, T., R. Takakusagi, et al. (2000). "*Static torque characteristics of permanent magnet type stepping motor with claw poles*." IEEE Transactions on Magnetics, 12th Conference of the Computation of Electromagnetic Fields (COMPUMAG '99), 25-28 Oct. 1999, 36(4, pt.1): 1854-7.
Jack, A., B. Mecrow, et al. (2000). "*Design and testing of a universal motor using a soft magnetic composite stator*." Industry Applications Conference, 2000. Conference Record of the 2000 IEEE, Vol. 1, p.46-50.

Jack, A. G., B. C. Mecrow, et al. (1999). "*Iron loss in machines with powdered iron stators*." Electric Machines and Drives, 1999. International Conference IEMD '99, p. 48-50.

Jack, A. G., B. C. Mecrow, et al. (1999). "*Combined radial and axial permanent magnet motors using soft magnetic composites*." Electrical Machines and Drives, 1999. Ninth International Conference on (Conf. Publ. No. 468)**:** 25-29.

Jack, A. G., B. C. Mecrow, et al. (1997). "*Claw pole armature permanent magnet machines exploiting soft iron powder metallurgy*." Proceedings of the 1997 IEEE International Electric Machines and Drives Conference, IEMDC, p. 1-5, May 18-21 1997, Milwaukee, WI, USA, IEEE, Piscataway, NJ, USA.

Jeong, Y. H. K., D.H.; Kim, J.M.; Jang, S.M. (2001). "*A design of transverse flux motor with permanent magnet shield*." Industrial Electronics, 2001. Proceedings. ISIE 2001. IEEE International Symposium on. Vol. 2, p. 995-999.

Kang, D. H., Y. H. Chun, et al. (2003). "*Analysis and optimal design of transverse flux linear motor with PM excitation for railway traction*." IEE Proceedings-Electric Power Applications 150(4): 493-9.

Kastinger, G. (2003). "*Design of a novel transverse flux machine*." Robert Bosch GmbH.

Kastinger, G. and A. Schumacher (2002). "*Reducing torque ripple of transverse flux machines by structural designs*." International Conference on: Power Electronics, Machines and Drives, Vol. 487, p.320-324, Apr 16-18 2002, Bath, United Kingdom, Institution of Electrical Engineers.

Kruse, R., G. Pfaff, et al. (1998). "*Transverse flux reluctance motor for direct servodrive applications*." Conference Record of 1998 IEEE Industry Applications Conference. Thirty-Third IAS Annual Meeting, Vol. 1, p. 655-662, 12-15 Oct. 1998, St. Louis, MO, USA, IEEE.

Kruse, R., G. Pfaff, et al. (1999). "*Optimisation of a direct servodrive with a transverse flux reluctance motor*." Electromotion 6: 25-29.

Kuppers, S. and G. Henneberger (1997). "*Numerical procedures for the calculation and design of automotive alternators*." IEEE Transactions on Magnetics Seventh Conference on Electromagnetic Field Computation - CEFEC, 18-20 March 1996 33(2, pt.2): 2022-5.

Laszlo, B. Danaher Motion, *personal communication*.

Lefebvre, L. P. and C. Gélinas (2001). "*Effect of Material Insulation and Part Geometry on the AC Magnetic Performances of P/M Soft Magnetic Composites*." Advances in Powder Metallurgy & Particulate Materials, MPIF Princeton, NJ 7: 36-50.

Maddison, C. P., B. C. Mecrow, et al. (1998). "*Claw Pole Geometries for High Performance Transverse Flux Machines*." ICEM 98, p. 340-345, Istanbul, Turkey.

Martinez-Munos, D. (2005). "*Design, Modelling and Control of Electrical Machines*." Doctoral thesis, Department of Industrial Electrical Engineering and Automation. Lund, Lund University: 324 p.

Martinez-Munoz, D. and M. Alakula (2003). "*Comparison between a novel claw-pole electrically magnetized synchronous machine without slip-rings and a permanent magnet machine*." International Electric Machines & Drives Conference, Vol. 3, p. 1351-6, 1-4 June 2003, Madison, WI, USA, IEEE.

Masahiro, S., I. Noboyuki, et al. (2005). "*Claw pole motor stator*." US Patent No 2005012427.

Mecrow, B. C., A. G. Jack, et al. (2002). "*High torque machines for power hand tool applications*." Proceedings of International Conference on Power Electronics Machines and Drives, Vol. 487, p.644-649, 16-18 April 2002, Bath, UK, IEE.

Moses, T. and J. Leicht (2004). "*Cutting core values [Cut your losses]*." Power Engineer [see also Power Engineering Journal] 18(4): 22-25.

MPIF (1999). "*Powder Metallurgy-Design Solutions*." U.S.A, Metal Powder Industries federation. ISBN 1-878-954-72-5.

Narasimhan, K. S. (2003). "*More power' call sparks soft compact research*." Metal Powder Report 58(5): 12-16.

Njeh, A., A. Masmoudi, et al. (2003). "*3D FEA based investigation of the cogging torque of a claw pole transverse flux permanent magnet machine*." International Electric Machines & Drives Conference, Vol. 1, p. 319-324,1-4 June 2003, Madison, WI, USA, IEEE.

Nord, G. and L.-O. Pennander (2004). "*Loss Calculations for Soft Magnetic Composites*." No. 170, 6p. 16th International Conference on Electrical Machines, ICEM 2004, Krakow Poland.

Payne, B. S., S. M. Husband, et al. (2002). "*Development of condition monitoring techniques for a transverse flux motor*." International Conference on: Power Electronics, Machines and Drives, Vol. 487, p. 139-144, Apr 16-18 2002, Bath, United Kingdom, Institution of Electrical Engineers.

Pennander, L.-O. (2005). Höganäs AB, *personal communication*.

Qin, D., Q. Ronghai, et al. (1999). "*A novel electric machine employing torque magnification and flux concentration effects*. "Industry Applications Conference, 1999. Thirty-Fourth IAS Annual Meeting. Conference Record of the 1999 IEEE, Vol. 1, p. 132-139.

Rang, Y., C. Gu, et al. (2002). "*Analytical design and modeling of a transverse flux permanent magnet machine*." PowerCon 2002, Vol. 4, p. 2164-7, 13-17 Oct. 2002, Kunming, China, IEEE.

Reinap, A. (2005). "*Design of Powder Core Motors*." Department of Industrial Electrical Engineering and Automation. Lund, Lund University: 220 p.

Reinap, A. and M. Alakula (2003). "*Study of a three-phase claw-to-claw pole machine*." International Electric Machines & Drives Conference, Vol. 1, p. 325-9, 1-4 June 2003, Madison, WI, USA, IEEE.

Skarrie, H. (2001). "*Design of Powder Core Inductors*." Licentiate Thesis, Department of Industrial Electrical Engineering and Automation. Lund, Lund University: 161 p.

Suzuki, Y., S. Fujitani, et al. (1998). "*Claw pole type synchronous motor*." United States Patent 5,818,143, Minebea Co., Ltd**:** 7p.

www.dahrentrad.se. April 2005.

Zhang, Z., F. Profumo, et al. (1997). "*Analysis and experimental validation of performance for an axial flux permanent magnet brushless dc motor with powder iron metallurgy cores*." IEEE Transactions on Magnetics 30(5): 4194-4196.